DETERMINATION OF DIFFUSIBLE AND TOTAL HYDROGEN CONCENTRATION IN COATED AND UNCOATED STEEL

vorgelegt von
MSc (Chemie)

Nonhlangabezo Mabho

aus der Republik von Süd Afrika

Von der Fakultät - Chemie

Universität Duisburg-Essen

zur Erlangung des akademischen Grades

Dr.rer.nat.

genehmigte Dissertation

Promotionsausschuß

Vorsitzender: Prof. W. Sand

Berichter 1: P.D. Dr. U. Telgheder

Berichter 2: Prof. Dr. H-M. Kuß

Tag der Prüfung: 23. September 2010

DECLARATION

I, Nonhlangabezo Mabho hereby declaring that all the results and data included in this thesis were totally obtained by the experiments I have conducted in ThyssenKrupp Steel Europe in Chemical Analytical Laboratory.

ACKNOWLEDGEMENTS

The following work was carried out in ThyssenKrupp Steel Europe during the three year project in the department of chemical analytics. For this reason I would like to thank all my colleagues for creating a comfortable working environment.

I specially thank Dr. J. Flock for providing me with an opportunity of being part of the great and interesting topic with valuable applicable information. For the experimental part I would to specially thank Mrs K. Bergers for constructive discussions, friendly support and great support.

For the support during analysis, I would like to thank Mr. D. Langbein, Dr. E. Pappert (ICP-OES analysis), Mr F. Pitch (Himmel furnace), Mr M. Nietz, Mr B. Mücke and Mr C. Volgermurth (LA-AES). I also thank Dr. I. Thomas for his friendly support and interesting discussions during the analysis of alloys microstructure.

I highly appreciate Mr T. Volmering for arranging the equipments needed for the work and assistance in every aspect. To a colleague and friend, Eric Camisão de Souza, I highly appreciate your hard work during construction of TDMS which made my analysis to flow easily.

I thank the workshop colleagues at ThyssenKrupp Steel Europe, Mr M. Derix, Mr C. Freiwald, and Mr M. Donath who were always willing to go an extra mile in assistance during sample preparation.

At the University of Duisburg-Essen, I specially thank Dr. U. Telgheder for challenging discussions based on the work, kindness and great motivation. I also thank Dr. H. Krohn for his assistance during electrolytic charging of steel with hydrogen.

I really thank all my friends for keeping on encouraging me during the course of the project.

I highly appreciate my mentor Prof. H-M Kuß for being a great inspiration in my career.

I thank my partner, family and parents for their greatest support and encouragement.

This work is dedicated to my late grandfather, Monde Collins Ndukwana who taught me that education is the key to success, wisdom and independence.

ABSTRACT

The new trend in the steel industry demands thin, flexible, high strength steels with low internal embrittlement. It is a well known fact that the atomic hydrogen which is picked up during production, fabrication and service embrittles the steel. This has led to an extensive research towards the improvement of the quality of metallic materials by focusing on total and diffusible hydrogen concentrations which are responsible for hydrogen embrittlement. Since the internal embrittlement cannot be foreseen, the concentrations of diffusible hydrogen work as indicators while the total hydrogen characterizes the absorbed quantities and quality of that particular product.

To meet these requirements, the analytical chemistry methods which include the already existing carrier gas melt (fusion) extraction methods that use infrared and thermal conductivity for total hydrogen detection were applied.

The newly constructed carrier gas thermal desorption mass spectroscopy was applied to monitor the diffusible concentration at specific temperatures and desorption rates of hydrogen which will contribute towards the quality of materials during service. The TDMS method also involved the characterization of the energy quantity (activation energy) required by hydrogen to be removed from traps of which irreversible traps are preferred because they enhance the stability of the product by inhibiting the mobility of hydrogen which is detrimental to the metallic structures. The instrumentation for TDMS is quite simple, compact, costs less and applicable to routine analysis.

To determine total and diffusible hydrogen, the influence of the following processes: chemical and mechanical zinc coating removal, sample cleaning with organic solvents, conditions for hydrogen absorption by electrolytic hydrogen charging, conditions of hydrogen desorption by storing the sample at room temperature, solid CO_2 and at temperatures of the drier was analysed.

The contribution of steel alloys towards diffusible and total hydrogen concentration was studied including the metallurgical microstructure formed by differently alloying metals.

CONTENTS

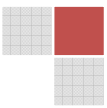

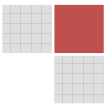

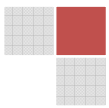

ABBREVIATIONS

α	Alpha
A	Ampere
amu	atomic mass unit
ɣ	Gamma
cm	Centimeter
CO_2	Carbon dioxide
CRM	Certified reference material
g	Gram
G_m	Molar Gibbs free energy
GDOS	Glow discharge optical spectroscopy
IR	Infrared
KJ/mol	Kilo joule per mole
$\mu g.g^{-1}$	Micro gram per gram
N_2	Nitrogen
ppm	Parts per million
RT	Room temperature
Σ	Sum
TCD	Thermal conductivity detector
TDMS	Thermal desorption Mass Spectrometry
TOF-SIMS	Time of flight secondary ion mass spectrometry

FIGURES

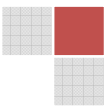

TABLES

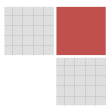

1. THEORY TO HYDROGEN AND STEEL

The huge development of new high strength, environmental friendly, coated and uncoated steel products has opened a wide market for steel producers. For instance the automobile industry have plans of producing light weight cars, fast water ships because water is the safest transport system for goods. This has led to an extensive research towards increasing more attention on improving the steel quality by focusing on a contaminant like hydrogen in flat coated and uncoated steel products because it contributes towards the embrittlement of steel. The new trend in the steel industry demands thin, flexible, high strength steels with low embrittlement. To meet these requirements, the analytical chemistry methods which include thermal desorption (hot extraction) and melt extraction were applied to monitor the total and diffusible hydrogen contents in steel. The diffusible hydrogen is very crucial because it is the indicator for the possibility of embrittlement occurrence. Thus, thermal desorption mass spectroscopy is a powerful tool in investigating the quality of steel before deterioration takes place. The steel analysis process included the analysis of hydrogen: in coated /uncoated samples, during absorption and desorption conditions, during alloying by evaluating the activation energies of hydrogen traps.

The contamination of steel by hydrogen is originated from production, fabrication and service conditions that the steel went through. For an example, the raw materials for steel production in electric arc furnace are recycled from e.g. old automobiles, construction site steel and many other scraps because steel has unique magnetic properties which make it easy for it to be recycled. Therefore, the recycled materials have already been affected by hydrogen before the production process hence there is always hydrogen in steel products. Steel is an environmental friendly material, very useful in everyday life but can be highly contaminated and embrittled.

Since the 1800 hundreds many cultures have produced steel in different forms. Henry Bessemer is generally credited with the first technique to produce steel in the middle of 1850s by using the technology that was based on Bessemer Process of blowing air through molten pig iron to oxidise the material and separate impurities.

In our days the blast furnace, basic oxygen furnace and electric arc furnace are used [1, 2]. The iron and steel manufacturing processes contribute towards hydrogen entrance into the final steel product. But this fact will be explained after the description of steel manufacturing process as indicated in figure 1-1.

The raw material for iron making consists of iron ore (Fe_2O_3), coke, limestone and additives which are poured into the blast furnace. Coke is added to the furnace as the source of carbon and it is oxidised to carbon monoxide. The calcium oxide is added as the fluxing material to collect silicon and other undesired substances to form a slag. Then, the carbon monoxide reduces the iron ore into a molten iron while the carburization is also taking place.

In the basic oxygen furnace (BOF) the oxygen is added to oxidise the carbon out of the molten steel. The residual oxygen in the steel is removed by deoxidizing agents such as silicon as silicon oxide (SiO_2) and aluminium as Al_2O_3.The oxygen can also be removed by vacuum degassing process.

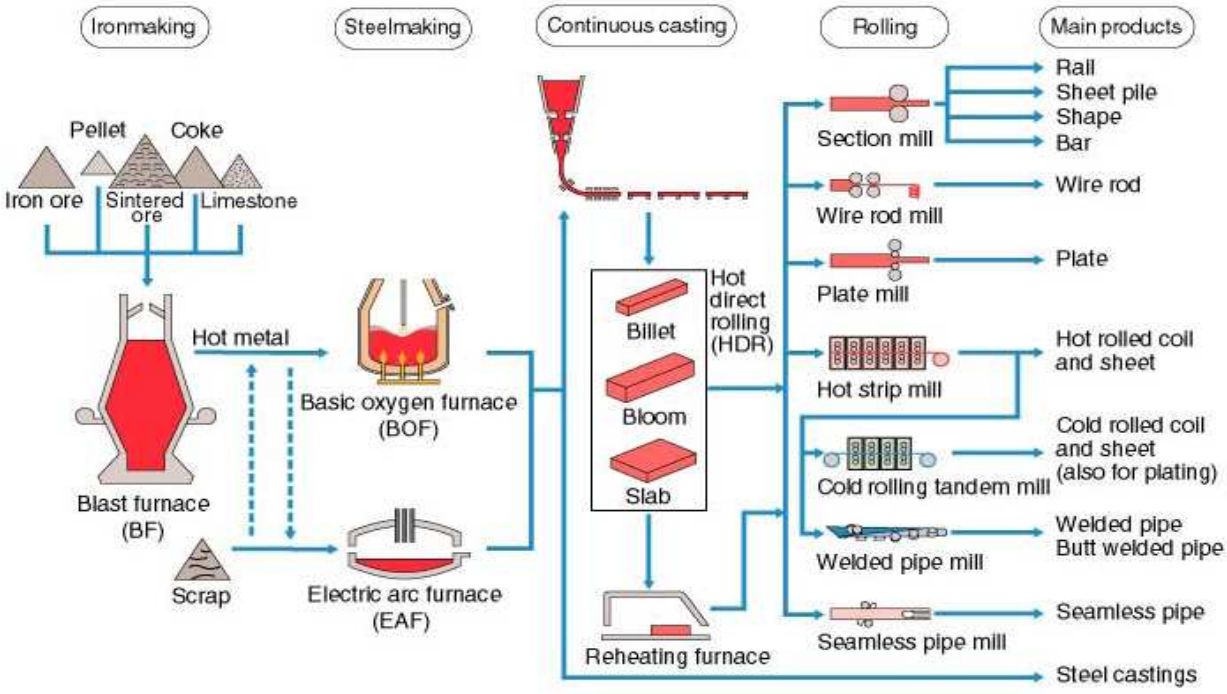

Figure 1-1: Steel making process [1].

Another method of steel production is the addition of scrap and iron ore into the electric arc furnace (EAF). The iron ore is reduced by natural gas consisting of hydrogen, carbon monoxide and methane. But any oxygen left will form inclusions in steel that attract hydrogen. The steel is considered to be clean if the total oxygen content is at least 3-6 ppm. Then the alloying elements are added in appropriate amounts and continuously casted at a certain temperature. The steel is obtained as slabs that are 20 cm thick which are highly prone to rusting if they are not properly treated further. Therefore the production processes and steel fabrication (finishing) processes that pick up hydrogen are discussed in chapter 1.1.1.

1.1 Hydrogen contamination during production processes

The hydrogen may be absorbed by metals during production, fabrication and service. For an example the production processes include calcium oxide and coke additions [3] to adjust slag chemistry. The work of C.R. Hurst [3] indicated that hydrogen pickup increased when both calcium oxide and coke were added to the molten slag in the blast furnace. Due to the moist atmospheric conditions in the ladle furnace, calcium oxide can become hydrated to form calcium hydroxide and when added to the iron melt it decomposes to form calcium oxide and

water vapor. But the capacity to absorb hydrogen increases as the steel becomes deoxidized. The water vapor formed reacts with the oxygen in the slag to form hydroxide. The hydroxide in the slag dissociates in the liquid steel surface causing the steel to pick hydrogen up and the slag remains with oxygen. The capacity of the melt to absorb the hydrogen decreases as the hydrogen content in the melt approaches the equilibrium value.

The hot metal from the blast furnace is injected with magnesium oxide or carbide to facilitate desulphurization process. The sulphur contents are impurities that increase hydrogen diffusion into the metallic materials and the critical limit of hydrogen concentration is quickly exceeded in their presence and this can form cracks.

The formation of flakes is also the harmful effect of hydrogen in steel. Flakes are normally formed around inclusions and in segregated areas of manganese (up to 150 $\mu g \cdot g^{-1}$), chrome and nickel steels. In figure 1-2 the flaking of steel was observed at various contents of manganese.

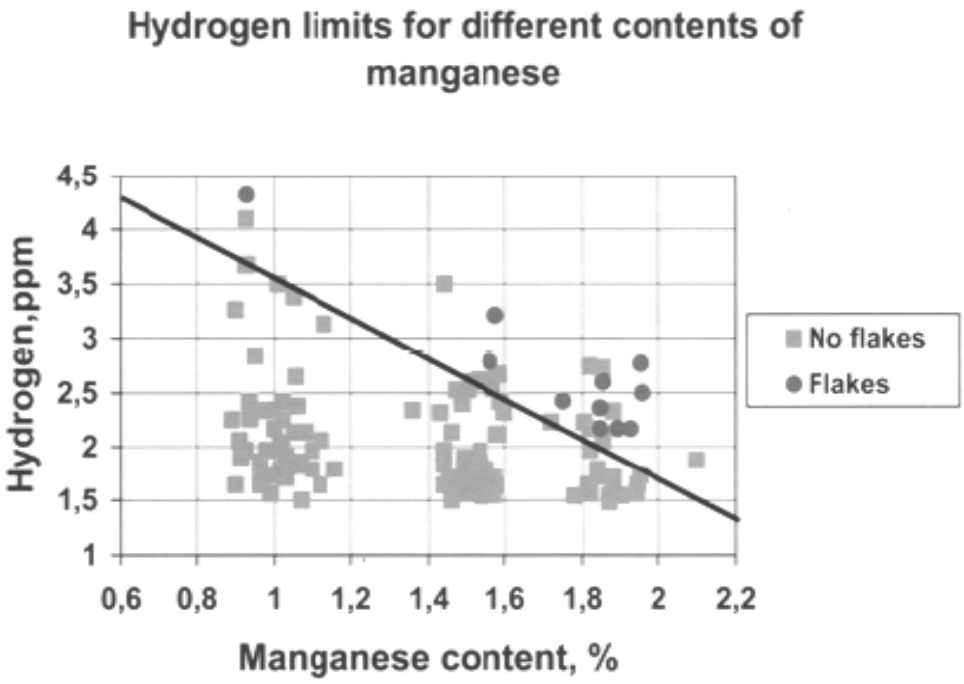

Figure 1-2: Increasing Mn contents require special care for hydrogen in steel [3].

Wet scrap additions [3]: the storage of the scrap to be used in electric arc furnace should be taken to great consideration because when the surface is exposed to an aqueous environment it becomes wet /rusted and engage in reactions that promote hydrogen pick-up in steel [3]. The water dissociates into hydrogen and oxygen that contaminate the iron and steel according to equation 1:

$$xFe + yH_2O \rightleftharpoons Fe_xO_y + 2y.H\cdot \quad (1)$$

The control of hydrogen content in steels is an important task of steelmakers during BOF and EAF steelmaking methods. The control of the pickup of hydrogen must include:

- the use of inputs with low moisture or hydrogen content,
- avoiding late addition of lime during smelting process
- minimizing the carry over slag
- carburization with low hydrogen pet coke,
- control of ladle slag basicity
- efficient degassing at deep vacuum and intense purging.

1.1.1 Influence of fabrication on hydrogen contamination

Steel rolling: the hot rolling takes place in rough rolling mill to reduce the thickness of steel slabs from 20 cm to 2.5 cm. The thin sheet is rolled to make coils of steel. The iron oxide scales formed on the steel surface can accumulate hydrogen contents. To clean the steel surface, pickling processes are applied (electrolytic) which lead to hydrogen adsorption according to *Volmer* reaction which will be discussed later in chapter1.2 which includes the entrance mechanism of hydrogen:

Electroplating [1]: the steel is cleaned chemically or electrochemically (pickling process) to prepare them for the electroplating process. The reaction of steel with the acid used for cleaning is such that some amount of hydrogen is adsorbed on the surface while some diffuses into the metallic material. Metals like Ti, Zr are sensitive to pickling processes because they exothermally dissolve large quantities of hydrogen which is very difficult to be released once it has been absorbed.

The problem of hydrogen embrittlement in electroplated products is complicated by the low rate of diffusion though most of the metals are used as electroplates. This low rate hinders the removal of hydrogen which can accumulate high concentrations and this becomes a problem in future. The zinc is chosen as the coating material because it is an element above iron in the electrochemical series and it is least expensive.

1.1.2 Influence of steel service environment on hydrogen contamination

Hydrogenous gases are used to prevent oxidation of metals that are being treated by heat e.g. in metallurgical processes hydrogen is mixed with N during heat treatment applications to remove oxygen by reacting with it to form HO whose oxidation potential is much lower compared to O [4]. But during the heat treatment, both the thermodynamics and kinetics favour the absorption of substantial quantities of atomic hydrogen from the gas phase.

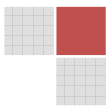

The metallic containers in petroleum industry where the raw material contain hydrogen sulphide (H_2S) as an impurity are highly affected by embrittlement due to hydrogen absorption. The sulphide ion on the metal surface acts as the promoter of hydrogen absorption into the bulk of metal. At high temperatures, the molecular hydrogen can actually dissociate to become the source of hydrogen atoms that are absorbed into the metal. However the hydrogen atoms that are obtained from all these processes will solubilise and diffuse into the steel material due to the influence of hydrogen parameters that are discussed in chapter 1.4.

1.2 Mechanism of hydrogen entrance into the steel

1.2.1 Electrolytic hydrogen entrance

In an electrolytic solution (aqueous environment) the hydrogen atoms are adsorbed on the metal surface by losing the electrons to become protons that interact with the metal lattice (*Volmer* reaction in figure 1-3). The rate of absorption of the adsorbed hydrogen atom from aqueous solution is affected by the presence of surface adsorbents known as poisons and inhibitors. The poisons e.g. S, P, As, Se, Sb, Te and CN^- promote the hydrogen absorption by blocking the recombination reactions that cause desorption of hydrogen. In contrast to that, the inhibitors block the absorption of the adsorbed hydrogen by forming chemisorptive bonds on active surface sites [5].

1.2.2 Gas phase hydrogen entrance

In the presence of a hydrogen gas, the molecular hydrogen can actually be adsorbed on the metal surface. It dissociates later on the surface into atoms. After adsorption, the absorption of a small content of hydrogen takes place because the hydrogen protons have a much smaller radius that permits them to diffuse fast and easily throughout the metallic crystal structure to occupy the interstitial sites. Due to the pressure exerted by the presence of hydrogen protons the structure becomes hard and brittle.

But the remaining hydrogen atoms that are adsorbed on the metal surface will recombine to form hydrogen molecule according to *Tafel* reaction [5, 6]. The hydrogen molecule will be desorbed out of the metal as gas when the partial pressure in the metal is exceeded by the atmospheric pressure. Otherwise the molecule will remain on the surface of the sample at favourable conditions.

The hydrogen protons that are in the inner crystal lattice regain the electron from the metal lattice electrons. This atom from the inner crystal structure recombines with the adsorbed atom on the metal surface (*Heyrovsky* reaction) [5, 6]. Then this hydrogen molecule will be adsorbed on the sample surface. The figure 1-3 shows the mechanisms of hydrogen entrance into the bulk of steel [5, 6, 7].

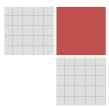

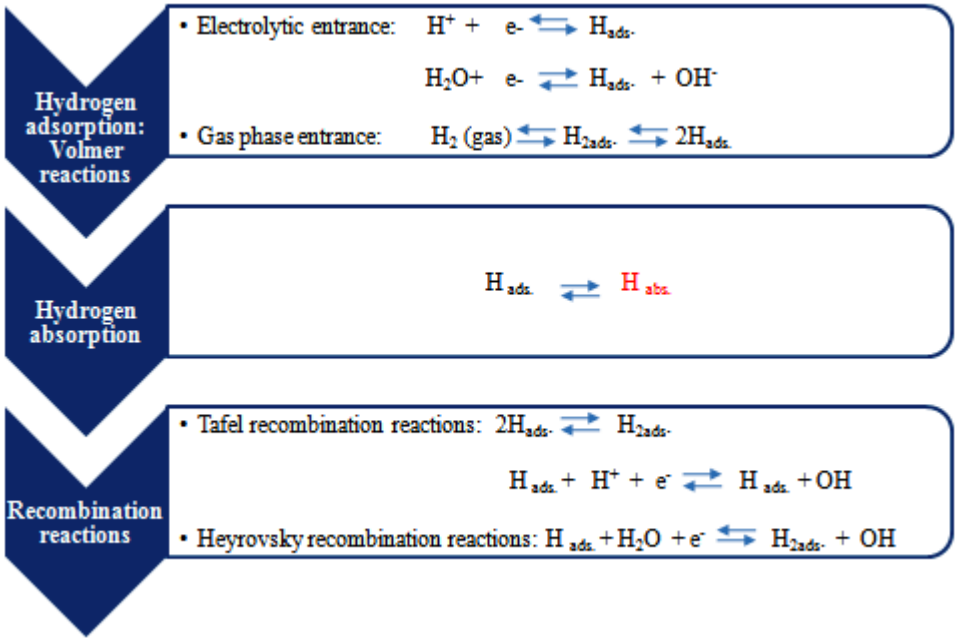

Figure 1-3: Mechanism of hydrogen entrance in steel.

These mechanisms of hydrogen interaction with steel result in adsorption of hydrogen on external steel surfaces (adsorption), absorption into the steel lattice ,localisation of hydrogen at internal sites of the bulk material (trapping) and desorption of hydrogen (recombination reactions) according to figure 1-4 [8].

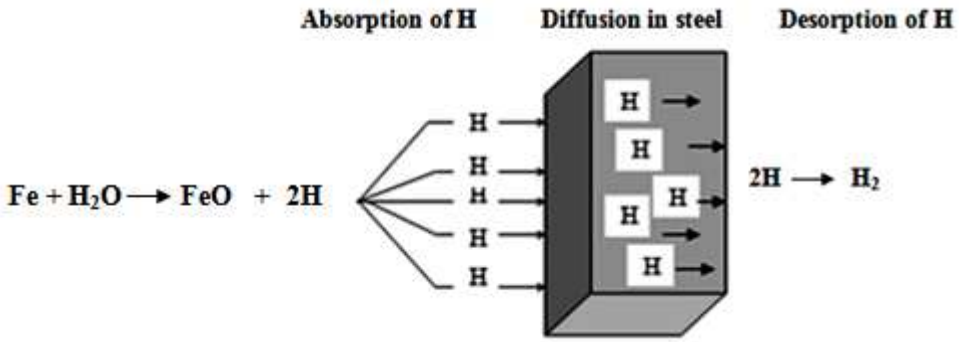

Figure 1-4: The transportation mechanism of hydrogen through the steel [8].

1.3 Hydrogen in steel

The main parameters that promote hydrogen absorption in the steel bulk are the solubility, diffusion, permeation and trapping. After the molecular hydrogen has been adsorbed on the surface, the main cause of hydrogen absorption is the presence of chemical species that affect the dissociation and recombination reactions of hydrogen atoms on the surface [refer to chapter 1.2].

These reactions lead to atomic hydrogen absorption or desorption at the metallic surface. Since hydrogen absorption takes place through the surface, the increase rate of hydrogen concentration in a specific volume of the metal is related to the surface to volume ratio. Therefore hydrogen embrittlement problems will be more frequent in fine wire and thin sheet where the surface to volume ratio is high. Conversely, metals in these forms will lose any dissolved hydrogen more rapidly on aging [9].

1.3.1 Solubility

The hydrogen diffuses into the steel in mono atomic form. If the hydrogen is absorbed from a gas phase at high temperatures (above 200 °C), the equilibrium concentration of the dissolved hydrogen is proportional to the square root of the gas pressure, according to *Sieverts* law [10]:

$$C_H = k\,(P_{H2})^{1/2} \qquad (2)$$

Where,

K: constant
C_H: concentration of the dissolved hydrogen

P_{H2}: partial pressure of hydrogen outside the metal

But the concentration of the absorbed hydrogen and the dependence of solubility on temperature imply that the solubility of metals differs widely. For instance during the solubilisation of hydrogen in La, Ce, Ti, Zr, Th, Hf, V, Nb, Ta, Pa, the reaction is exothermic [11]. Thus, the solubility decreases with increasing temperature at constant pressure. Such metals dissolve large quantities of hydrogen by forming ordered solutions or definite hydrides. In contrast, metals such as Cu, Ag, Cr, Mo, W, Fe, Co, Ni, Al, and Pt have higher hydrogen solubility as the temperature is increased.

In pure Fe the solubility of hydrogen at room temperature is $3*10^{-6}$ atoms per 100 atoms, while in the solid phase at the melting point it is $4.3*10^{-2}$ atoms per 100 atoms.

Therefore, the solubility of hydrogen in steel is affected by pressure, temperature and the crystal structure as shown by the iron hydrogen system done by C.A. Zapffe [11, 12] in figure 1-5. His work indicated that the solubility of hydrogen in liquid iron is much higher than the solid phases of iron.

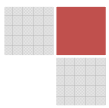

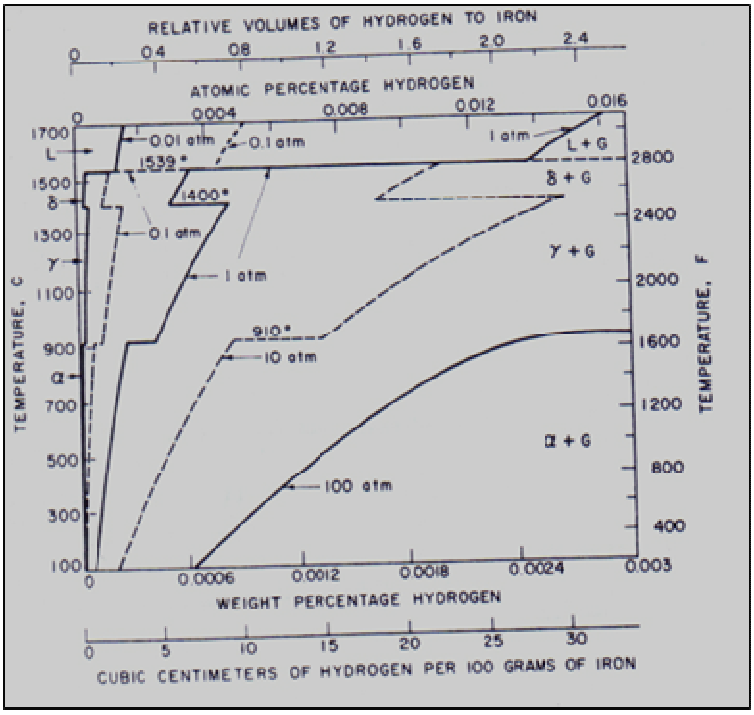

Figure 1-5: Equilibrium diagram of iron hydrogen system by C.A. Zapffe [11]

At temperatures above 400°C which was the lower limit, the small fraction of soluble hydrogen is contained as atomic hydrogen at the interstices of the metal lattice. This hydrogen which is responsible for hydrogen induced cracking of metals. On the other hand, at temperatures below 400°C, an insoluble or excess hydrogen is retained at trapping sites e.g. inclusions, grain and phase boundaries as the total hydrogen.

The solubility of hydrogen in solid ɣ, gamma iron (FCC) is much higher than in α, alpha (BCC) [13]. But in both gamma iron and alpha iron, the hydrogen solubility decreases with as the temperatures are lowered although the difference in hydrogen concentration of gamma iron ($C_H{}^{\gamma}$) to alpha iron ($C_H{}^{\alpha}$) becomes larger.

When the iron is alloyed with Ni-Cr (fcc crystal structure), there is a great temperature dependence and the diffusion is lower. Therefore the bcc and fcc structure have opposite ways of reacting towards diffusion. The work done by Beke [15] indicated that the lattice diffusion of interstitial hydrogen atoms at temperatures below 200 °C was low and required high activation energies upon the addition of alloys. In this case the diffusion at lower temperatures was hindered by the presence of traps which captured and delayed the migrating hydrogen atoms hence high activation energy was required. In gamma iron the hydrogen diffusion is lower than in alpha iron. Also the highly alloyed austenitic stainless steel has low hydrogen diffusion [14, 15].

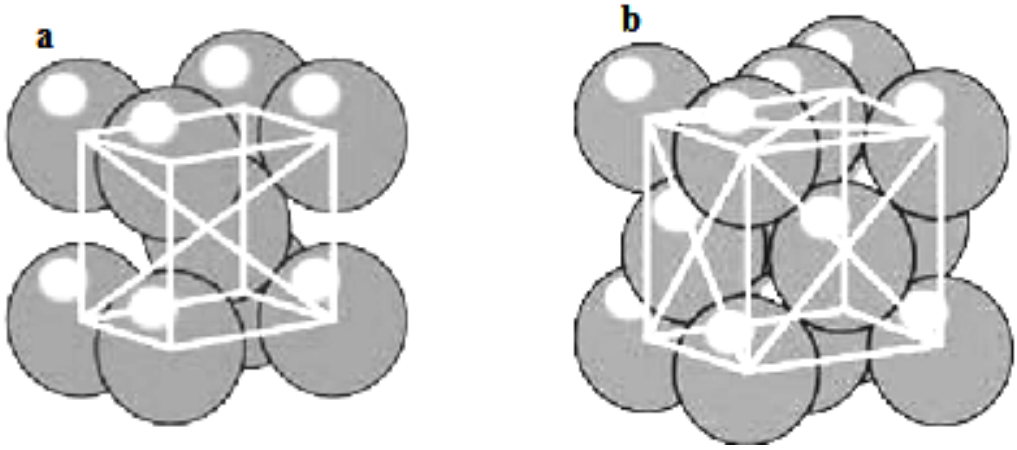

Figure 1-6: (a) Base centred cubic structure and **(b)** face centred cubic structure [13].

Pressouyre and Interrante managed to show that the environmental factors can influence the hydrogen solubility by governing the effective pressure of hydrogen [16]. For an example, a steel product with a constant number of trapping sites can be affected by a pH of a charging medium, immediately both the saturation concentration and the rate of absorption will be affected e.g. the saturated hydrogen concentration will increase from 1 ppm at pH of 8 to 30 ppm at a pH of 1.4.Therefore, according to *Sievert`s* law, high pressure will exert high stress and high localization of hydrogen. In figure 1-7 the various factors that contribute to the solubility of hydrogen in steel are summarized.

Material factors like cold working or the presence of non-metallic inclusion (sulfur) increase the number of hydrogen trapping sites to contain the total hydrogen. The area and volume of the internal voids can increase as well as the solubility of hydrogen thus more diffusible hydrogen can exist. The work done by Darken and Smith [17] showed that un-worked metal has low concentration of saturated hydrogen. However, a large percentage of excess hydrogen that remained in steel or iron after solidification diffuses into pores, cracks and lattice imperfections and form high pressure molecular hydrogen as the temperature drops.

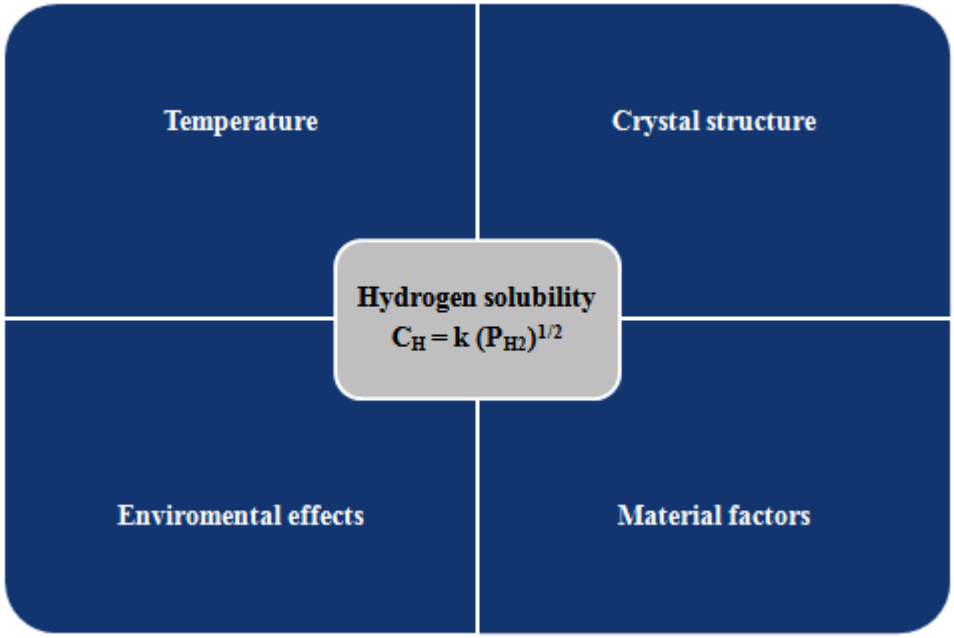

Figure 1-7: The solubility of hydrogen in a metal.

1.3.2 Diffusion

The diffusion rate of hydrogen atoms is driven by the concentration gradient in the crystal lattice which is equivalent to the activities of hydrogen in solution according to *Fick`s* law [18, 19, 20] as shown by the equation below.

$$j\infty = -D\frac{\Delta c}{\Delta x} \qquad (3)$$

Where

$j\infty$: state flux of hydrogen

D: diffusion coefficient

Δx: distance

Δc: concentration difference

In absence of alloys in pure α Fe, the absorbed hydrogen interacts with the material by diffusing at about $5*10^{-9}$ m^2 / sec at 25°C, the temperature dependence is small and the activation energy is 8.0 kJ / mol [21].

As a result of high mobility of hydrogen in metals, diffusion under the influence of temperature has a significance e.g. Zr alloy was exposed to temperature gradient, the hydrogen redistributes itself mostly at the cold end until the solubility limit has been reached, then hydrides begin to precipitate.

This phenomenon can cause failure of the zirconium alloy in nuclear reactors that use pressurized water for heat transfer. The diffusion coefficient increases with temperature and decreases in the presence of carbides. Actually the carbides in steel lower the diffusion or mobility of hydrogen. These facts were represented by the work done by Astaf`ev and Crank [18, 19].

The stress in the metal produced by notches, inclusions, cracks, bending moments, elastic stress field of dislocation can provide a driving force for hydrogen diffusion into these fields [19]. When the stress is first applied, the chemical potential of hydrogen may be lower than the equilibrium value because the solubility is increased at these local sites as a result of tensile stresses. In triaxially stressed regions, the energy of the interstial hydrogen is lower and this prompts a net flow of hydrogen into this region to be solubilised. Then, the triaxial stressed regions are crucial in steel for delayed failure behaviour. The content of hydrogen that flows into these sites is proportional to the triaxial stress components. But the saturated hydrogen concentration is observed when the stressed region relieves itself by an extension of cracks. Then, the hydrogen may even precipitate from solution in the lattice or can react chemically.

1.3.3 Hydrogen movement by dislocation

The hydrogen movement occurs via entrapment by dislocations moving in response to the applied stress. The dragged hydrogen would be motivated to move faster over long distance than diffusion which is encouraged by concentration gradients [22]. Normally the dislocations initiate at the surface and progress into the interior. Therefore, they may also have an effect on entrance or exit of the hydrogen adsorbed on the sample surface.

As the moving dislocations annihilate, they deposit hydrogen [23]. The following scientists [24, 25, 26] worked further to investigate the hydrogen deposited by dislocation, of which they discovered that it occupied the microvoids and developed higher pressure than the input activity,a_1. The hydrogen pressure supported the growth of the pre- existing micro voids and thereby contributed towards hydrogen embrittlement.

Yu and Li [27] developed an idea that the stress induced a large concentration of dissolved hydrogen which becomes supersaturated when the stress is relaxed by separation formation at the inclusion matrix interface. Therefore the supersaturated and dissolved hydrogen enter the microvoids and exert an intensive pressure causing the microvoids to grow.

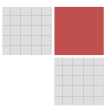

1.3.4 Hydrogen Trapping

The nature of the traps controls the jump probabilities for hydrogen atoms. Pressouyre [28] presented the energy as the function of hydrogen atoms positions as they move through a series of equilibrium positions in a lattice. The driving forces of an atom movement towards a trap are the driving forces of diffusion in chapter 1.3.2.

There is an attractive trap e.g. low angled boundary, which is a region in the crystal lattice that draws the hydrogen atoms by the force. These traps have an activation energy that is less than 30 kJ/mol at temperatures of 200 °C and below are reversible [29]. It is easier for hydrogen atom to leave an attractive trap because it requires small jump increments to be released. Such traps maintain an equilibrium concentration with hydrogen atoms present in normal interstitial lattice sites.

The physical trap is a modified crystal lattice that is energetically more favourable site for hydrogen to stay e.g. high angled grain boundaries, incoherent particle matrix interferences, micro voids and dislocations [30]. In physical trap more binding energy is required e.g. 50-60 kJ/mol which requires temperatures above 200 °C. For hydrogen atom to leave the physical trap is very difficult because one large jump is needed and more activation energy is required. Therefore, a physical trap is a non reversible trap of hydrogen. The irreversible traps reduce the amount of diffusible hydrogen content and hydrogen induced cracking (HIC). Therefore, they must be identified and characterized within the micro structure.

Thus, the amount of hydrogen in both types of traps is controlled by the diffusion, solubility, concentration of hydrogen in the lattice (which is a function of the effective pressure of hydrogen in the environment), and the nature of the traps. Hydrogen traps can be in a particle or atomic form but in order for them to be beneficial some conditions must be fulfilled [16, 29, 30]. As an example:

- The type of the trap should increase the critical hydrogen concentration, thus resist crack initiation
- Traps should be in sufficient quantities to lower the hydrogen concentration of bad defects with low critical concentration.
- They should be irreversible because if they release hydrogen, the conditions can accelerate cracks.
- Homogeneously distributed in the matrix because segregations on grain boundaries of traps will be detrimental to steel because in such areas there is always a low critical concentration.

More examples of traps including activation energies are listed in table 5-23.

1.3.5 Permeability

The permeation process through the steel involves the hydrogen entrance at one surface and its exit at the other surface. The permeation rate of hydrogen can be determined from the diffusion, the thickness of the sample, the difference between hydrogen concentration at the entrance and exit surface [31]. Thus,

$$P = D (C_1-C_2)/ L \quad (4)$$

Where,

L: thickness of the sample, [mm]

C_1: hydrogen concentration at the entrance, [ppm]

C_2: hydrogen concentration at the exit [ppm]

D: effective diffusion. [ppm / mm]

If an exit surface is exposed to the environment that reduces the value of hydrogen (C_2), the permeation is governed by effective diffusion value and the lattice solubility of hydrogen at the entrance surface, C_1.

At low temperatures, trapping will occur and hinders diffusion; therefore the measured C_1 and C_2 will not represent an equilibrium concentration. As the traps are filled, the permeation rates will increase slowly with time until the traps are completely filled. Then steady state permeation occurs at the rate that is controlled by interstitial concentration gradient. Therefore, the permeation behaviour of hydrogen atoms is influenced by interstitial diffusion rate and the trapping behaviour. Also the presence of elastic stresses appeared to increase the hydrogen permeation while the plastic deformation reduced it [32].

Since the hydrogen diffusion is not inhibited by trapping either at high temperatures or at lower temperatures, after reaching the steady state permeation condition, the traps are filled to the appropriate level of C_H that exists throughout the sample. Under these conditions, P is given by the following equation [31]:

$$P = D C_1 / L = D S / L \quad (5)$$

Where S is the solubility of hydrogen. This establishes the relationship between diffusion, permeability and solubility which is P = S x D. In contrast to solubility (S), hydrogen permeability (P) is higher in ferrite (body centred cubic structure) than in austenite (face centred cubic structure). This characteristic facilitates the removal of hydrogen in steel by heating. But permeability is also affected by alloying materials e.g. carbon decreases the permeability of hydrogen. At high temperatures the hydrogen decarbonizes the Fe_3C. During permeability manganese plays a small role but molybdenum does not participate.

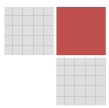

Silicon decreases permeability in steel while chromium has no effect in austenite but decreases permeability in ferrite. Nickel (6 %) increases permeability but higher percentages of it decreases hydrogen. The influence of alloying elements is explained more in chapter 1.6.4.

1.4 Hydrogen defects in steel

When the hydrogen has entered the material, it is trapped in lattice defects like inclusions, grain and phase boundaries as bulk hydrogen [33]. The diffusible form exists in interstitial sites within the ferrite lattice. When the hydrogen is negatively influenced by temperature, pressure, environmental conditions (acidity), material variables (stress) and steel alloys, quality deterioration occur in steel.

1.4.1 Low temperature defects for hydrogen embrittlement

The industrial processes that are good examples where embrittlement can take place are petroleum, ammonia and crude oil production because they generate atomic hydrogen, gas and water which are responsible for the embrittlement of steel. Hydrogen embrittlement takes place in a variety of forms depending on the temperatures and components of steel products according to Rogers [9] and figure 1-8.

Hydrogen blisters [API 579-1/ASME FFS-1]: The blisters occur mostly in carbon containing steel with high sulfur content (S > 0.01%). The atomic hydrogen diffuses through the steel until it reaches a sulfide inclusion, where the atoms recombine into H_2 molecules. The hydrogen molecules become trapped because they are large to diffuse through the steel. As the additional H_2 is trapped within the S inclusions, the H_2 gas pressure builds up and creates a bulge on the surface, which can result into a blister in the absence of the applied stress.

Hydrogen induced cracking (HIC) [API 579-1/ASME FFS-1]: The hydrogen induced cracking occurs in the same manner as hydrogen blister formation but without noticing the bulging on the steel surface at first because of low sulfur content (S < 0.01%). The trapped H_2 molecules cause internal cracking that is parallel to the steel surface. The neighboring cracks on slightly different planes link up, resulting in a stepwise cracking pattern. In hydrogen charging environment, the cracks increase in size and in number over time.

*Stress oriented hydrogen induced cracking (SOHIC):*In case of welded steel products like line pipes, when the HIC approaches a weld, cracks change the direction and propagate along the fusion boundary and this process entails a high risk of brittle fracture than HIC because the former results in cracks that are nominally perpendicular to the applied stress.

Delayed hydrogen cracking in the weld heat affected zone (HAZ): The cracks can also form at the areas that were affected by heat during welding due to the sufficient dissolved atomic hydrogen, sufficient concentration, high hardness, and tensile residual stress. The cracking is delayed and occurs several hours after welding. In moist welding conditions, the hydrogen atom can be absorbed at ambient temperatures. In a hydrogen charging service of line pipes, the dissolved hydrogen can migrate to the weld unless the material is out gassed before welding. The dissolved hydrogen tends to be concentrated at the heat affected zones because the hydrogen solubility is higher than either at the weld or the base metal. The HAZ can be prevented, by heating the steel product after welding before it cools down to ambient temperature.

Hydrogen assisted cracking under applied stress: The solubility of atomic hydrogen decreases at ambient temperature in most alloys. But the solubility increases by several orders of magnitude at the tip of the crack under a stress. The high local concentration of the hydrogen causes the material at the tip to become embrittled which results in crack propagation. The propagation of the crack is slow and stable initially, but once the critical size is reached, the catastrophic failure occurs. The susceptibility of hydrogen assisted cracking tends to increase with an increasing tensile strength of the material.

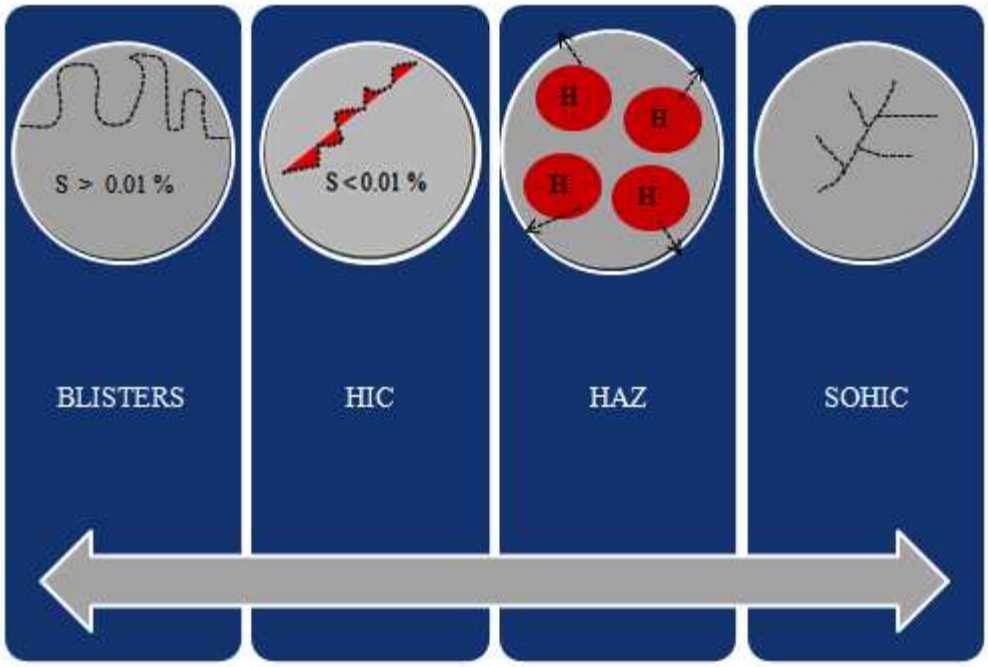

Figure 1-8: The hydrogen embrittlement processes acting on steel**.**

The explanation of embrittlement is complex due to numerous influences that can that bring about deformations which result to embrittlement. For instance plasticity is very critical because it enhances the brittle fracture. In another case the damage in the structure is brought by different hydrogenation methods e.g. such grain boundaries versus precipitate interface may compete differently for hydrogen depending on the relative coherency of each boundary.

The initiation may favour grain boundary failure in one instance and precipitate shearing in another. Either way, the results may be favoured by changing the external state of stress, yield strength level or thermal history makes a general separation between stress criteria and strain criteria for hydrogen enhanced fracture an unresolved issue. Local softening does not result from a stress free material instead from plastic strain relief. The factors that contribute towards steel embrittlement are hydrogen, stress and the material summarized in figure 1-9.

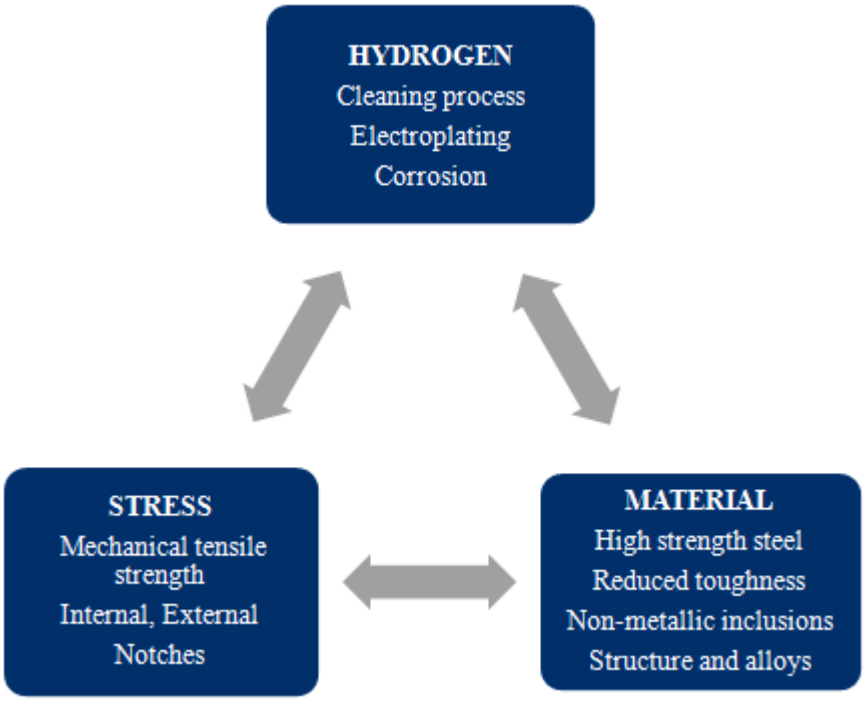

Figure 1-9: The influences of steel embrittlement [34].

1.5 Mechanisms of hydrogen embrittlement

Decohesion theory is based on embrittlement of metals depending on the varying amounts of hydrogen concentration in the region of maximum triaxiality in the lattice [35]. The accumulation of hydrogen at the regions of high triaxial decrease the cohesive strength of the lattice and causes embrittlement. The theory is concerned with the hydrogen in metal lattice positions and in voids. Less hydrogen embrittlement at low temperatures is associated with the decrease in hydrogen diffusion, whereas at high temperatures the opposite occurs. The mechanism of decohesion theory and hydrogen embrittlement is explained as the pyramid according to figure 1-10.

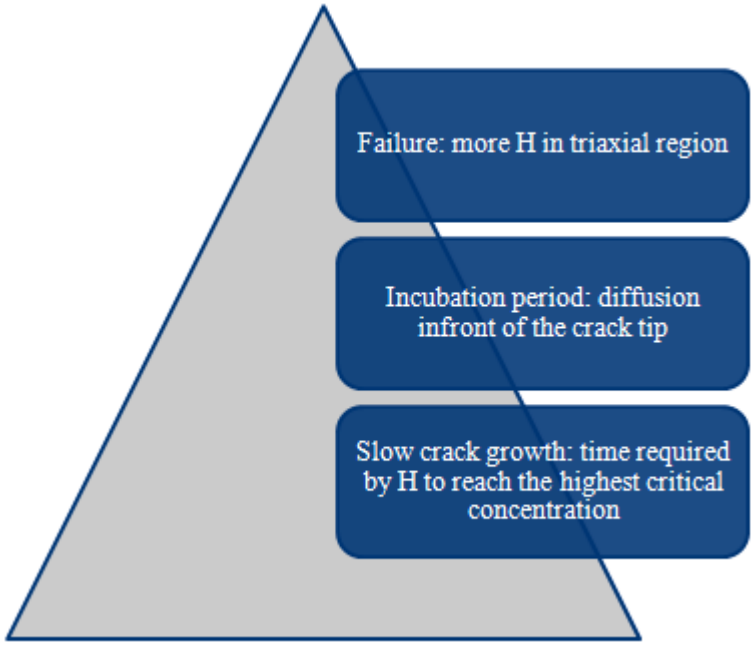

Figure 1-10: The mechanism of decohesion in the metal lattice**.**

Troiano [36, 37] speculated that the hydrogen atoms in solution of transition metals donate their electrons to the d band of the metallic core thus increasing the repulsion of metallic cores. This theory predicted that addition of copper (Cu) to nickel (Ni) would increase embrittlement initially, and then decrease it eventually as the 3d in Ni is progressively filled.

Zapffe and Sims [11] described the decohesion theory as the change of steel properties because of atomic hydrogen solubility in the tensile strength field (at the tip of the crack), in the tension field of the edge dislocations and in the areas within the internal tensile strength. The increased hydrogen solubility in the mentioned places decreases the atomic binding forces of the metal lattice. The stress influence results in a premature brittle material fracture along the grain boundaries.

1.5.1 Internal pressure theory

The hydrogen accumulates at voids until an equilibrium pressure has been reached [11].When the pressure attains the value that is close to the elastic strength of the metal, embrittlement takes place. This implies that the crack growth is facilitated by the energy released by the expanding hydrogen gas in cracks [38].

1.5.2 Adsorption theory

The hydrogen is adsorbed on the metal surface to reduce the energy required by the surface to form a crack and thus lowers the fracture stress [23]. The presence of the following chemical species e.g. amines, alcohols, alkenes, heteroaromatics etc. on the sample surface can encourage dissociation reactions which can lead to adsorption [65]. The recombination reactions which result into hydrogen desorption can be promoted by As, Se, Sb etc.

1.5.3 Substitution theory

The hydrogen enhanced localized plasticity occurs when there is an accumulation of hydrogen also in the field stresses (tips of cracks) or in the stress areas of dislocations (carriers of plastic deformation in the metal grid or elastic obstacles) [39]. By introducing the external stress, the dislocation movement within the metallic structure can be initiated. But the active hydrogen atoms within the structure shield the fields of stress of dislocations against each other and retard the dislocation movement which results in less stress available. Therefore low dislocation movement (sliding localization) of metallic particles will occur at low levels of shearing stress which is caused by hydrogen shielding mechanism. The small sliding localization leads to micro pores which create micro cracks. This localized plasticity limits the ductibility of metals such as Fe and Ni by fracture formation. Most measurements have been done with a technique of in situ TEM environmental cell deformation and fracture.

The dislocation promotion process consisted of formation of a hydrogen rich phase which is most associated with hydride, methane or steam embrittlement. The hydrogen rich phase has mechanical properties that differ from those of the matrix [40].

The dislocation restriction of hydrogen dislocation mobility occurs to provide more localised hydrogen accumulations that will embrittle the lattice [22, 41].

1.6 Influence of different factors on hydrogen embrittlement

1.6.1 Crystal Lattice defects

There are portions within the lattice grains caused by contaminants, whereby the regularity of iron atoms is lost and these areas are known as lattice defects which are listed below:

Vacancies are point like defects where the iron atom is missing at the lattice point. The vacancies contribute a lot during hydrogen diffusion and plastic deformation which occurs when dislocations move. Dislocations are linear defects caused by stress within the metallic lattice which can induce high concentrations of supersaturated hydrogen.

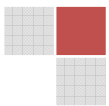

In general the impurities or foreign atoms exist in the crystal structure in two forms as shown in figure 1-13, [42].

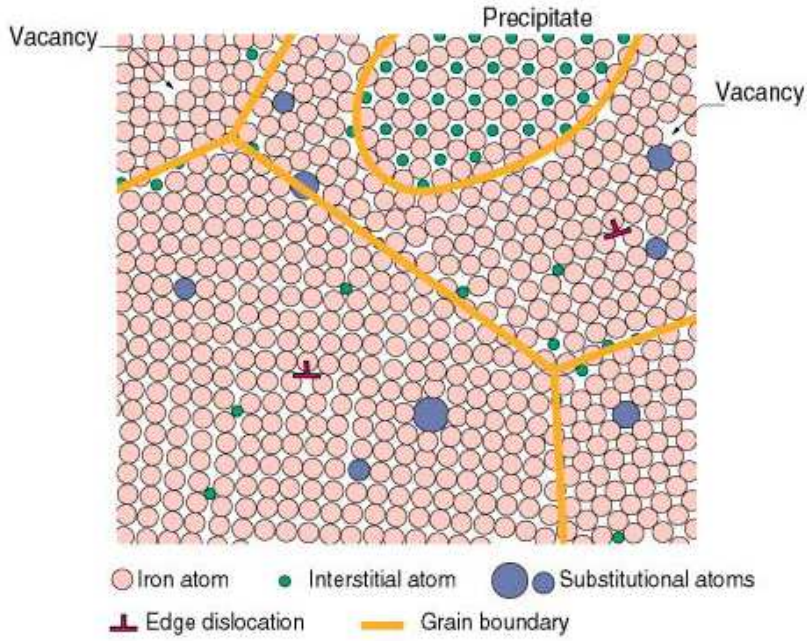

Figure 1-11: The iron crystallic structure, the influence of alloys and impurities [42].

In solid solutions the particles are divided into interstitial and substitution atoms. The atoms with the smallest radius than Fe atoms e.g. H, N, O can dwell between iron atoms at interstitial sites. During substitution, solid solutions atoms with bigger radius than Fe atoms e.g. Ti, Al or atoms with almost the same size as Fe atoms e.g. Cr, Ni or a bit smaller than Fe e.g. Si, P occupy the iron atom spaces in the lattice.

In the precipitates the contaminants create another crystal structure within the grain or at grain boundaries of the metallic structure. The polycrystalline structure will be composed of different grains with different orientations. The grain boundary has an excess energy, therefore when it becomes necessary for the atomic diffusion to occur, the area boundary decreases and the grain growth progresses. To avoid the grain influence on the crystal structure, the grains must be kept small because they improve the strength and toughness of steel.

1.6.2 Material defects

In the material defect class, the parameters like element`s distribution, density will affect interstitial, substitution or segregation atoms, while the rest of the parameters will affect inclusions and particles.

1.6.3 Microstructure defects

The steels with identical microstructure can have different hydrogen embrittlement behaviour due to the different impurities in traps.

Choo and Lee reported that the pure iron has defects like grain boundary, dislocation, and microvoids which act as trapping sites [31]. The microvoid has the biggest trap with the activation energy of 36.5 kJ/mol^{-1}.They found out that the evolution peak of hydrogen released from the grain boundary in their thermal analysis of pure iron appeared at 391K. While Lee [43] reported that in A4340 steel the evolution peak of hydrogen from ferrite carbide interface in his thermal analysis was at 388K. The evolution rate of hydrogen from ferrite carbide in the spheroidized carbide structure is higher than the pearlitic structure. This difference in structures is due to hydrogen trapping at ferrite carbide interface at low temperature.

The solubility of hydrogen in pure iron increases as the temperature decreases below 573K and the trapping tendencies starts to appear. But once the steel is alloyed, for example AISI 4340 steel, the trapping started at 673K which implied that there are new defects that formed when the steel is alloyed. The studies by Lee revealed that in AISI4340 steel, there are defects like ferrite carbide, dislocation, micro void and MnS interface which is the strongest hydrogen trapping site with activation energy of 72.3kJ/mol. That is why the hydrogen trapping temperature in pure iron (573K) moved to 673K in AISI4340 steel. Banstein and Pressouyre insisted that the interface of TiC is the strongest trapping site with activation energy of 71.4kJ/mol-88.2kJ/mol [30].

According to ferritic steel the quenched and tempered structures have fine and rounder carbides that are resistant to hydrogen with fine dislocations. But the normalized (pearlitic) structures have coarse angular structures which are susceptible to hydrogen embrittlement [44].The order of decreasing susceptibility of ferritic steel towards embrittlemment is shown below.

Untempered martensite > Normalized bainite > Normalized steel > Normalized and tempered > quenched and tempered spheroidized steels

Decreasing susceptibility to hydrogen embrittlement

Mostly in austenitic steel, martenisite plays an important role but this can lead to carbide precipitation resulting from straining and sensitization treatments [45, 46]. In stainless steel AISI 316 and AISI 434 LHC, there was high hydrogen embrittlement susceptibility because of high diffusion coefficients and low solubility values at room temperature. The austenitic sintered stainless steel was also characterised by hydrogen embrittlement susceptibility although the hydrogen diffusion was coefficients were low at room temperature.

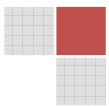

The embrittlement could have been caused by the presence of the micropores in the region around the crack.
The hydrogen diffuses very slowly in fcc lattice, but, when it finds a micropore, it is deeply trapped. This process can increase the internal hydrogen pressure and crack growth in connection with the recombination reactions that take place [47].

During the studies of 301stainless steel conducted by Perng, it was suggested that as the content of alpha martensites increases the threshold stress intensity increases at room temperature [48]. Therefore, the larger the contents of alpha martenisite distributed throughout the bulk of the specimen, the easier for the hydrogen to be highly distributed in the specimen. Then, it becomes more difficult for hydrogen to be in excess at the crack tip and this causes hydrogen embrittlement.

The work done by Hanninen and Hakariner [49] showed that the susceptibility of 304 steel types to hydrogen embrittlement resulted from cold working at 77 K. During the cold working process, martenisites are generated; dislocation density is enhanced and increases the brittleness of steel.

The high strength martenise steel is highly affected by hydrogen embrittlement because both the time required for failure and the minimum stress for failure decrease as the strength is increased. The work of Zackey et al [50] was based on cathodic charging of TRIP steels with hydrogen. Large C shaped plastic zones ahead of the tip of the fatigue crack were produced by application of stress. Since the plastic zone contained a large amount of strain induced maternisite, this effect could bring hydrogen embrittlement at the crack tip. The bcc structure is more susceptible to hydrogen embrittlement. It was also established that homogenization of treatment apparently lowers high hydrogen concentration by reducing further cracking.

1.6.4 Alloying elements

The damages that are caused by hydrogen diffusion into the steel e.g. brittle cracking, reduced ductility, and blistering can also depend on the type of alloy and the chemical composition involved. The steel has to be alloyed to achieve the product that is applicable for a specific purpose as explained below.

Carbon [51]: when 2 % carbon is added, it tends to fit into the interstial spaces in between the clusters of iron atoms. It strengthens the steel and gives it the ability to harden by heat treatment. At the same time, more carbon concentration (> 0.25 %) in steel creates a hard microstructure that is susceptible to hydrogen cracking. The carbon forms carbides with other alloying elements e.g. Iron carbide, chrome carbide etc. The coarser the carbide particles the less influence they have on the strength of steel [52].

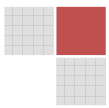

Vanadium [53]: The vanadium is added to iron to increase strength and hardness of steel. The added vanadium results in a pearlitic ferrite structure with refined spacing (fine structure). The presence of vanadium results in formation of precipitates of vanadium carbides or vanadium nitrides depending on the amounts of nitrogen present in the steel and the temperature. The presence of these precipitates, increase the strength and hardness.

But their positive influence decreases when they are precipitated at high temperatures into coarse particles. If the nitrogen content is too high during alloying, there is an increased tendency to form VN at high temperatures instead of fine vanadium carbides at lower temperatures. More VN formation brings about detrimental effects to the steel when the amount of nitrogen is more than 0.003 % in the alloying oven. [54].

Addition of carbon to vanadium ferrite facilitates a lower transformation temperature and hence finer interlamellar spacing. It forms a hard cementite and fine intermellar spacing within the structure that provides wear resistance in pipelines. This involves networks of embrittling cementite at grain boundaries. The vanadium carbides (VC) form an irreversible hydrogen trap with activation energy of 82.3kJ/mol according to the work done by analysts in reference [44]. The vanadium carbonitride (C, N) particles can be found at the interphases of ferrite precipitate colonies and also in the ferrite of the pearlite colonies.

In low vanadium and medium carbon alloyed steel, pearlitic ferrite steel is formed. Within the ferrite interphase, the precipitation of vanadium carbide occurs in the form of linear uniformly sized and shaped arrays of particles. During the formation of a pearlite, two distinctive morphologies exist as lamellar and non lamellar spheroidised types of pearlite. In the pearlitic formation from both morphologies, the VC precipitation at the interphase occurs.

In lamellar type of pearlite, VC precipitates are in the form of curved, uniformly shaped and sized particles whose direction is perpendicular to the cementite long axis. Whereas in non-lamellar, the VC particles are randomly distributed. It was found out that the VC interphase precipitation always occurred at the austenite/ferrite boundaries at all temperatures of pearlitic transformation [46].

Titanium is a highly active element that is added in steel to fix elements like carbon, oxygen, nitrogen, hydrogen and sulphur by forming stable compounds. It can absorb up to 60 % of hydrogen which can be removed by annealing in a vacuum [54]. Titanium refines ferrite grains and reduces pearlite formation. During solidification it binds with free N and form TiN which is very stable at high temperatures of approximately 1000°C. It inhibits the growth of austenite grains by having TiN and T (C, N) precipitates which are formed upon the addition of carbon and are difficult to dissolve during heating [55].

The TiN eliminates the free unwanted nitrogen because it reduces the toughness of steel. More distribution of TiN in the steel matrix reduces the grain growth so that the steel grain size is refined.

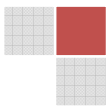

Lastly, TiN impacts toughness on the heat affected zones, for example during welding processes. But coarse TiN can have negative impacts on steel because they are sharp angled and few in number, limiting the hardening and the refinement of the structure which leads to deterioration in toughness and ductility due to embrittlement. To avoid this problem, the Ti alloying should not exceed 0.03% so that precipitation in liquid steel can be inhibited because it can cause detrimental effects. When titanium is combined with carbon it can form a pearlite structure combined with bainite. Otherwise ferrotitanium has a polygonal ferrite structure.

Silicon: is added in ferrite for enhancement of the steel strength of the pearlitic ferrite. Normally silicon addition to steel retards recrystallisation. It also inhibits austenite grain formation and accelerates the polygonal ferrite transformation [56]. It has a multiphase microstructure consisting of ferrite, bianite and retained austenite at room temperature. The cooling periods of FeSiC must be restricted by the formation of pearlite and cementite. The FeSiC forms grain boundary precipitates during cooling because the carbon exceeds its solubility in ferrite at room temperature. When the sample is quenched at temperatures that are lower or higher than 800°C, coarse precipitates remain in the grain boundaries [57]. Addition of silicon to iron changes the toughness of steel especially at low temperatures. It forms a coarse ferrite structure. The higher concentrations of silicon (2-3%), phosphorus and nitrogen in the presence of heat treatment within the range of 450-520°C whereby there is a slow cooling process, brittle fractures of steel can occur. This is due to the presence of horophyllic elements at grain boundaries [58].

Upon the addition of silicon during steel alloying, the growth of ferrite crystals occurs during recrystallisation. The structure showed heterogeneity due to the complex and irregular deformations. These structural heterogeneities make it possible to obtain large variety of transition structures that facilitate the analysis of the redistribution of dislocations during hot plastic deformation. The enlargement of polygons and growth of the sub grains result mainly from annihilation of the low angle dislocation boundaries [59]. In a ferrosilicon steel there is low saturation of hydrogen due to the fact that the dislocations are not mobile (static) [60].

Vanadium, titanium, manganese, zirconium and tantalum increase hydrogen solubility, particularly at low and moderate temperatures [61]. These metals are highly capable of trapping hydrogen but it all depends on their distribution in the lattice of the steel [62]. The nickel increases hydrogen solubility, when the solubility is proportional to nickel content. Molybdenum has no effect on solubility, while tungsten decreases it. Silicon decreases the hydrogen solubility, as well as aluminium. Chromium contents up to 10% increase hydrogen solubility, but higher concentrations decrease it. The effect is explained in terms of crystal structure. In table 1-1 there is a list of alloying elements which includes the way they distribute themselves within the metallic structure during alloying.

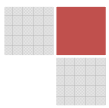

Table 1-1: The distribution trends of alloying elements in steel [62].

Element	Dissolved in ferrite	Combined in Carbide	In special nonmetallic inclusions	In special intermetallic compounds	In elemental state
Nickel	Ni				
Silicon	Si		$SiO_2.M_xO_y$	NiSi, Ni_3Al	
Aluminium	Al		Al_2O_3	Al_xN_y	
Zirconium	Zr		ZrO_2	Zr_xN_y	
Manganese	Mn	Mn	$MnS, MnO.SiO_2$		
Chromium	Cr	Cr	Cr_xO_y		
Tungstein	W	W			
Molybodenum	Mo	Mo			
Vanadium	V	V	V_xO_y	V_xN_y	
Titanium	Ti	Ti	Ti_xO_y	$Ti_xN_yC_z$, Ti_xN_y	
Columbium	Cb	Cb			
Phosphorus	P				
Sulfur	S		(MnFe)S, ZrS		
Copper	Cu				Cu≥ 0.8%
Lead	Pb				

1.7 Investigation of hydrogen role in embrittlement

1.7.1 Supporting views regarding embrittlement

In order for the hydrogen embrittlement to occur by decohesion, internal pressure, substitution, dislocation etc., regardless of the mechanism, the defects are present and also the amount of hydrogen concentration absorbed at these sites exceeds the hydrogen critical value of that particular material [11, 36-39]. Then, the hydrogen embrittlement mechanisms affect the properties and behaviour of steel. The mechanisms depend principally on hydrogen concentration (or effective hydrogen pressure) and the strength level of steel. The best solution explained by most of the authors was to increase the critical concentration in order to decrease the concentration of absorbed hydrogen.

1.7.2 Opposition in relation to dissolved hydrogen and dislocations

Beachem [39] pointed out that the importance of hydrogen action is to diffuse into the lattice ahead of the crack tip and becomes an aid to the plastic deformation processes that are taking place in the system.

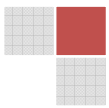

But, this is quite opposite because the interpretation seems to be that the large hydrogen gas pressures generated at microcracks and voids force their expansion by increasing the plastic deformation whereby the process leads to embrittlement (9, 11, 63-64).

Petch and Stables [23] suggested that the surface free energy of a clean metal surface is lowered by adsorption of hydrogen which can lead to embrittlement. But Oriani and Josephic [65] did not verify that suggestion, because the adsorption of H required for creating a new surface was not linked to the mechanism for crack formation on the surface. They mentioned that the suggestion is true for thermodynamic reasoning.

Bastien and Anzou [22] suggested that the dissolved hydrogen can be carried along by moving dislocations and precipitated elsewhere. But the mechanism does not contribute towards the embrittlement mechanism.

1.7.3 Improvements on reduction of hydrogen embrittlement in metallic materials

In spite of any mechanism acting on hydrogen in any defect, a crack will be initiated by high critical hydrogen concentration and the concentration of the trapped hydrogen. The industries have developed methods to reduce activities of hydrogen on steel in order to hinder embrittlement.

Directly formed barriers (coating) [16]: the barriers deposited on metallic surface lower the hydrogen diffusion and they also have low solubility for hydrogen. The application of steel at high temperatures and pressures require less permeability to withstand hydrogen e.g. Cu, M, Al, Ag and W coating. Also heating the metal to form oxide layer creates an impermeable surface.

External hydrogen activity [65]: in either gaseous or liquid environment, the hydrogen is reduced by the presence of an inhibitor which reduces the activity of hydrogen with steel by preventing the formation of H^+ ions e.g. alcohols, amines, alkenes, heteroaromatics and polymerized aromatics compounds.

Trap additions [16]: traps must be applied as an advantage to avoid hydrogen embrittlement. The characteristics of traps have been already discussed in chapter 1.3.4. If there is an existing hydrogen source with high activity around the metal, the trap may slowly saturate hydrogen because they decrease the diffusion process but the hydrogen will accumulate somewhere else within the metallic structure.

Figure1-14 summarises the hydrogen effects and solutions applied on reducing the concentration of absorbed hydrogen.

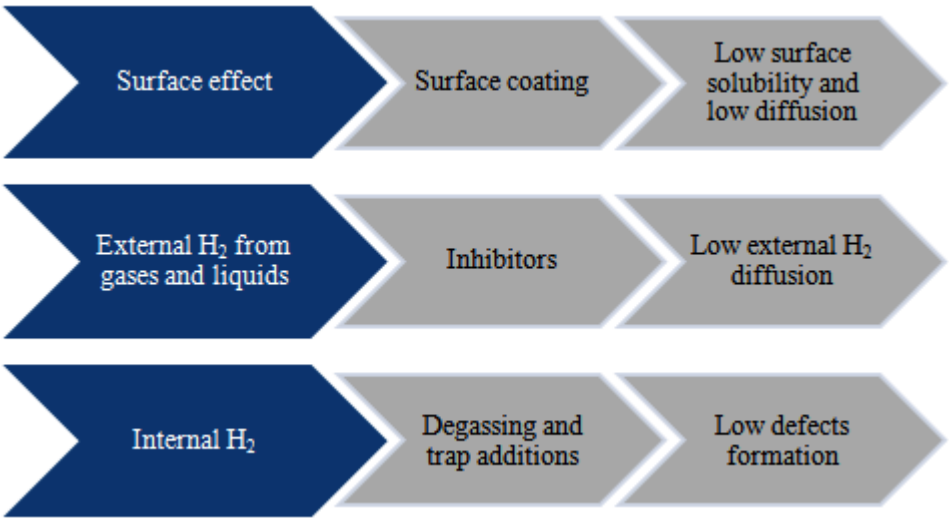

Figure 1-12: The effects and solutions applied to decrease absorbed hydrogen in steel**.**

2. HYDROGEN DETERMINATION METHODS

At the beginning of the last century, in the thirties, it was already observed by the emerging metallurgical research that internal cracks, which appear in the steel during hot-rolling and forging, were caused by the diffusion of atomic hydrogen through the lattice and the recombination into molecular hydrogen inside the material.

Furthermore, the formation of blisters and micro-cracks in the steel during cooling was also observed. The slow cooling of large steel profiles was then applied as a solution for this problem. However, with the increasing demand for better materials, analytical methods for the determination of hydrogen started to be developed in the seventies.

The first onsite analysis was the “probe sampling”-method, which consists in the measurement of the hydrogen released from the solidification of a sample from the molten steel. This method was improved with better sampling methods and modified into more accurate versions such as the ESP-method [66].

Further efforts to develop a direct online determination of hydrogen in the ladle furnace and the manifold led to the Hydris system, which is able to measure hydrogen semi-continuously directly from the molten steel [67].

However, the presence and the influence of hydrogen in steel are not limited to the production steps. The development of high performance steel demands a detailed characterization of physical-chemical properties from the material. In view of this, efforts are being made to improve the analytical methods for the determination of hydrogen in steel.

Several equipments are currently being used in laboratories for the analysis of hydrogen by solid and melt extraction. Thermal conductivity and infrared detection are the most usual for the determination of bulk and diffusible hydrogen. The use of GDOS (Glow Discharge Optical Emission Spectrometry) and SIMS (Secondary Ion Mass Spectrometry) to determine the distribution of hydrogen in the sample is also being studied.

2.1 Vacuum techniques

Vacuum fusion (melt extraction) and vacuum hot extraction are used to determine hydrogen in steel materials by heating the sample and measurement of the hydrogen gases evolved by mass spectrometer [68]. Since many gases are released from heating the steel, hydrogen was determined by measuring the pressure difference after diffusion of the hydrogen through a palladium-silver tube into a calibrated volume. Therefore, the hydrogen can be determined by measuring the difference between the pressure of the total gas evolved and that of the gas remaining after oxidation of hydrogen to water.

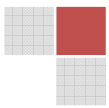

Both methods do not require the use of reference materials. Vacuum hot extraction was considered to be more precise than vacuum fusion after investigation by ASTM committee [69]. The same techniques can be used for detection of hydrogen by using thermal conductive detector.

Berkowitz [70] developed a technique which uses the calibrated pumping speed of a vacuum system and a mass spectrometer to provide a dynamic analysis of gases evolved from the samples. He analysed an Armco iron sample which released hydrogen within 20 seconds.

According to Martin [71] the hydrogen concentration measured by palladium membrane technique in HY80 steel sample was in agreement with the mass spectrometric method with reproducible results within $0.1 \mu g \cdot g^{-1}$. But thermal conductivity yield poorer values with a difference of $1 \mu g \cdot g^{-1}$.

Although the vacuum techniques are well recognised in research but they are the quite expensive, slow for routine analysis and occupy large space. Hence more rapid, fast and compact equipment like carrier gas systems are more attractive to the industries.

2.2 Carrier Gas Techniques

The carrier gas techniques can be adapted to both fusion (melt) and hot extraction methods [72]. The nitrogen or argon gas carries the analyte (hydrogen) after heating the sample inductively to the thermal conductive detector. During the use of induction furnace to extract hydrogen, nitrogen is mostly preferred because argon couples with the induction field and forms a discharge [73]. In carrier gas-hot extraction technique the kinetics of hydrogen evolution as a function of temperature can be followed.

The carrier gas techniques for melt (fusion) extraction have been developed to electrode furnaces which use a graphite crucible for holding the sample while it is melted at high temperatures. The resistance furnace for hot extraction method was also discovered for hydrogen analysis in samples that are equal to or more than 2g.

But there are challenges that face carrier gas systems with electrode furnaces that use N_2 in the presence of graphite crucibles [74]. For an example the use of nitrogen as the analyte carrier gas at temperatures that are approximately 3000°C causes the reaction of nitrogen with hydrogen from the sample to form ammonia (NH_4). The carbon from the graphite crucible can also react with hydrogen and nitrogen to form hydrogen cyanide (HCN). But the melting temperatures of approximately 2000°C cannot promote the reaction of nitrogen with the hydrogen hence they were applied to this recent work.

When Ar is used as a carrier gas at 2000°C in an electrode furnace, also the reaction of hydrogen and carbon from the graphite crucible occurs.

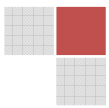

To counteract the graphite crucible problems, the measurements were done by fluxing the material with pure tin to lower the melting point and prevent the corrosion of the crucible by the metallic material.

But this action contributed towards the re-adsorption of the hydrogen released from the sample by the flux (getter effect) hence low analyte concentrations can be expected after the analysis.

But for more precise information regarding the susceptibility of steel materials towards hydrogen embrittlement, attention must be given to the following parameters: activation energies of hydrogen interaction with traps in various alloys desorption rates at different temperatures that are responsible for dehydrogenation [10, 31]. During this measurement, there was less matrix influence on the signal from the sample contents, carrier gas and the reagents of the measuring system In the present work the above mentioned hydrogen characterisation was achieved by coupling MS to the hot extraction analyser which is described in more details in chapter 5.1.4. Compared to the already existing thermal desorption mass spectrometry (vacuum technique), the newly developed one is simpler and useful for routine analysis.

Graphite crucible challenges in carrier gas System: the work done by Degrève and Jardin [75] on aluminium alloys applied vacuum hot extraction and nitrogen carrier gas fusion (melting) method. The fusion extraction technique involved heating the sample to 1000°C for 15min in a graphite crucible placed in a quartz tube furnace by induction in the presence of nitrogen carrier gas and hydrogen detection was done with thermal conductive detector. The vacuum hot extraction was performed by heating the sample up to 400°C for 25min and the hydrogen determination was done with mass spectrometer. The total/bulk hydrogen concentration measured by carrier gas fusion (melt) extraction was similar to diffusible hydrogen determined by vacuum hot extraction method. Hydrogen concentration extracted from melted and solid sample is governed by diffusion phenomenon. Therefore higher total hydrogen concentrations can be expected to be released after melting the sample while lower diffusible hydrogen can be recovered from the solid sample.

The low total hydrogen recoveries in carrier gas fusion (melt) extraction method could be due to the reaction of carbon released from graphite crucible, hydrogen from the sample at elevated temperatures [73,76,77]. The advantage of induction furnace (quartz tube) is that it permits analysis of larger samples e.g. 2g, 5g, 7g etc.

But application of carrier gas in fusion extraction techniques, require quartz crucibles to lower the possibilities of hydrogen retrapping reactions in the oven or crucibles before it reaches the detector.

Therefore the carrier gas fusion extraction was improved by melting the sample while floating (levitation) in between the metallic coil [77]. The sample was melted by magnetic pressure generated by high frequency magnetic field to the specimen placed inside the induction coil.

Although this technique is similar to carrier gas fusion extraction, the use of the graphite crucible for carrying sample was totally eliminated. But there is a high possibility of the induction coil erosion by the melt and this can influence the results on hydrogen concentration. Therefore, after melting the sample the coil must be properly cleaned and this process can be inconvenient for routine analysis because the cleaning step can take a long time before the next sample measurement. Another way of maintaining the stability of the measurement is to remove the coil which is more costly. The main drawback of this method is that it can only be applicable to conductive metallic materials implying that the temperature control can be critical.

This implied that melting the sample without using a sample holder is ideally required for more accurate analysis. But practically it is still having more disadvantages due to getter effects. In the recent work the small, pyrocoated graphite crucible was used for holding the sample by putting it inside a bigger crucible that is directly placed between the upper and the lower electrode in order to conduct electricity for melting the sample. Then the heat is uniformly distributed from the outer crucible to the inner hence corrosion of the outer crucible by the sample is impossible. Also the precision of the measurement is improved due to the optimal sample heating conditions in an inner crucible.

Challenges in carrier gas systems: the melt extraction method was found to yield lower hydrogen contents than the nuclear resonance analysis in stainless steel according to the work done by Westernberg, Wallen, Hjörvarssorn and Mathewson [78]. The difference in results was explained by the fact that the hydrogen was not fully extracted due to strong trapping, diffusion barriers or the hydrogen content in the sample bulk was not the same as at the near surface region (0.7µm). They stated that the hydrogen concentration which resulted from extraction methods resembled the transportation properties of hydrogen from the sample bulk to the vacuum phase and not the total hydrogen concentration in the sample. This is contradiction because after high heating energy was applied more hydrogen was supposed to be released from traps because higher temperatures enhance hydrogen diffusion.

It is very important to have a good variation of sample temperature versus time and to measure the maximum temperature to be reached so that the kinetics of dehydrogenation is quick enough to respond [75]. The reduction in hydrogen recoveries during extraction could be also due to sample preparation method which included high cleaning temperatures (121°C), long cleaning time (10min) and hot sample drying conditions (80°C in an oven), whereby the hydrogen could have been dehydrogenated. Due to such insecurities, in the recent work, sample cleaning methods were compared by measuring the H_2 concentrations with IR and TCD to observe any influence from the systems of measuring techniques.

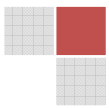

2.3 Autoradiography

Sastri [76] applied tritium transmission electron microscopic autoradiography for observing trap sites of hydrogen in solution treated austenitic stainless steel (type 316 L).They discovered that hydrogen was trapped by defects or precipitates at grain boundaries and by triple points where the three boundaries intersect. But this autoradiographical method could not determine the hydrogen concentration in the respective trap sites.

2.4 Electrodes for hydrogen analysis

The hydrogen analyses include the use of electrodes, whereby the hydrogen ionized form can be detected by the current produced by the movement of ions. Berman and Argawala [79] made use of Ni/Ni oxide polarizing electrode that was coupled to the steel surface and measured the current as hydrogen diffused out of the sample. The method was able to detect down to $1 \mu g \cdot g^{-1}$ concentrations of diffusible hydrogen. But this electrode had to be fixed on a smooth surface otherwise any curves e.g. the rough, concave or convex surface brought errors to the analysis.

Macher de Krenk and Schoonman also discussed an electrochemical sensor responsible for determination of the activities of mobile elemental hydrogen [80]. The principle of the electrode was based on the concentration cell that recorded the response of the detector to the hydrogen in potential units (volts) which were difficult to be translated to the usual concentration units hence suitable calibration techniques like IR, TCD and MS are required.

2.5 Nuclear techniques

Nuclear techniques such as small angle neutron scattering (SANS) and quasielastic neutron scattering (QENS) are also useful in studying hydrogen in solid metallic materials [82]. These techniques are valuable for determining hydrogen diffusion constants, trapping and binding phenomena but they are unable to quantify the hydrogen concentration.

On the other hand, iron filtered neutron beam technique is applicable in the analysis of hydrogen concentration in large steel samples of 1-2 cm in size and film coatings of 200 µm in size [83]. The detection limit is $2 \mu g \cdot g^{-1}$. While the notched neutrons beam technique can detect up to 0.2 $\mu g \cdot g^{-1}$ of hydrogen in similar samples. But it can only measure hydrogen in a sample whose elements are composed of mass numbers that are greater than or equal to 12 amu.

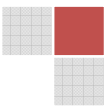

Although both neutron methods are non-destructive to the solid samples the experimental protocol required the placement of sample in neutrons field for 6-24 hours during the measurement which makes the neutron methods less rapid.

2.6 Potentiostatic techniques

Potentiostatic techniques for measuring samples in disk shaped samples were discussed by Pressouyre and Faure [81]. Although the technique was limited to samples of a particular size and thickness, the hydrogen concentration of 1 $\mu g \cdot g^{-1}$ was measured based on current density.

2.7 On site hydrogen analysis

The onsite hydrogen determination methods have been developed in the recent years to facilitate more understanding on hydrogen pick-up in molten steel [67]. This method offers the accuracy in identifying hydrogen levels on production line. The measurements experience help to manage hydrogen sources during production which lead to steel defects like embrittlement. Also it is easier to process hydrogen critical steel grades.

2.8 Hydrogen profiling in steel

The refinement of steel sheets with metallic and organic coat is quickly progressing. The importance of steel surface as the base material and as the uncoated steel is increasing. The surface properties that influence the coating and also the properties of the final steel product such as paint ability and corrosion behavior are crucial. Thus, the chemical composition is important for the surface properties. Therefore, techniques for profiling contaminants like hydrogen are highly on demand hence the following equipment is used.

2.8.1 Glow discharge optical spectroscopy

The GDOS is a powerful tool in quantitative depth profiling, surface and interface analysis [34]. It is applied in the optimization of the development and manufacturing processes. It is a widely applied technique in steel and car manufacturing industry especially in characterisation of coating material. It is a powerful and inexpensive tool in the surface analysis. The hydrogen added during the coating of steel materials can be stored at an interface between the coating and steel. Some of the hydrogen can also diffuse into the material and this can lead to the embrittlement, which is why depth profiling of coated samples is also very important to evaluate the effects of the hydrogen added during coating processes.

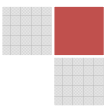

2.8.2 Time of Flight Secondary Ion Mass Spectrometry

Time of flight secondary ion mass spectrometry is a well established method for surface spectroscopy, depth profiling, and surface imaging for three dimensional analyses [84, 85]. It provides detailed information about a mass spectrum that surveys all atomic masses over a range of 0-10,000 amu, the rastered beam produces maps of any mass of interest on a sub-micron scale, and depth profiles are produced by removal of surface layers by sputtering under the ion beam. It has a high surface sensitivity (< 1 nm) and the high depth resolution (< 1 nm). This method characterizes semiconductors, polymers, paint, coatings, glass, paper, metals, ceramics, biomaterials, pharmaceuticals and organic tissue. Unlike X-ray photoelectron spectroscopy (XPS) and Atomic emission spectroscopy (AES) which combine several atomic layers during analysis, the TOFSIMS analyses each atomic layer individually.

3. STEEL SAMPLING FOR HYDROGEN ANALYSIS

To proceed with laboratory hydrogen analysis the samples to be analyzed must be properly sampled for accurate analysis. Sampling techniques are crucial because it is common to find some significant heterogeneous matter on steel during solidification which has not been removed during processing [66]. For an example, the convective currents that form during casting and cooling processes produce a refining action that carries impurities like oxides to the core of the material. The heat treatments produce depletions and enrichments of elements on the outer surface and near the outer surface of the material shape. Therefore, the main purpose for proper sampling of steel is to have an accurate analysis of the analytes e.g. hydrogen, oxygen and nitrogen in the original sample. An accurate sampling method is valuable for quality control of steel products. The sampling can take place from solid finished steel sheet, blocks or in the molten steel bath.

3.1 Sampling solid steel material

When sampling the solid steel sample it is highly advisable to take the middle section due to the information in chapter 3. The longitudinally rolled sheets must be sampled by cutting out a section across the entire width of the sheet perpendicular to the rolling direction. The transversely rolled sheets should be sampled by cutting out a section midway between the middle and the end. The billets are cut into full cross sectional slices; blooms, slabs are drilled on their end face about one half distances from the centre to the edge in the direction parallel to the main axis.

For hydrogen determinations it is highly required that less heat should be applied during sampling since hydrogen is highly mobile in low and medium alloyed steel. The samples should be kept in liquid nitrogen (-176°C) or in solid carbon dioxide (-78°C) to preserve their contents.

3.2 Sampling molten steel

Open quenched Sampling: a pin is quenched to freeze the hydrogen inside [67].

Copper mould quenching: the sample is sampled into copper mould by a spoon. The copper provides a chilling atmosphere to the sample. Then, the sample is quickly removed from the mould and cooled in water. The removal of the sample from the mould is critical and requires two skilful workers [67].

Pin sample:

ferrostatic filling: the silica tube is immersed in the molten steel so that it can be filled with the sample by ferrostatic pressure. The silica tube is initially cooled in water which can lead to formation of cracks. Therefore, the sample cooling step is critical.

The cracks provide a free surface for hydrogen diffusion out of the sample and that results in low hydrogen recoveries during the analysis in the laboratory [67].

Vacuum Filling: the quartz tube (pin) sample is also immersed in molten steel and the sample is driven into the tube by pressure. When the tube is opened prematurely then poor hydrogen measurement will result [67].

Comparison of molten sampling technique: the hydrogen content in ferrostatic filled samples was compared to vacuum filled samples by thermal conductive detection. According to figure 3-1, the ferrostatic filled samples had higher hydrogen concentrations. The comparison between the copper mould and ferrostatic filled samples resulted in scattered data [66, 67].

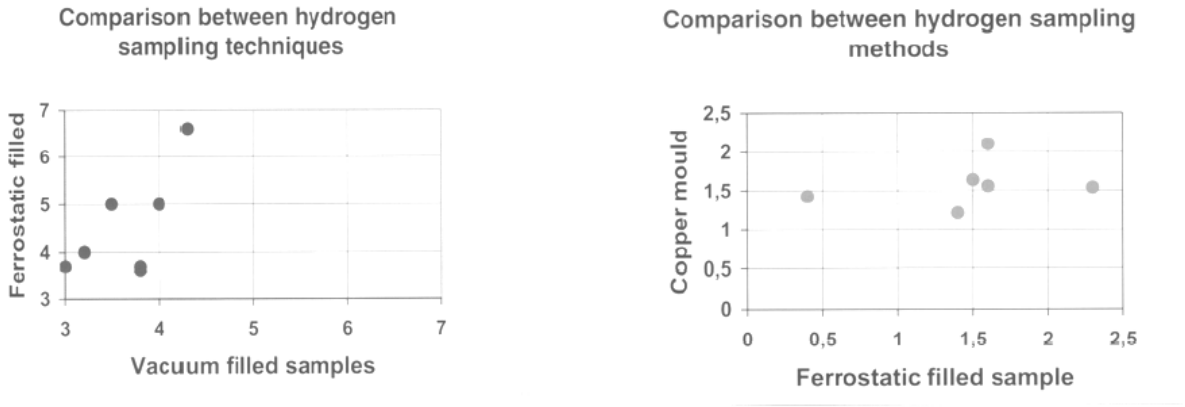

Figure 3-1: (a) Ferro static versus vacuum sampling **(b)** Copper mould versus ferro static sampling [67].

4. AIM OF THE WORK

The aim of this work is to optimize the already existing carrier gas fusion (melt) extraction methods for quantification of total/bulk hydrogen and development of a rapid routine technique for characterization of diffusible hydrogen by carrier gas hot extraction technique. For instance the carrier gas fusion (melt) techniques that applied TCD and IR for hydrogen detection can only determine the bulk/total of steel sample. Hence in the present work they will be complemented by carrier gas hot extraction coupled to the mass spectrometer to characterise hydrogen desorption rates at specific temperatures, activation energies of traps and the diffusible concentration evolved in each peak area. Calibration in carrier gas methods can be very critically, therefore, gas calibration will be applied to ensure the stability of the measurements.

The first step is to compare the total hydrogen concentration measured in molten steel onsite with the concentration measured in melted sample in laboratory. In both conditions the analyte is detected by thermal conductivity. This gives an idea about the interaction of the particular material with hydrogen onsite and the quality of the metallic material after it has been sampled.

This work will contain experiments that will thoroughly explain coated and uncoated sample handling before hydrogen analysis in order to yield reliable results. The influential parameters on bulk and diffusible hydrogen concentration during sample preparation will involve sample storage, hydrogen absorption conditions, desorption conditions of total and diffusible hydrogen concentrations will be studied to identify the interaction characteristics of the material with hydrogen.

The contribution of the micro structures from differently alloyed steel to hydrogen concentration in steel shall be also evaluated by measuring the hydrogen desorption rates, temperature and activation energies from traps of alloyed steel. The activation energies for hydrogen desorption will be associated with the morphology studies to identify the lattice sites e.g. compounds that interact with hydrogen to form reversible or irreversible traps within the sample.

The whole work will clarify the possibility of the emergence embrittlement by quantifying the steel threatening diffusible hydrogen concentration compared to bulk hydrogen. Figure 4-1 gives an overview about the steps of hydrogen analysis.

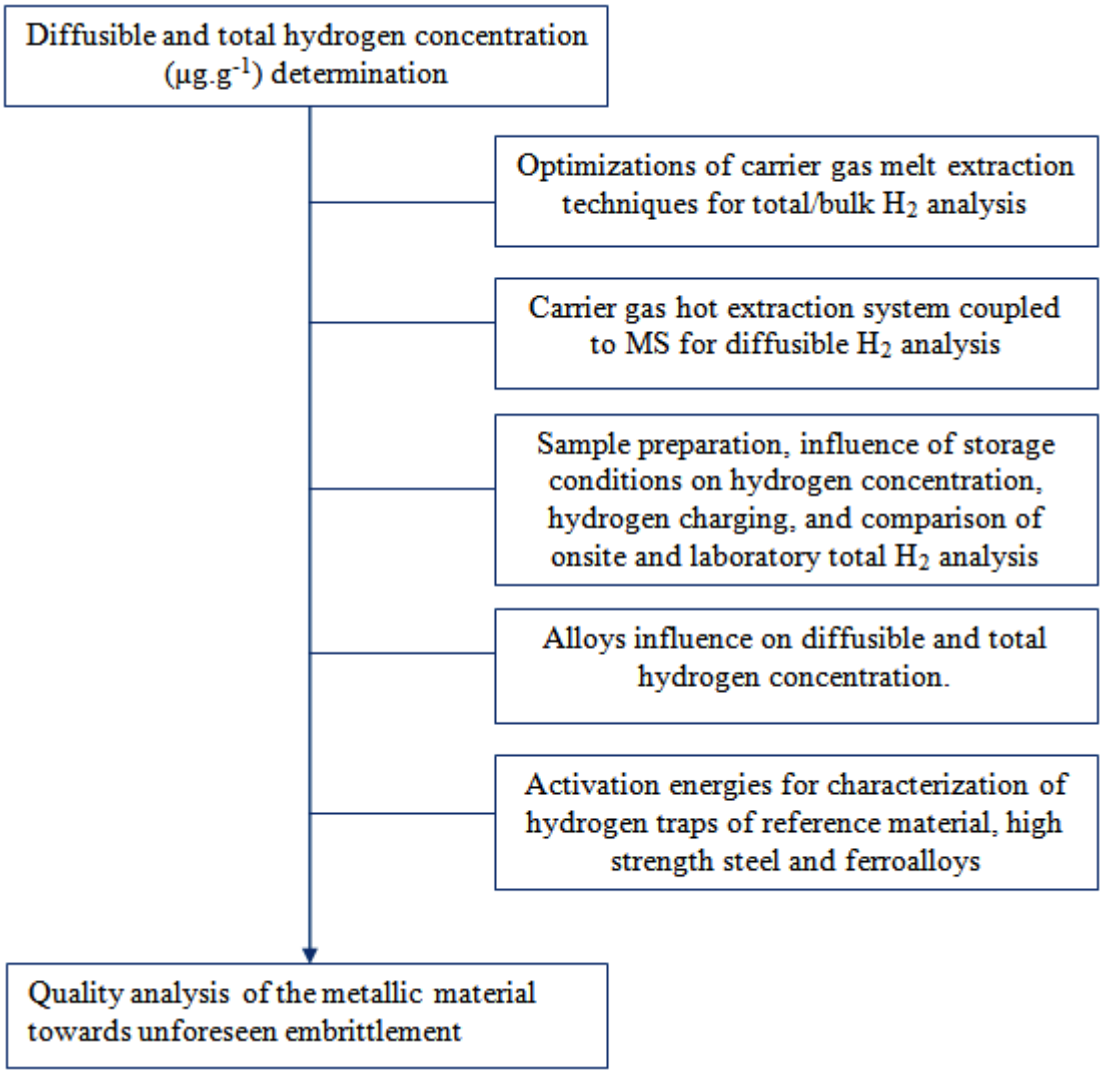

Figure 4-1: Total and diffusible hydrogen analysis in laboratory.

5. EXPERIMENTAL PART

5.1 Application of hydrogen analysis techniques

This part of the work contains the techniques that were involved during the analysis of total and diffusible hydrogen in the laboratory. The total hydrogen analysis equipment at the steel production site is shortly explained because it was used for measurement comparing purposes.

The purity of the material depends on the concentration of interfering compounds like hydrogen gas. In the steel and metal marketing industry the demand on hydrogen analysis has increased because the new products are being established and the customers have to be assured about the quality.

5.1.1 Total / bulk hydrogen analysis by thermal conductivity detection.

The Eltra 2000 OHN instrument [87] measures the thermal conductivity of hydrogen at $\mu g \cdot g^{-1}$ level. The measuring principle is shown in figure 5-1. It can alternatively operate as a simultaneous O_2 / N_2 or as O_2 / H_2 analyzer. Here the second alternative is described. The sample in the electrically heated graphite crucible is completely melted at approximately 2200 °C. Before the nitrogen carrier gas enters the furnace, it is cleaned with sodium hydroxide to remove carbon dioxide and with magnesium perchloride to remove any moisture within the gas.

The dust particles are removed by cotton wool. The carbon from the graphite crucible reacts with oxygen and produces carbon monoxide. The carbon monoxide is oxidised to carbon dioxide in the presence of a catalyst (Schütze reagent: Iodinepentoxide (I_2O_5) on silica).

The oxygen is measured as CO_2 by infrared detection. Afterwards CO_2 is absorbed by sodium hydroxide so that it would not be transported to the thermal conductivity detector. The moisture formed during the gas transportation is removed by an anhydrone (magnesium perchlorate). The hydrogen then is carried by pure nitrogen gas to the thermal conductive detector.

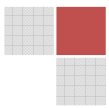

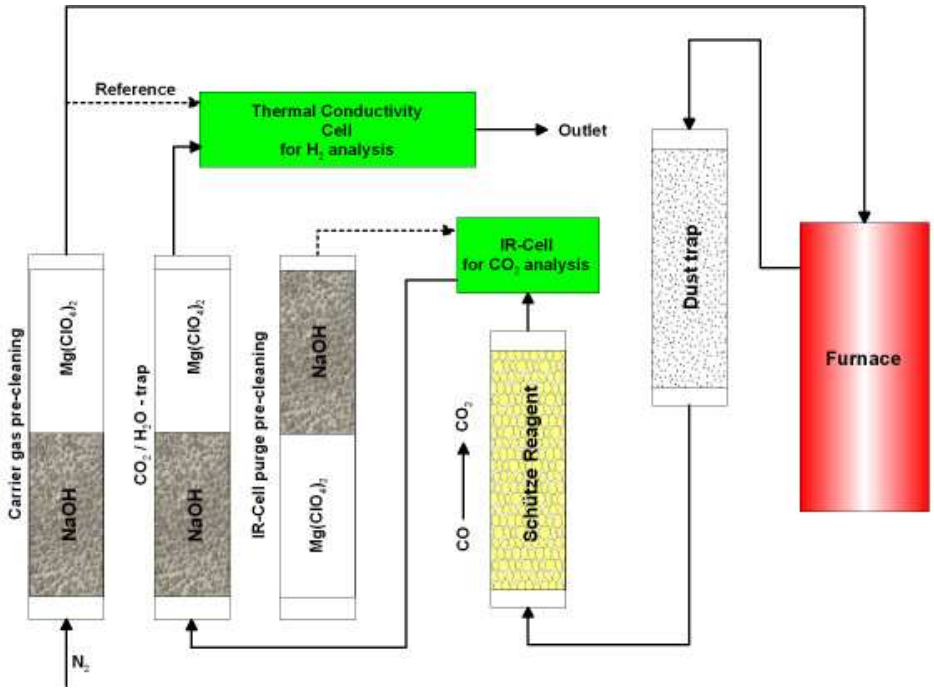

Figure 5-1: Experimental set up of Eltra OHN 2000 - determination of hydrogen by melt extraction and thermal conductivity detection.

Thermal Conductive Detector Principle: (figure 5-2): The difference in thermal conductivity between the carrier gas and the analyte (hydrogen) which is called the effluent flow and the carrier gas known as the reference gas is determined. The gases are switched over a filament at a rate of 5 times per second by using a solenoid valve. It produces a voltage that is proportional to the thermal conductivity difference. This voltage is released as an output signal. The optimum parameters should be the ratio of the effluent gas flow, reference gas flow, the resistance of the filament and the temperature of the detector. The reference flow should be 3 times the effluent flow. The temperature should be low as possible. The filament should have 11-to 13 ohms when it is warm. Because of the difference in thermal conductivity of hydrogen and nitrogen, the hydrogen passes through the column first while nitrogen passes 45 seconds later and cannot be measured.

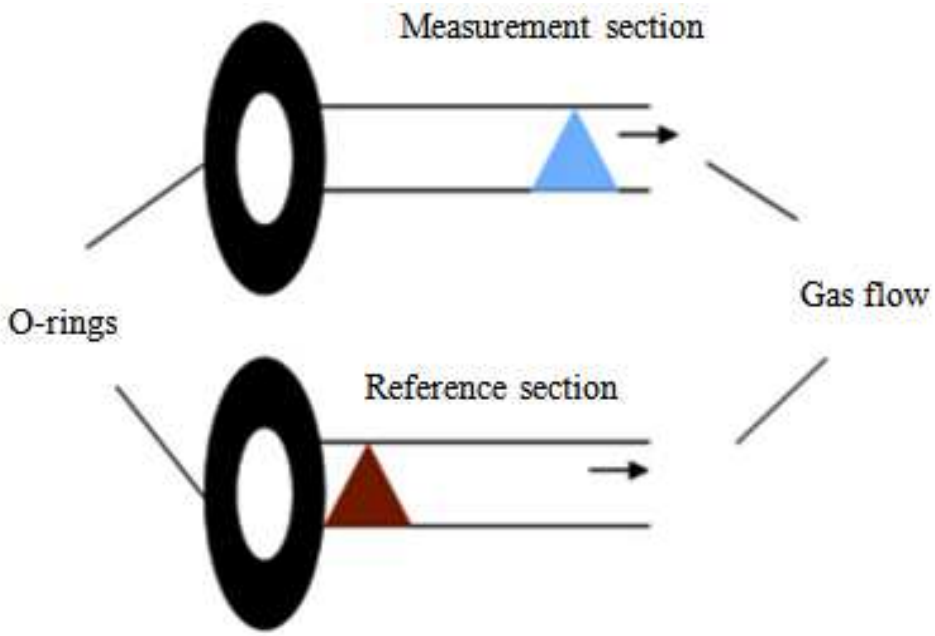

Figure 5-2: Sketch of thermal conductivity detection cell.

5.1.2 Total / bulk hydrogen analysis by infrared detection.

The Leco TCH600 [88] uses the similar melting principle but the released hydrogen is converted to H_2O and is analyzed by infrared detection as shown in figure 5-3. After melting the sample at approximately 2200 °C, the gases like hydrogen, oxygen and nitrogen are released and carried by helium to CO and CO_2 sensitive IR cells. Then the copper oxide wire converts carbon monoxide (from oxygen and carbon in the graphite crucible) to carbon dioxide and hydrogen to H_2O. The gases pass through the next IR detectors for total hydrogen determination as H_2O. The oxygen result is measured by a combination of the two carbon dioxide and carbon monoxide sensitive IR cells. Afterwards the carbon dioxide is absorbed by sodium hydroxide and H_2O by magnesium-perchlorate to prevent their detection by the following TC detector. The helium is added at the dynamic cell to maintain a constant gas flow after removal of CO_2 and H_2O. Nitrogen is carried by helium further to the thermal conductivity detector.

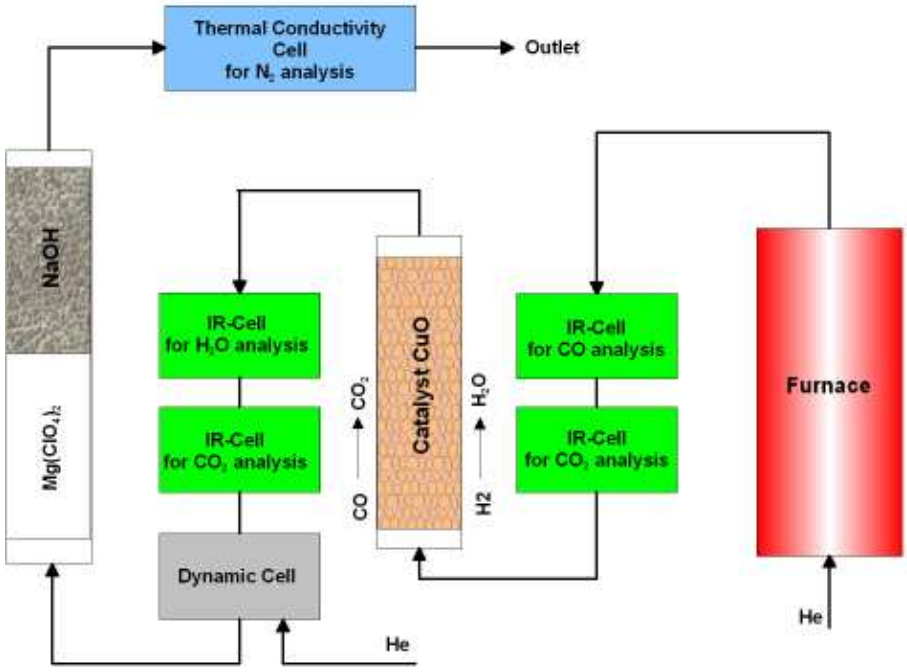

Figure 5-3: Experimental set up of Leco TCH 600 - determination of hydrogen by melt extraction and infrared detection.

Infrared Detector Principle: As the volume of gas passes through the infrared radiation, the analyte absorbs radiation at specific wavelengths. There are two infrared light sources with two wavelengths and one infrared detector (figure 5-4). The intensity within the absorption wavelength and outside the absorption wavelength is measured by the infrared light detector. If the gas e.g. H_2O intervenes by radiation absorption between the infrared light source and the infrared detector, then the amount of radiation falling on the detector is reduced. The concentration of the analyte is obtained by comparing the relative values between the two wavelengths.

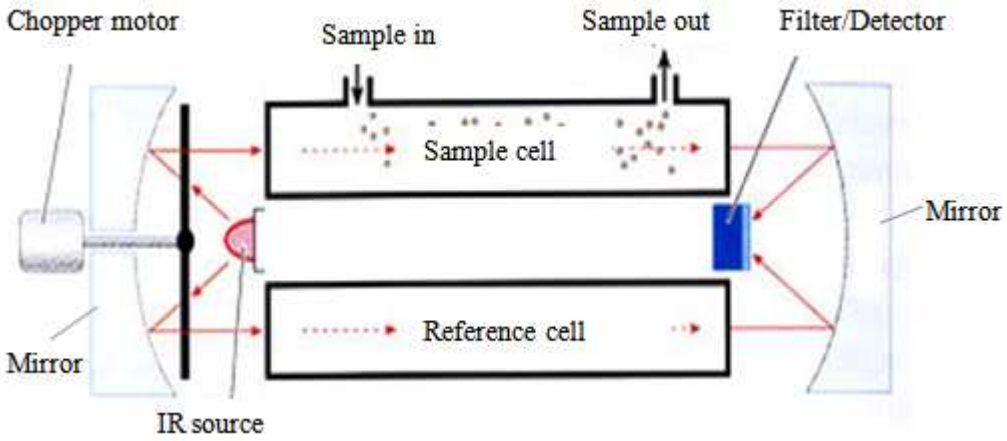

Figure 5-4: Schematic diagram of a dual infrared detector [89].

5.1.3 Total hydrogen analysis by TCD at the production site

The Hydris is a system and process for the rapid, accurate, economical analysis of soluble gases in molten metal melts whereby an inert carrier gas (99.99% N_2) is bubbled through the molten metal at a controlled rate to pick up hydrogen in steel [67]. When the equilibrium is reached between the hydrogen dissolved in the melt and the hydrogen in the carrier gas, the process is stopped. Then the detector measures the final value reported in ppm (mg/kg).

This technique measures hydrogen concentration in carrier gas by applying *Sievert's* law which states that the concentration of hydrogen is equal to the square root of the of the partial pressure in the melt. The equation is as follows [67]:

$$[H] = \frac{K}{f}\sqrt{P}\ (H_2) \qquad (6)$$

[H]: Hydrogen content in the steel melt (mg/kg)

K: -1900/T + 1.9 (T in K)

F: Hydrogen interaction coefficient

P [H_2]: Hydrogen partial pressure in the melt (hPa)

The measured gas is continually exhausted and immediately disposed into the atmosphere. The principle of the Hydris is illustrated in figure 5-5.

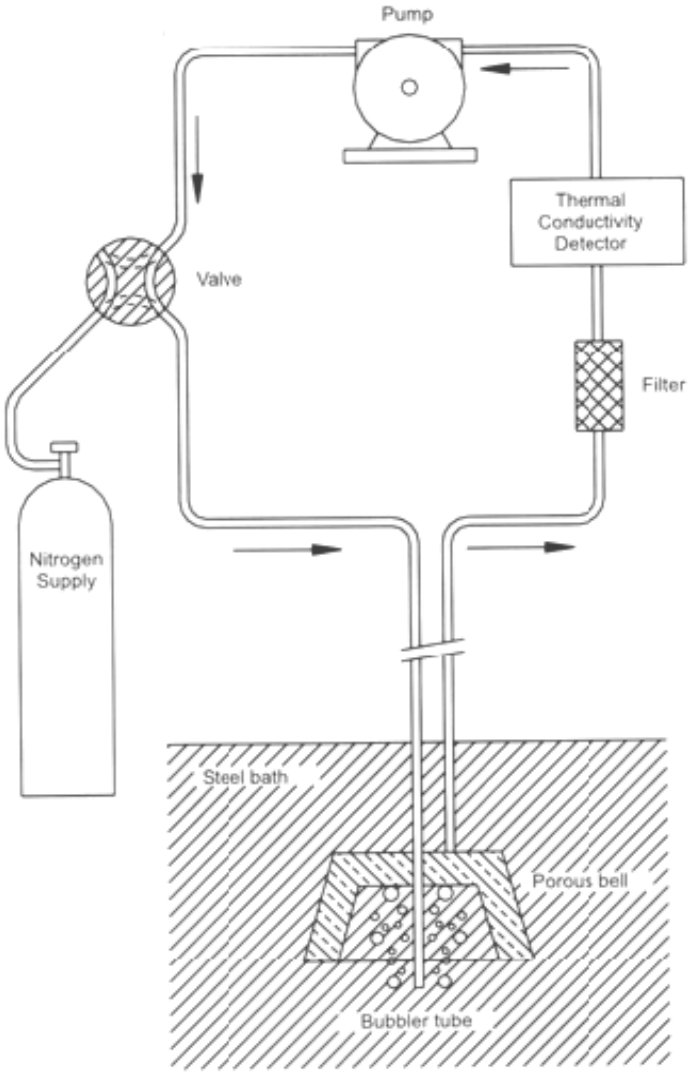

Figure 5-5: The measurement principle of the Hydris [67]

5.1.4 Diffusible hydrogen analysis by thermal conductivity detection

This method involved heating the sample below the melting point so that the diffusible hydrogen residing in traps like dislocations, grain boundaries and microvoids can escape out of the sample [90-92].
The Bruker Juwe H-mat 122 instrument in figure 5-6 has a smaller quartz tube furnace which can heat the sample by resistance from the temperature of 50 °C to 1050°C to release the hydrogen that is located in traps. It also has the bigger quartz furnace that applied infrared for heating the sample from 50 °C to 950 °C for hydrogen desorption.

The (99, 99 %) pure nitrogen gas is carrier gas that flows at 0.9 L / min throughout the system and shields the measurement from the interfering gases outside the open end of the furnace.
The nitrogen gas was purified by molecular sieve that removed oxides, carbon dioxides and other interfering gases.
During solid extraction of hydrogen from steel samples, the carbon and oxygen react into forming carbon monoxide which is oxidized by Schützes reagent into carbon dioxide. Then, the carbon dioxide is removed by sodium hydroxide. The hydrogen is carried by pure nitrogen to the thermal conductive detector as shown in figure 5-2. The use of the quartz as a sample holder has a great advantage because there are less getter effects than using graphite crucible (refer to chapter 2.2).

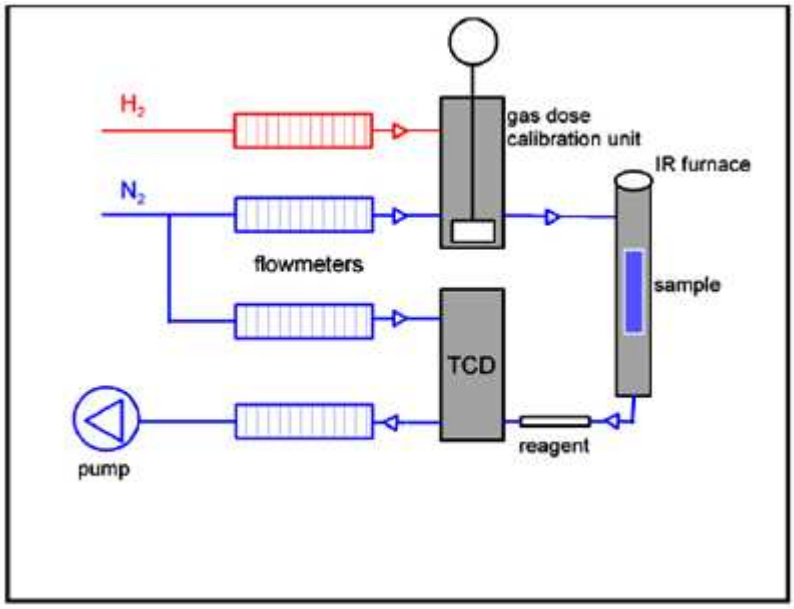

Figure 5-6: The hot extraction setup for diffusible hydrogen analysis [93].

5.1.5 Diffusible hydrogen determination by mass spectrometry

The thermal desorption spectrometry method has been used for quantification of diffusible hydrogen and it has been explored by other analysts [10, 90-92, 94]. Their equipment consisted of an expensive, slow and complex designed ultra high vacuum system that occupies a huge space in the laboratory. This method is important in characterising the mobility of hydrogen in steel because it reveals the possibility of embrittlement occurrence. In the recent work the thermal desorption mass spectrometry has been simplified by coupling an already existing carrier gas hot extraction analyser with quadrupole mass spectrometer (figure 5-8) to have a compact and rapid hydrogen analysis system that is highly applicable to routine analysis.

During the analysis of the sample, the infrared quartz tube was heat from 50° to 950°C and this temperature should correspond with the temperature of the sample. Therefore, a Pt-Rh thermocouple was used to optimize the temperature conditions.

The quadrupole mass analyser (figure 5-7) is the most popular mass spectrometer available in the market because it is more compact, less expensive, allows high scanning rates and suitable for continuous multiple ion detection [95]. It consists of an inlet which introduces very small gas volumes of the sample into the ion source that converts the gas into a stream of positive and a few negative ions. The positive ions are accelerated to the mass analyser which filters the targeted mass over charge ratio from the ion stream and the transducer detects the target molecule (H_2^+) while the vacuum pump maintains the required low pressure in the vacuum system [96]. Therefore the vacuum is important for the ions to have a free run without hitting air molecules while travelling through the instrument.

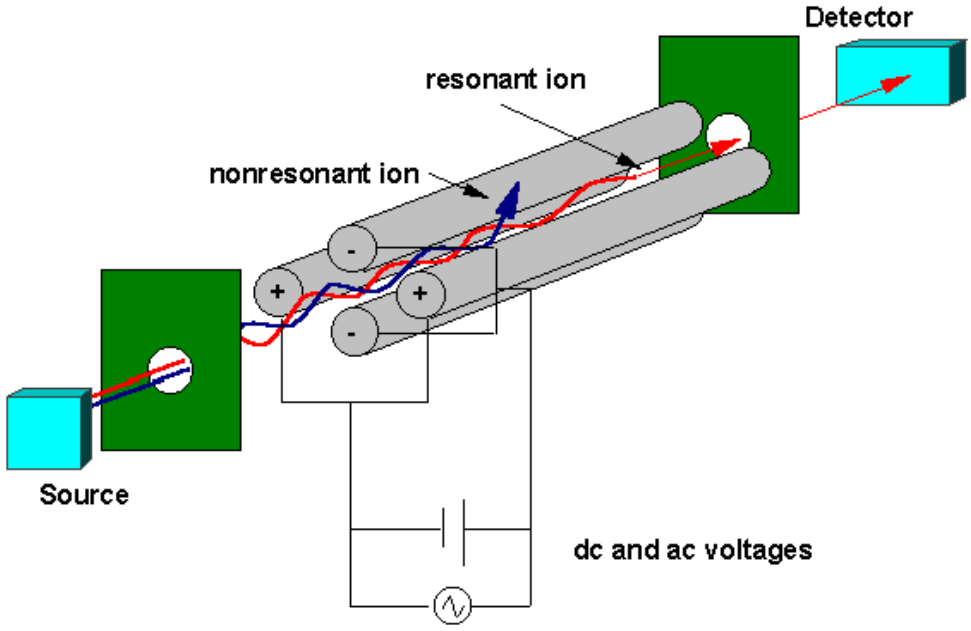

Figure 5-7: Schematic diagram of the quadrupole mass filter [97]

The quadrupole mass analyser consists of four cylindrical rods that are parallel to each other and they serve as electrodes. The two pairs are oppositely charged. Each pair is connected to a pole of direct current source and subjected to variable radio frequency alternative current potentials.

The gas analyte is ionised and fragmented by electrons released from the hot wire filament with an electric current running through it as soon as it is introduced into the ion source.

The ionized particles are accelerated through the centre axis between the rods which isolate the targeted ions by mass over charge (m/z) ratio. The unwanted ions or other m/z ratios become unstable, strike the sides of the rods and become neutralised.

The analyte ions move towards the electron multiplier detector where they are neutralised by the electrons jumping from the metal box of the detector. The jumped electron leaves a space in the metal and the other electrons shuffle each other in order to fill in that space. This electron movement is detected as the electric current. Therefore, the more ions arriving in the detection cell, the more neutralisation will take place and greater production of current will occur [97].

5.1.5.1 TDMS connection

The compact quadrupole GSD 300 O mass spectrometer from Balzers AG was coupled with the solid/hot extraction analyser from Juwe Bruker H-mat 221 by means of a 5 meter long stainless steel capillary with an inner diameter of 0.15 mm (figure 5-9).

The capillary is followed by a platinum nozzle to complete the interface to the ion source and the quadrupole mass analyser in the vacuum chamber. For ion detection both the channeltron and faraday transducers are available.

A turbo molecular drag pump generates an ultimate pressure of about 10^{-8} mbar in the ultra high vacuum chamber [98].

The low pressure was achieved by connection of the T-shaped metallic tube between thermal desorption detector, the pump and the mass spectrometer capillary. After the sample has left the TCD, it is transported by the carrier gas through the stainless steel capillary to the mass spectrometer.

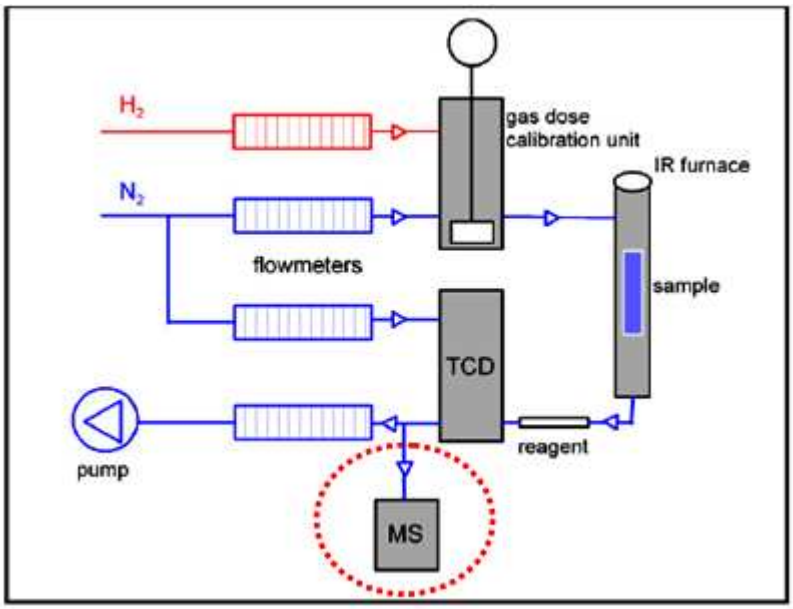

Figure 5-8: The diagram of thermal desorption mass spectrometry equipment achieved by connecting hot/solid extraction instrument from Juwe Bruker H-mat 122 to the quadrupole mass spectrometer.

5.1.5.2 Pressure regulation in TDMS

The diffusible hydrogen was determined by thermal conductivity detector or with mass spectrometry depending on the type of analysis performed. The Juwe Bruker instrument (solid extraction analyser) was coupled with a mass spectrometer in order to quantify the hydrogen desorption rate from steel over a long analysis time. Mass spectrometers have a high ability for the determination of hydrogen with higher sensitivity and a lower drift throughout the thermal desorption analysis.

In this system nitrogen was used as the carrier gas for transporting the gases that are released from the sample to the detector. The advantage of using mass spectrometry is that the carrier gas which usually contains carbon oxides and H_2O during analysis does not contaminate the measurement because the MS contains a mass analyser which filters the gaseous ion stream.

In case of using TCD the step of removing carbon oxides and H_2O is necessary because they can interfere with the signal of hydrogen during detection.

The carrier gas system in Juwe Bruker instrument maintains a specific atmospheric pressure while the mass spectrometer must remain under ultra high vacuum. Therefore to connect the two systems, the one step pressure reduction capillary was constructed to allow the transition of the gas pressure [96].

The pressure was reduced from 0.1 bars in Juwe Bruker to 10 mbar in the mass spectrometer. The connecting capillary was made from stainless steel with a small inner diameter that allowed the carrier gas /analyte to fall from a pressure of 10^3 mbar to the ultra high vacuum pressure of 10^{-5} mbar as indicated by figure 5-9.

The carrier gas system is simple to be constructed and less expensive to maintain. But due to the long travelling paths between the furnace and mass analyser, the gas flow can be highly influenced which can lead to unknown variables in the measurement and this may decrease the quality of thermal desorption analysis.

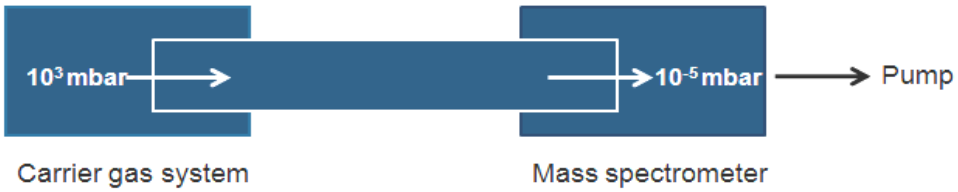

Figure 5-9: The pressure transition between atmospheric pressure and vacuum systems.

5.2 Calibration

5.2.1 Gas calibration

The gas calibration has an advantage of having a flow regulator which allows the gas volume that is required for calibration to enter into the measuring instrument and none is wasted (less costs).

Melt extraction techniques: In this work a two point gas calibration system was used in Eltra OHN 2000. The calibration gas at the first point was a mixture of helium 4.6 and nitrogen 4.0. For the second point pure helium (4.0) was used. The gas yields a constant flow rate with reproducible results during calibration (table 5-1). The gas calibration actually confirms the stability of the measuring instrument before any material can be measured.

Table 5-1: Gas calibration points in Eltra OHN 2000 detected by TCD (n = 10).

Calibration points	Reference value ($\mu g \cdot g^{-1}$)	Mean value ($\mu g \cdot g^{-1}$)	Std. deviation ($\mu g \cdot g^{-1}$)
1	2.5	2.51	0.04
2	12.5	12.42	0.03

Hot/Solid extraction techniques: The Juwe Bruker H-mat 221 is equipped with a calibration module as shown in figure 6-1 and 6-4 which consists of ten different chambers to mix the volumes of the calibration gas (H_2) to the carrier gas (N_2) at different ratios. The gas calibration was performed with 99.999 % pure hydrogen gas (flow rate, 0.2 L / min) which was carried by 99.99% pure nitrogen (flow rate 0.9 L / min) to the TCD. The precisely defined volumes of the calibration gas were injected through a special valve into the carrier gas which flowed through the infrared or resistance furnace. The gas reached the thermal conductivity detector first for hydrogen to be analyzed. The calibration was done by five calibration volumes and each volume was repeated three times as shown in table 5-2.

Table 5-2: The calibration volumes in Juwe H-mat 221 measured by TCD.

Volume	Integral mean value (n=3)	Standard deviation (%)
1	21915	2.9
2	50436	1.2
3	102952	0.9
4	151045	0.9
5	206985	1.5

Applying TDMS for hydrogen analysis the five-point-calibration was also performed by allowing the carrier gas and hydrogen to move further to the T-connection in figure 5-8 which directed it to the mass spectrometer. The small volume of the gas flowed through the stainless steel capillary into the ion source of the mass spectrometry while the rest of the gas was pumped out of the system during the ionisation of hydrogen gas. Both H^+ and H_2^+ were produced, therefore the multiple ion detector was optimised to measure the targeted fragment (H_2^+) which corresponded to 2.16 amu. The signals of the MS that corresponded to the measured volumes of the calibration gas are in figure 5-10.

The gas flow is very important parameter for the stability of this measurement and the baseline.

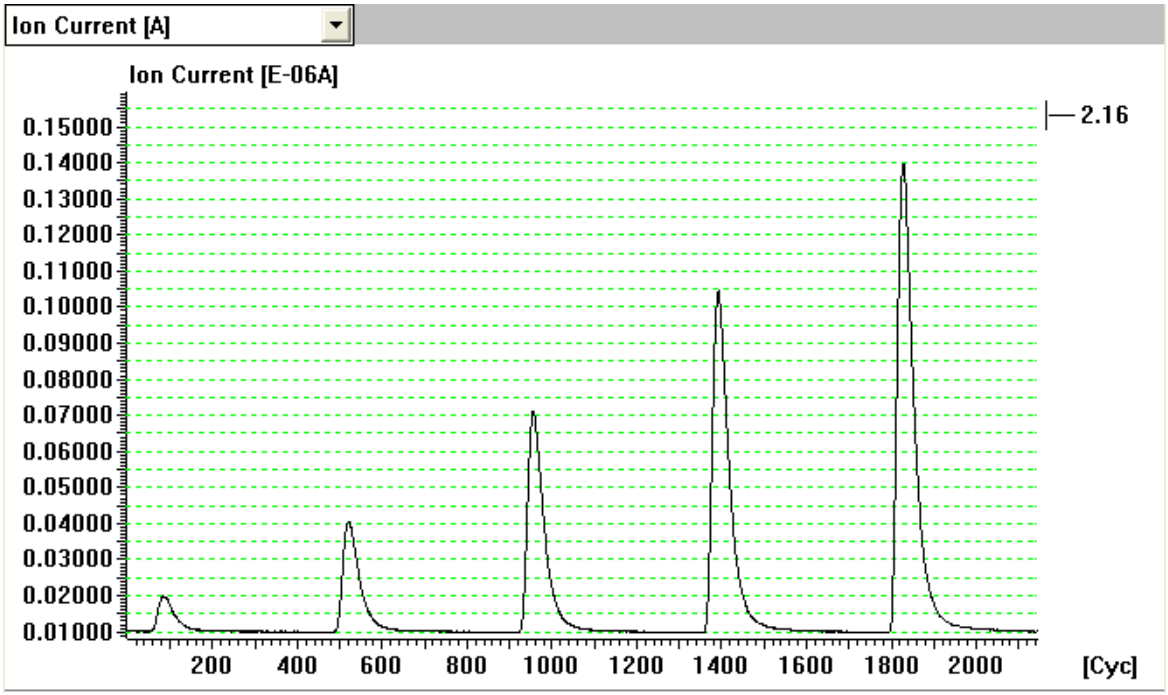

Figure 5-10: The 5-point-calibration signal of the TDMS system.

The calibration factor for the MS was obtained by integration of the raw signal in figure 5-10. The relation of different volumes to the integrated signal of the MS was proven to be sufficiently linear to allow an extrapolation of the factor with five-points-calibration. The internal system measured the temperature and pressure of the injected hydrogen volume during calibration. These parameters were used to calculate the corresponding mass of hydrogen according to the ideal gas law:

$$p \cdot V = n \cdot R \cdot T \qquad (7)$$

Therefore, $m_{H_2} = \frac{p \cdot V \cdot \tilde{M}}{R \cdot T}$

Where,

p: internal pressure of the instrument (mbar)

V: hydrogen volume (ml)

n: number of moles (mol)

R: gas constant (8.314 $JK^{-1}mol^{-1}$)

T: internal temperature of the instrument (°C)

M: molecular mass ($g.mol^{-1}$)

The factor of the measurement is equal to:

$$fc = \frac{Integral}{m_{H_2}} \qquad (8)$$

Where,

Integral: hydrogen signal from MS (10^{-7} mA·s)

mH_2: hydrogen mass (µg)

fc: calibration factor (mA·s /µg)

The factor of the measurement is used as the indicator of the measurement stability by comparing it every day with previous measurements.

Signal Analysis

The results obtained from the spectrum consisted of ion current (A) versus time (s) as shown in figure 5-10. The diffusible hydrogen concentration was directly calculated by:

$cH_2 = Integral \times factor \times sample\ mass$ (9)

Integral: (10^{-7} mA· s)

Sample mass: (g)

Factor: (mA·s /µg)

$cH_2 = (\mu g \cdot g^{-1})$

To simplify the interpretation of the thermal desorption mass spectrum, the signal was converted to desorption rate using the calibration factor and the sample mass.

$$\dot{d} = \frac{s}{fc \cdot m} \quad (10)$$

Where,

d: hydrogen desorption rate from the sample ($\mu g \cdot g^{-1}$/min)

S: signal obtained from the measurement (10^{-7} mA· s)

fc: hydrogen calibration factor (mA·s /µg)

m: sample mass (g)

The conversion of results to desorption rate form enabled the visibility of temperatures where the hydrogen has been released.

5.2.2 Calibration with reference material

There are various certified reference materials for total hydrogen analysis in the market. Therefore, they were analysed by the melt extraction method with Eltra OHN 2000 as described in chapter 5.1.1.to verify their certified values. The instrument was calibrated by gas and then the reference materials were analysed after cleaning them with dichloromethane for 5 minutes in ultrasonic bath. The measurements were continuously repeated for a period of one month.

Data analysis: The results of hydrogen concentration from the TCD were automatically calculated according to the following equation:

$$cH_2 = Factor\ (Integral/Rate/\ Sample\ mass) \quad (11)$$

Factor: calibration factor

cH_2: hydrogen concentration ($\mu g \cdot g^{-1}$)

Rate: volume flow of carrier gas (L/h)

Sample mass: sample weighed in grams (g)

The results for the hydrogen concentrations in Leco reference materials were stable and in agreement with their certified values as shown in table 5-3. The alpha reference materials showed that they can be used during the analysis of samples that contain very low hydrogen contents.

In this work it is recommended to use gas calibration when using Eltra OHN 2000 system. The reference materials are used for controlling the measurement during sample analysis.

But during hydrogen analysis using Leco TCH 600 system (chapter 5.1.2), the Leco reference material was used for calibration

The calibration with reference materials can be influenced either by sample packaging or storage which can change the certified values. This was problem was demonstrated by the instability of certain reference materials in table 5-3.

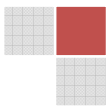

Table 5-3: The total hydrogen concentration in reference materials.

Sample code	Certified value ($\mu g \cdot g^{-1}$)	Measured value ($\mu g \cdot g^{-1}$)	Std. dev. ($\mu g \cdot g^{-1}$)	Number of measurements
Leco 501-529	6.00 ± 0.2	5.80	0.20	19
Leco 747-762	1.70 ± 0.4	1.80	0.20	34
AR 546	0.61 ± 0.2	0.74	0.14	13
AR 555	2.50 ± 0.2	1.30	0.04	5
H 901S-1 (SKF balls)	1.97 ± 0.15	1.05	0.05	5
H 800S-1 (SKF balls)	4.55 ± 0.25	2.38	0.22	9
BS-HON-2	1.70 ± 0.30	2.40	0.02	3

The total hydrogen concentrations in certified reference materials were compared to the diffusible hydrogen content. The diffusible hydrogen content was firstly measured in samples at approximately 1050°C with the Juwe H-mat-221 system. Immediately after that the total hydrogen was analysed in the same samples at approximately 2155 °C with the Eltra OHN 2000 system. The results are listed in table 5-4.

The diffusible hydrogen content in BS HON-2 and Leco 501-529 was higher than the total hydrogen content. This could imply that most of the hydrogen amount in these reference samples was reversibly trapped hence more hydrogen was released during hot extraction by ramping heating the sample from 50 °C to 1050 °C.

The diffusible hydrogen content in the Ar 546 and Leco 762-747 samples was lower than the total hydrogen content. The remaining hydrogen after hot extraction was probably strongly trapped by lattice sites formed by steel alloys. But the trapping properties of steel alloying elements are going to be discussed later in steel alloying topic in chapter 5.7 and 5.8. Therefore, more heat energy was required to remove the rest of hydrogen from the sample content by completely melting the sample at approximately 2155 °C.

The sum of the diffusible and total hydrogen concentration obtained by measurements was in agreement with the certified hydrogen values from the reference materials.

The results could imply that each material has a unique way of interacting with hydrogen. For an example more diffusible hydrogen in the Leco 501-529 and BS HON-2 sample can mean that such materials have very low energy for trapping hydrogen hence more diffusible concentration was obtained.

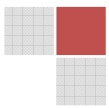

According to the literature [5, 6, 7], hydrogen enters the metal structure in an atomic proton form, therefore more recombination reactions could have occurred due to the temperature, pressure and microstructure influence. Therefore, the lattice sites for solubilising hydrogen in this case could have been less effective hence low total hydrogen was recovered.

Table 5-4: Hydrogen concentration in µg·g-1 measured by hot and melts extraction with TCD.

Reference material	Total Certified H_2 ($\mu g \cdot g^{-1}$)	Diffusible H_2 ($\mu g \cdot g^{-1}$)	Bulk H_2 ($\mu g \cdot g^{-1}$)	Σ (Diff + Bulk) = Total H_2 ($\mu g \cdot g^{-1}$)
Ar 546	0.61 ± 0.2	0.11	0.40	0.51
Leco 501-529	6.00 ± 0.2	5.50	0.70	6.20
Leco 501-529	1.70 ± 0.4	0.40	1.30	1.70
BS HON-2	1.90 ± 0.2	1.50	0.70	2.20

5.3 Influence of operating parameters

In order to quantify total or diffusible hydrogen, the measuring parameters must be well optimised because the extraction of hydrogen from solid or molten metal is highly governed by the diffusion phenomenon according to *Ficks* law in equation 3. Therefore it is crucial to record the variation of sample temperature versus time to measure at the maximum temperature to be reached so that the kinetics of dehydrogenation is quick enough to occur. To ensure that accurate analysis and correct characterisation of the material, the operating parameters were optimised:

5.3.1 Melt extraction

Sample form and weight: The investigations on the influence of sample weight and form on the determination of the hydrogen concentration were conducted in high strength and alloyed steel (austenitic, uncoated flat steel). The sample blocks or cubes and chips were weighed into various masses from 0.1 g to 1 g which were analysed by TCD with the Eltra OHN 2000 system. The results in figure 5-11 showed that hydrogen concentrations were high in sample chips than in sample blocks. Also, in samples with more weight, less hydrogen contents were released. There was no satisfactory explanation for these effects except that it could be the influence of surface effects or insufficient analysis time.

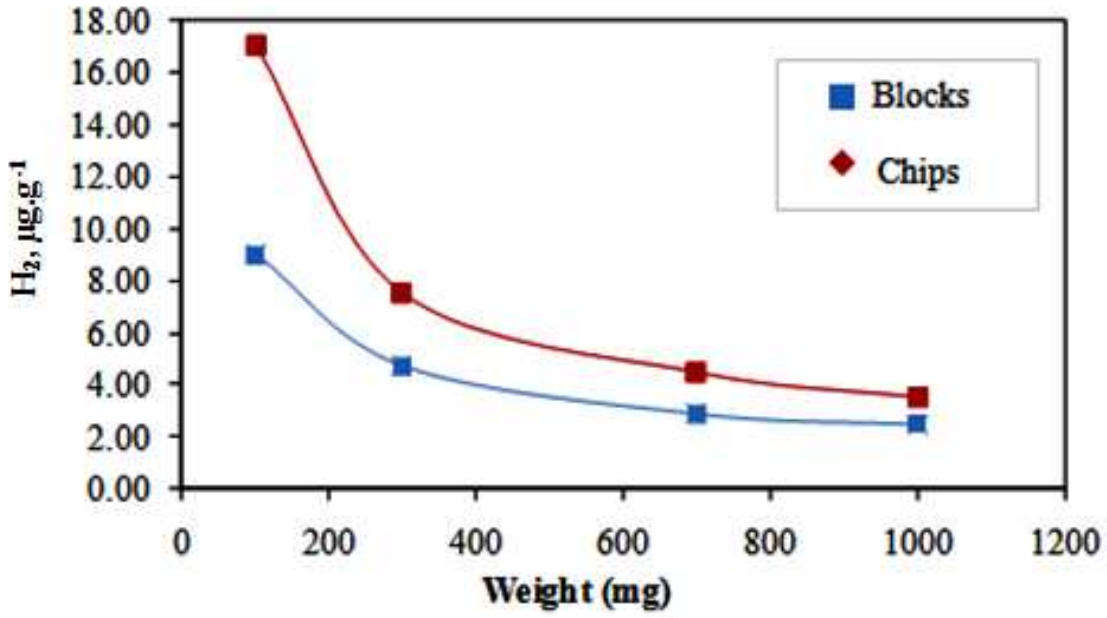

Figure 5-11: Hydrogen ($\mu g \cdot g^{-1}$) in manganese steel prepared in blocks and chip form.

To investigate whether the concentration difference in weight was caused by alloy composition, form and weight, an uncoated HCT780C material was analysed with the standard parameters of Eltra OHN 2000. The sample was weighed to different weights as illustrated by the resulting hydrogen peaks in figure 5-12. According to the instrument`s producer, the high hydrogen concentrations in light samples was caused by the tailing towards the end of the real hydrogen peak which is also detected together with hydrogen from the sample. The interfering hydrogen originated within the equipment and it contaminated the signal. Since the relation between tailing and the analyte peak is larger, therefore light sample weight can be easily falsified towards having higher hydrogen contents. To prove that tailing is the real hydrogen detected and not a negative effect from the thermal conductive detector, the samples were analysed by the mass spectrometer that was connected to the Eltra OHN 2000 system. More work on this part is required for clearing this point.

It was concluded that 1g will be the mass used throughout the analysis because at this mass, stable signals were obtained as it is shown in figure 5-12.

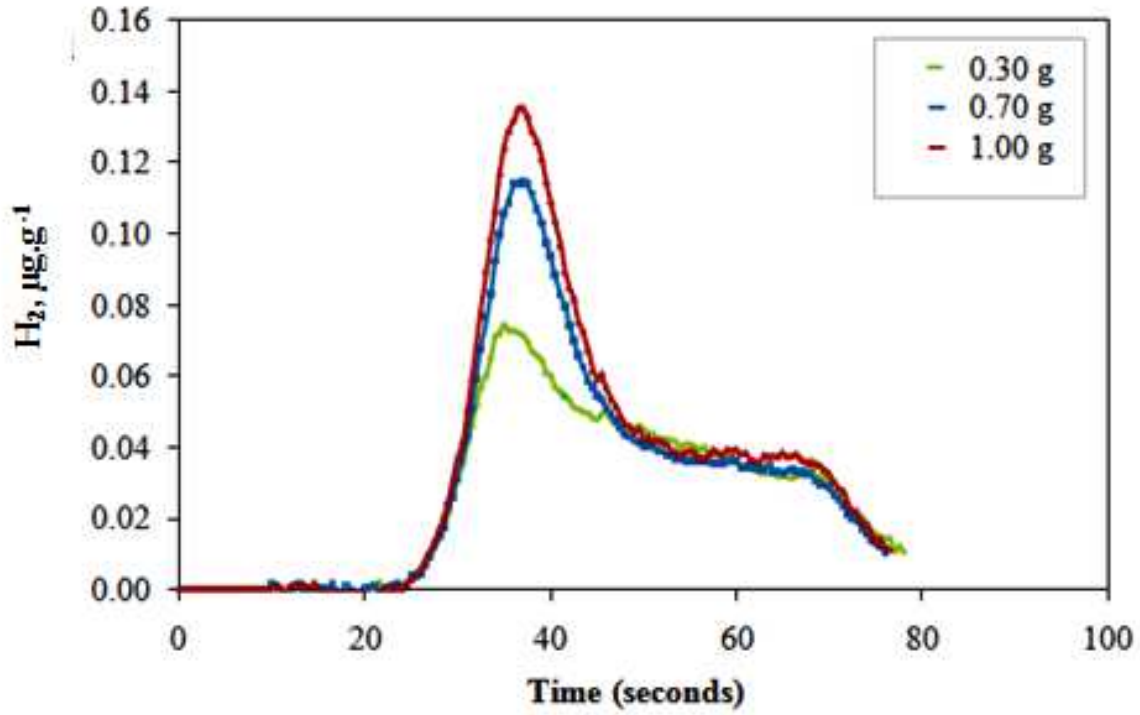

Figure 5-12: The total hydrogen signal of 0.3, 0.7 and 1.0 g. in uncoated steel (HCT780C) (TCD).

Melting power and time: The melting power was varied over 50s to identify the optimal conditions for extracting hydrogen amount from Leco 762-747 reference material which contained 1.8 ± 0.4 µg·g-1 of H_2. As shown in figure 5-13.and table 5-5, the hydrogen depends on the applied power. With increasing power also the hydrogen concentration is increased.

This may have been caused by violent reactions of the analyte gas with the graphite crucible. The peak signal contained two signals of which the first peak could be from hydrogen in the sample and the second peak from carbon hydrides that caused peak tailing.

The hydrides may have originated from the reaction of carbon from the graphite crucible and the hydrogen gas from the sample.

The low power at 1.95 kW did not completely melt the sample hence low hydrogen concentration from the reference materials was obtained. Therefore, the optimum melting power was 3.90 kW within 50s.

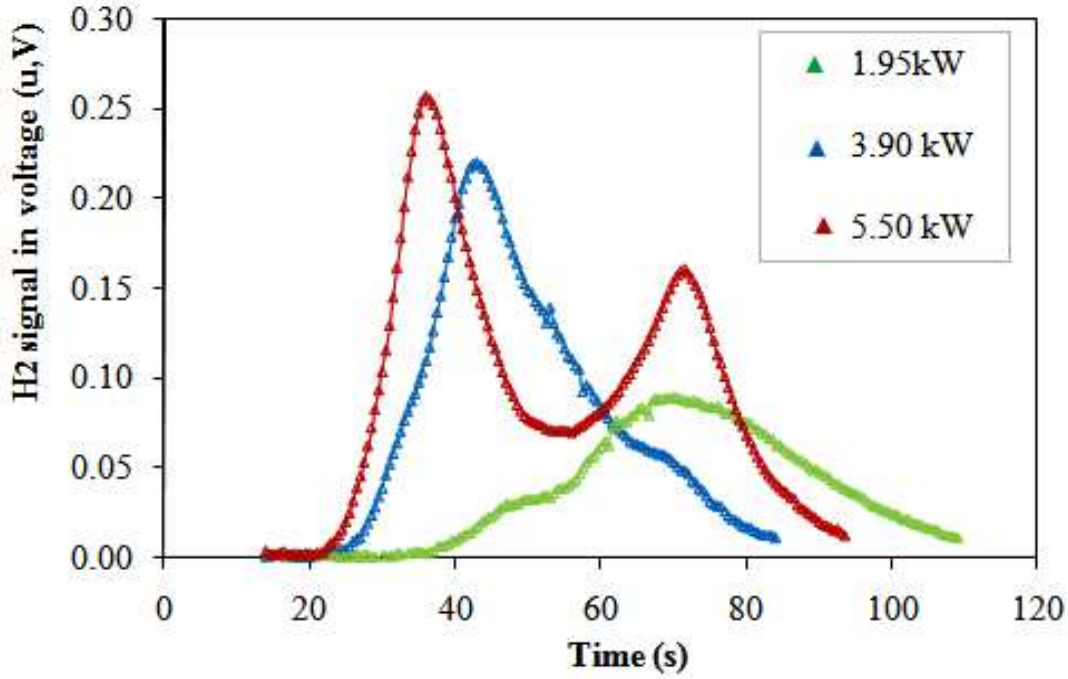

Figure 5-13: Hydrogen concentration ($\mu g \cdot g^{-1}$) obtained by melt extraction of steel samples varying the power (kW) of the furnace.

Table 5-5: Parameters for the determination of hydrogen in the Leco 762-747 reference sample.

Reference Material	Power (kW)	Temperature (°C) approximately	Time (s)	H_2 ($\mu g \cdot g^{-1}$)
Leco 762-747 (1.8±0.4)	1.95	1500	50	1.38
	3.50	2100	50	2.18
	5.50	2500	50	2.98

Graphite crucibles and electrode furnace: the crucibles that are used for application in the Eltra OHN 2000 and Leco TCH 600 instruments were made of pure pyrocoated graphite in order to inhibit corrosion by the gases when the power has been applied. The electrical power is directly applied to the outer crucible. Then the inner crucible is uniformly heated to melt the sample (figure 5-14). The contact between the graphite crucible and the electrode tip is very crucial for melting the sample. The graphite tip for holding the crucible was worn out after approximately 30 days of successive measurements. Then, the crucible could not perfectly fit on the tip.

This reduced the contact between the crucible and the electrode tip decreasing the resistivity. Hence less electricity was deposited to the crucible to melt the sample. Therefore, this case can result in lower hydrogen concentration recoveries.

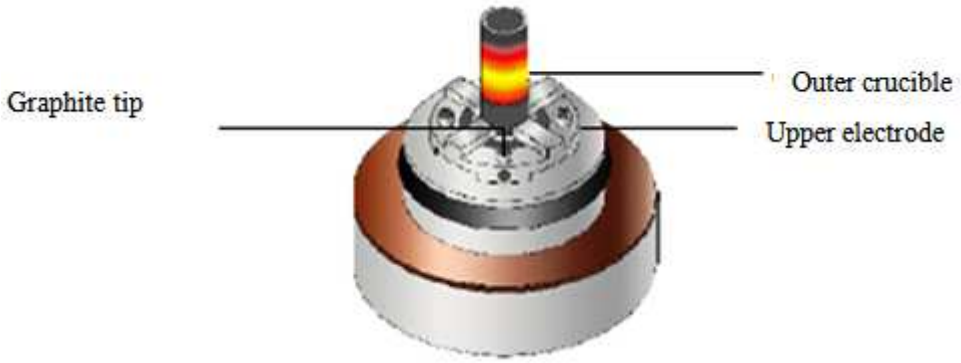

Figure 5-14: The deposition of electricity on the upper electrode, graphite crucible and the graphite tip [84].

Controlling interfering combustion products: Since the melt extraction method has a carrier gas system, the gases released from the sample had to be removed before the analyte (hydrogen) reached the thermal conductivity detector. The carbon dioxide was absorbed by sodium hydroxide (NaOH) while the moisture was absorbed by magnesium perchlorate ($Mg(ClO_4)_2$) before the sample reached the thermal conductivity detector.

The hydrogen released from the sample may be absorbed onto carbon deposited on the electrode surfaces. Hence low recoveries were obtained as shown in figure 5-15. The reference material from Leco 762-747 with c (H_2) = 1.8 ± 0.4µg·g^{-1} was used as an example, due to the re-trapping of hydrogen to dirt/carbon on the electrodes, less hydrogen recoveries were observed.

Then, the upper and the lower furnace electrodes were thoroughly cleaned with a cloth after three measurements. This was done to eliminate the carbon or other interfering substances released when melting the steel that can heavily contaminate the furnace and re-trap hydrogen (getter effects). The cleaning improved the results.

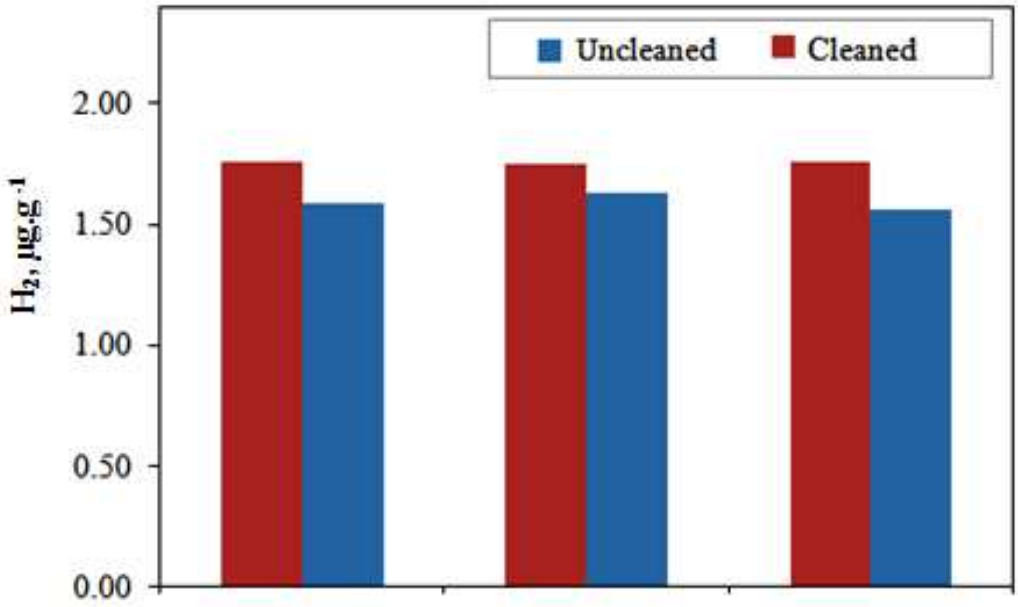

Figure 5-15: Influence of the conditions of the furnace on hydrogen concentrations in reference material (Leco 762-747 ($1.8 \pm 0.4 \mu g \cdot g^{-1}$))

5.3.2 Solid extraction

Sample weight: The influence of different weights on diffusible hydrogen analysis by solid/hot extraction was tested by analysing a highly pure iron block. The sample was cut into block/cubes which were weighing 1, 5 and 15 g. The hot extraction analyser with resistance and infrared furnace in chapter 5.1.4 was used to conduct this analysis with both furnaces. The total hydrogen was also analysed by Eltra OHN 2000 by using TCD. The hydrogen concentration of 1.01 $\mu g \cdot g^{-1}$ has been achieved.

The results in table 5-6 did not identify any significant difference concerning the weight of the sample. The small difference in diffusible hydrogen concentrations could have caused by the resistance furnace extraction temperature of 1020 °C. Otherwise the influence of the weight difference was not observed.

Table 5-6: Diffusible hydrogen concentrations in different samples weights measured by infrared and resistance furnace (n= 2-3).

Sample weight of pure Fe blocks (g)	H_2 analysis ($\mu g \cdot g^{-1}$) in infrared furnace at 950 °C	H_2 analysis ($\mu g \cdot g^{-1}$) in resistance furnace at 1020 °C
1	0.09 ± 0.02	0.13 ± 0.03
2	0.07 ± 0.02	0.12 ± 0.02
15	0.08 ± 0.03	____

5.4 Samples preparation

The flat, zinc coated and uncoated steel samples listed in table.5-7 have been sampled from the middle as illustrated by figure 5-16 and cut by plate shear into block pieces. The 0.5 mm × 0.5 mm was prepared for melt extraction techniques because it uses smaller crucibles.

For the analysis of total hydrogen by melt extraction with Eltra OHN 2000, the 5 pieces of DC06 samples (0.8mm thick) or 3 pieces of HCT780C samples (1.5 mm thick) were weighed to 1g.

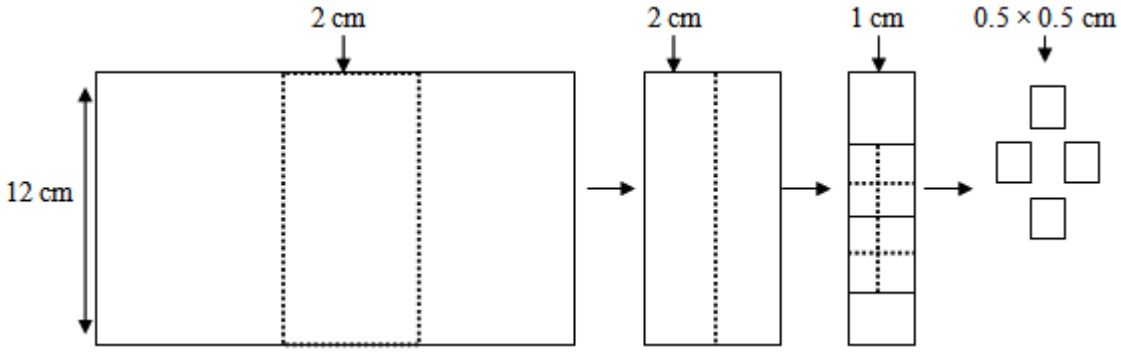

Figure 5-16: Sampling the flat steel for hydrogen analysis.

Table 5-7: The ferritic steel samples consisted of DC06 and HCT780C steel types.

Sample	Coated	Uncoated	Thickness (mm)
DC06	A, B	E	0.8
HCT780C	C, D	F	1.5

5.4.1 Cleaning steel samples

The zinc coated and the uncoated samples contained oil on the surface which is a protective layer. The oil must be removed before hydrogen analysis because it can interfere with hydrogen contents in the steel. As shown in table 5-7, the surface contaminants of the samples E and F were removed by the below listed organic solvents to obtain original hydrogen concentrations in steel.

- Dichloromethane for 5 minutes in ultrasonic bath, dry with air
- Rinsing the samples quickly with acetone, ethanol and dry with nitrogen
- Tetra chloromethane for 5 minutes and dry with air
- Ridoline C72 (alkaline steel cleaner), 5 minutes and dry with nitrogen.

After cleaning the samples, the solvent is totally removed from the material by gently drying it off with air to avoid any interference during the analysis and loss of hydrogen from the sample

The total hydrogen in the samples was measured by TCD and IR systems as described in chapter 5.1.1 and 5.1.2.
Concluding the results in figure 5-17, dichloromethane was chosen as a better organic cleaning solvent for oil and oxides removal on steel. It is a polar solvent with a high volatility which makes it as an ideal solvent for removing grease and other contaminants from steel surfaces.

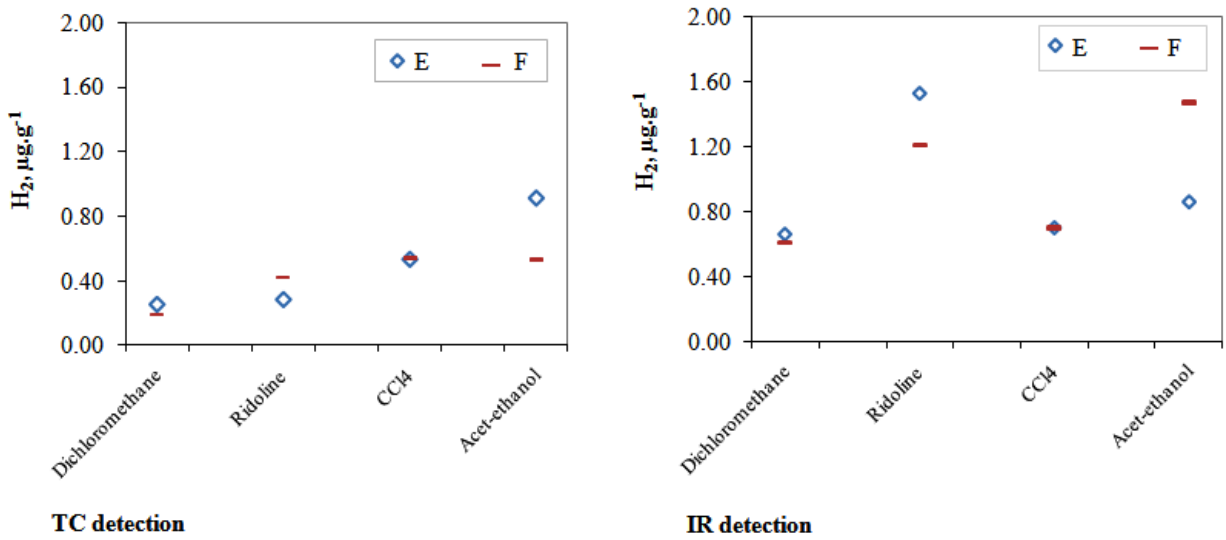

Figure 5-17: Influence of the cleaning solvents on the hydrogen concentration in uncoated samples E and F measured by (a) TC and (b) IR detection.

5.4.2 Zinc coating removal

Zinc has been widely applied as a steel protection layer from hydrogen embrittlement and corrosion. The zinc coating hinders the iron oxidation by having a higher oxidation potential than iron. The schematic diagram in figure 5-18 showed that the hydrogen which interacted with zinc remained in the intermetallic layer between the zinc and the steel. The hydrogen in the intermetallic layer is stored in the form of hydroxides and some hydrogen is absorbed into the metallic layer as H^+ or trapped in metallic particles as H_2. To determine the diffusible or the total amount of hydrogen in steel, the zinc coating must be carefully removed because the contaminants that interacted with zinc can have a negative influence on actual hydrogen concentration.

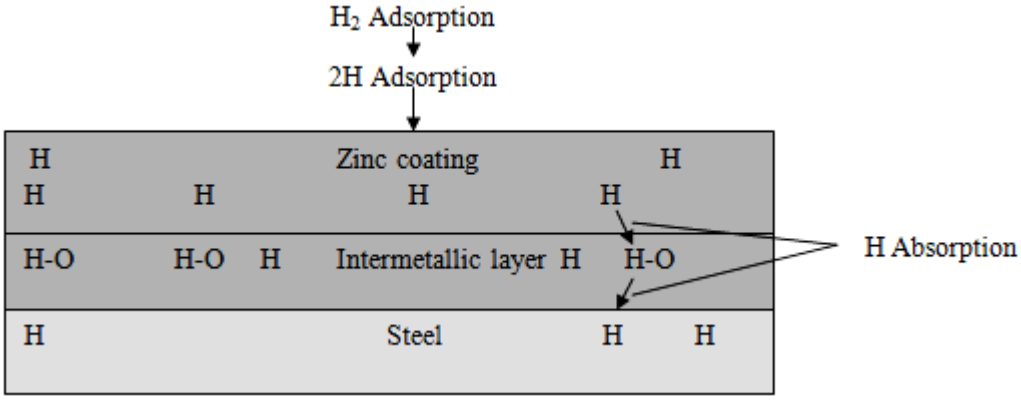

Figure 5-18: Zinc coating on steel and hydrogen interactions.

5.4.2.1 Chemical removal of zinc coating

The zinc coated samples were prepared in the same way as illustrated in figure 5-16 before hydrogen analysis. The coating in 0.5 mm × 0.5 mm sample pieces was chemically removed by 16 % HCl etching in the presence of 0.5 % hexamethylenetetramine (as an inhibitor) until no more gas was developed. The samples were neutralised by immersing in 0.5 % NaOH solution and were quickly dried with the cloth. Then they were cleaned further with dichloromethane in ultrasonic bath for 5 minutes.

Another etching method was to apply a mixture of 68 % nitric acid, 100 % acetic acid and 85 % phosphoric acid. During zinc coating removal the released gas was very slow and the process took more time. The samples were rinsed three times by dipping them in three containers with distilled water. They were also dried with a cloth and cleaned further with methanol for 5 minutes in ultrasonic bath.

The total hydrogen was analysed by melt extraction techniques and detection by TCD and IR. (chapter 5.1.1 and 5.1.2). The results in figure 5-19, table 5-7 and 5-8, indicated that there was a slightly higher hydrogen concentration obtained from HCl etched samples than with NAP etching. The presence of the inhibitor (hexamethylenetetramine) during etching with HCl may have prevented the hydrogen from diffusing in or out of the steel during the zinc removal. It can also inhibit the recombination reaction of the adsorbed hydrogen on the sample surface in acidic environment by forming a monolayer [20, 65, 98].
The application of NAP mixture indicated lower amounts of hydrogen. The adsorbed hydrogen atoms on the sample surface may have diffused out due to recombination reactions of the hydrogen atoms during etching. Hence lower concentrations of H_2 were obtained.

The same trend was observed by the results obtained from the analysis of the same samples by infrared detection. The hydrogen concentration determined by IR depended on the total conversion of H_2 to H_2O in the presence of copper oxide catalyst. Then, H_2O absorbed the radiation at a specific wavelength. Therefore, the accuracy of the measurement depends on the sample composition and the purity of copper oxide. These two factors can have minor influences on the results e.g. higher recoveries of hydrogen concentration.

On the other side the accuracy of hydrogen analysis by applying thermal conductive detection, depended strongly on the separation of H_2 from the carrier gas (N_2). The volume flow and the purity of the carrier gas have a big influence on complete separation of hydrogen. Therefore, less concentration of hydrogen can be measured by TC because of retention of a partial amount of hydrogen in the carrier gas.

Furthermore, it is possible that reaction of oxygen from the sample with carbon from the graphite crucible occurred over the catalyst (iodine pentoxide). If the catalyst is less active oxygen reacts with hydrogen to form moisture (H_2O) which is removed by magnesium perchlorate before hydrogen analysis by TC detection. Hence low results can be obtained.

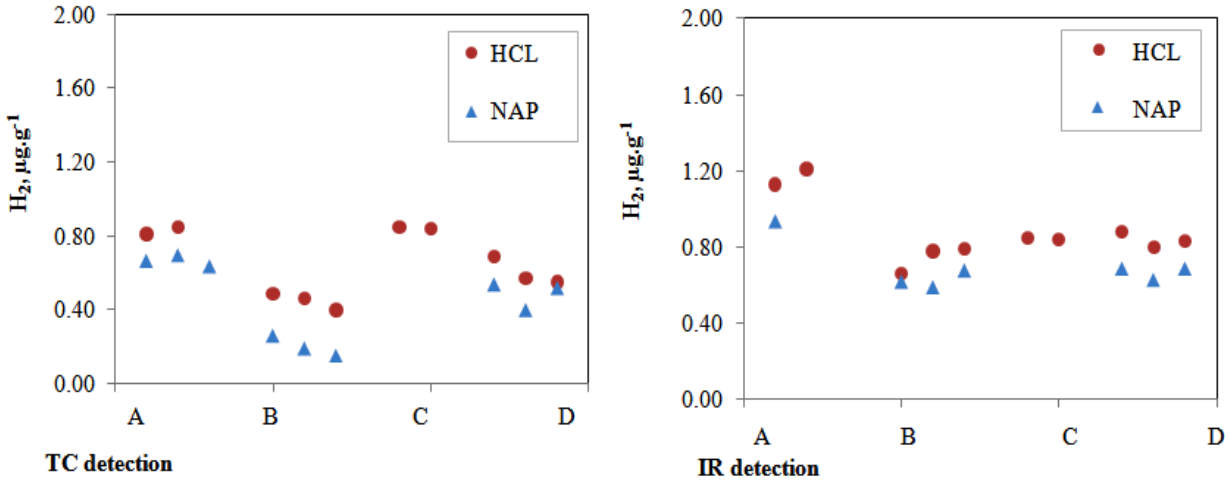

Figure 5-19: Determination of total hydrogen concentration by (a) thermal conductive detection and (b) infrared detection at µg g^{-1} in A, B, C, D samples etched with HCl, NAP.

Table 5-8: Zinc etching with HCl, NAP and hydrogen analysis by TCD (µg·g^{-1}).

Zn etching method	A	B	C	D
HCl	0.83 ± 0.03	0.48 ± 0.03	0.93 ± 0.13	0.62 ± 0.12
NAP	0.62 ± 0.10	0.31 ± 0.03		0.55 ± 0.11

Table 5-9: Zinc etching with HCl, NAP and hydrogen analysis by IR (µg·g^{-1}).

Zn etching method	A	B	C	D
HCl	1.17 ± 0.06	0.73 ± 0.07	0.85 ± 0.01	0.82 ± 0.10
NAP	0.94 ± 0.00	0.61 ± 0.03		0.68 ± 0.03

The diffusible hydrogen was analysed by TDMS in the temperature range of 50 °C to 950 °C at the rate of 600 °C/h. The zinc coated sample in HCT780 in table 5-6 was cut into 20 mm ×10 mm pieces which weighed 2g. The concentration of 0.67 $\mu g \cdot g^{-1}$ was determined from the MS spectrum in figure 5-20. The diffusible hydrogen from the coated surface was released at the temperature of 100 °C to 300 °C. As the hydrogen desorption continued with increasing temperature, the sharp hydrogen peak between 300 to 400 °C was observed. It could have originated from the intermetallic layer between the coating and the steel. Then, the last peak from 400 °C to 650 °C should be the rest of the hydrogen content in steel. The overlapping of different desorption peaks which are related to trapping sites in the coating as well as in the interface between them.

Therefore, the diffusion and retrapping processes of hydrogen coming especially from the inside the material are strongly influenced by the intermetallic and zinc layer on the sample surface.

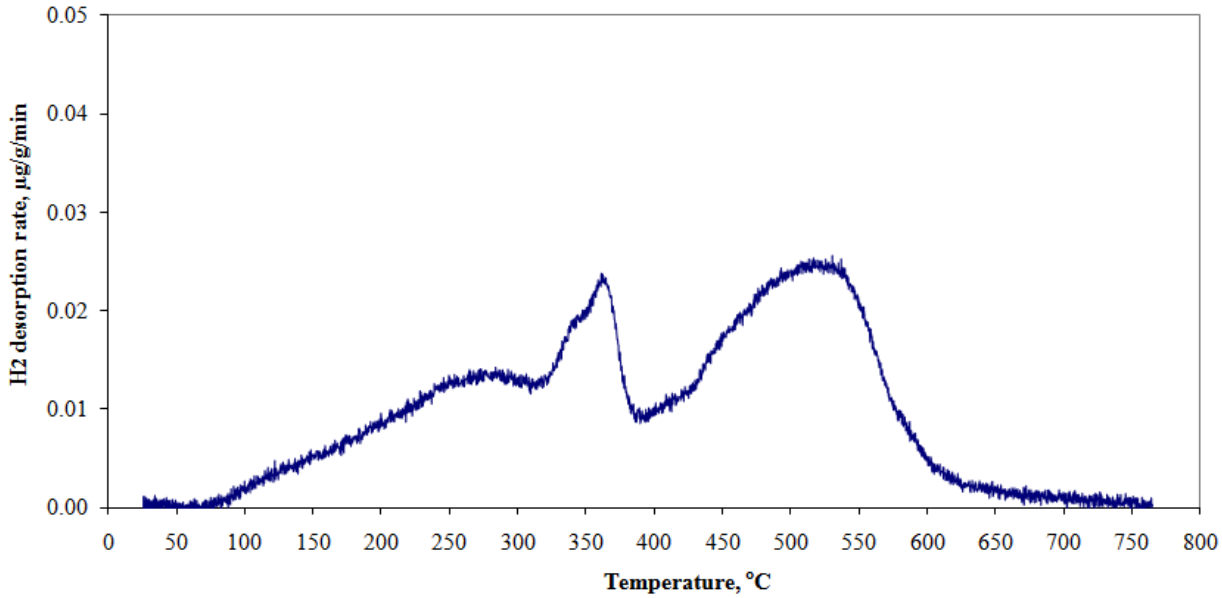

Figure 5-20: The desorption rate of hydrogen ($\mu g \cdot g^{-1}$/min.) from zinc coated HCT780C sample.

The same coated material was etched with HCl solution as described in chapter 5.4.2.1. The diffusible hydrogen was analysed in 2g sample by TDMS which applied the temperature from 50 °C to 950 °C at the rate of 1200 °C/h.

The resulting spectrum in figure 5-21 showed well separated hydrogen desorption peak at 150 °C. This peak could be related to the hydrogen adsorbed on the material during pickling. The second peak was observed at about 550 °C which could be similar to the one observed in same region of the zinc coated sample.

The total hydrogen concentration of 0.37µg·g^{-1} was obtained in the etched sample. The first peak corresponded to 0.20 µg·g-1 which could be the hydrogen added during pickling/etching and the remaining concentration of 0.17 µg·g^{-1} is probably the actual hydrogen content in the steel beneath the coating.

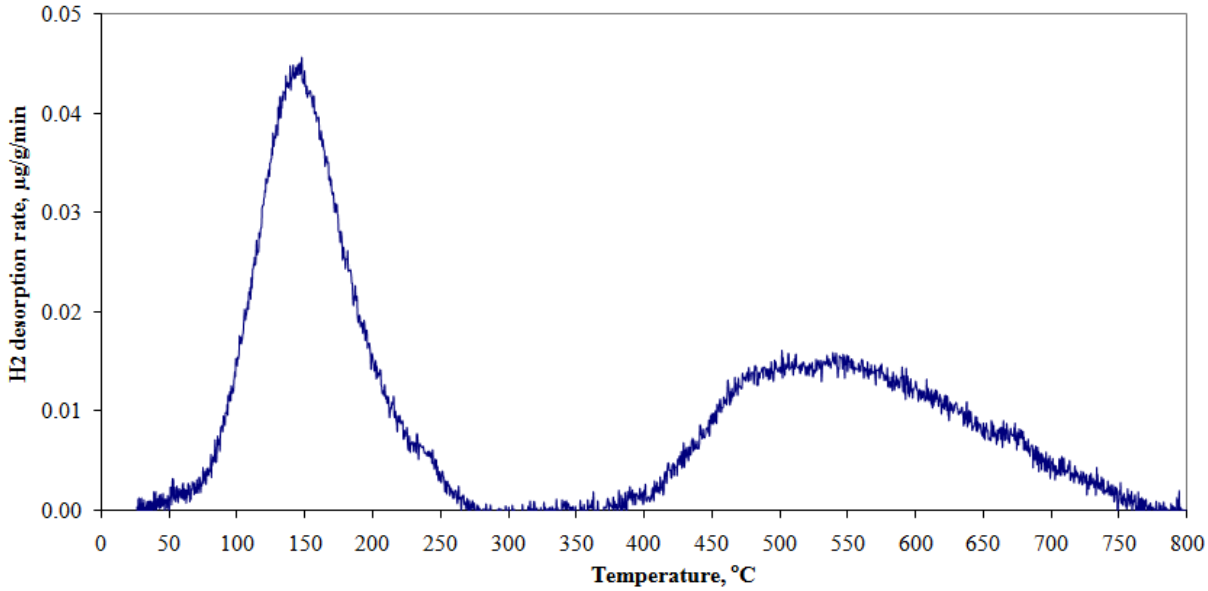

Figure 5-21: The desorption rate of hydrogen (µg·g^{-1}/min.) from HCT780C sample etched by HCl in the presence of hexamethylenetetramine (inhibitor).

Influence of an inhibitor on diffusible hydrogen during steel coating removal: The same HCT780C material was left at room temperature at 22 °C for one year. After those tests were conducted to observe the influence of an inhibitor on hydrogen content, the sample was etched with the same concentration of HCl solution which contained no inhibitor. The etching took place for 30 seconds, 5 minutes and 10 minutes.

According to the results in table 5-10 and figure 5-22, etching the steel without an inhibitor encouraged more hydrogen diffusion in steel due to the higher diffusible and total hydrogen concentrations obtained. As the etching period was increased from 30 seconds to 5 minutes more hydrogen was obtained. This could be due to the hydrogen absorption into the internal lattice sites of the metal e.g. precipitates, inclusions, grain boundaries which causes more accumulation of hydrogen concentration. Then, more concentrations of hydrogen in metallic grains can lead to high pressure which causes the recombination reactions of hydrogen and diffusible hydrogen escape.

The values of the diffusible hydrogen concentration were lower during 10 minutes etching period than in 5 minutes period while the total hydrogen had increased. There was no explanation for this value except that it can be an outlier.

The results indicated that HCl etching with an inhibitor hindered most of the hydrogen from being absorbed into the steel because the total hydrogen did not differ much in samples that were etched for 30s, 5min and 10 min. This also explains the importance of the substances surrounding the steel surface because they can either promote or hinder the hydrogen entrance and steel embrittlement.

This test also showed that acidic conditions enhance hydrogen absorption/adsorption during long time exposure of ferritic steel materials to aqueous environmental circumstances.

The influence of acidic conditions on hydrogen concentration due to exposure period of metallic materials to acidic environments will be described later in chapter.5.5.2.

Table 5-10: The diffusible and total hydrogen concentration ($\mu g \cdot g^{-1}$) in HCT 780C sample etched with HCl with and without an inhibitor.

Etching period	Zn etching conditions	Diffusible H_2, $\mu g \cdot g^{-1}$	Total H_2, $\mu g \cdot g^{-1}$
30 s	HCl with $C_6H_{12}N_4$	0.05 ± 0.03	0.8 ± 0.10
	HCl	0.11 ± 0.04	1.05 ± 0.07
5 min	HCl with $C_6H_{12}N_4$	0.14 ± 0.06	1.05 ± 0.09
	HCl	0.26 ± 0.07	1.18 ± 0.04
10 min	HCl with $C_6H_{12}N_4$	0.12 ± 0.04	0.91 ± 0.11
	HCl	0.16 ± 0.05	1.24 ± 0.03

Column 1: HCl with $C_6H_{12}N_4$ **Column 2**: HCl

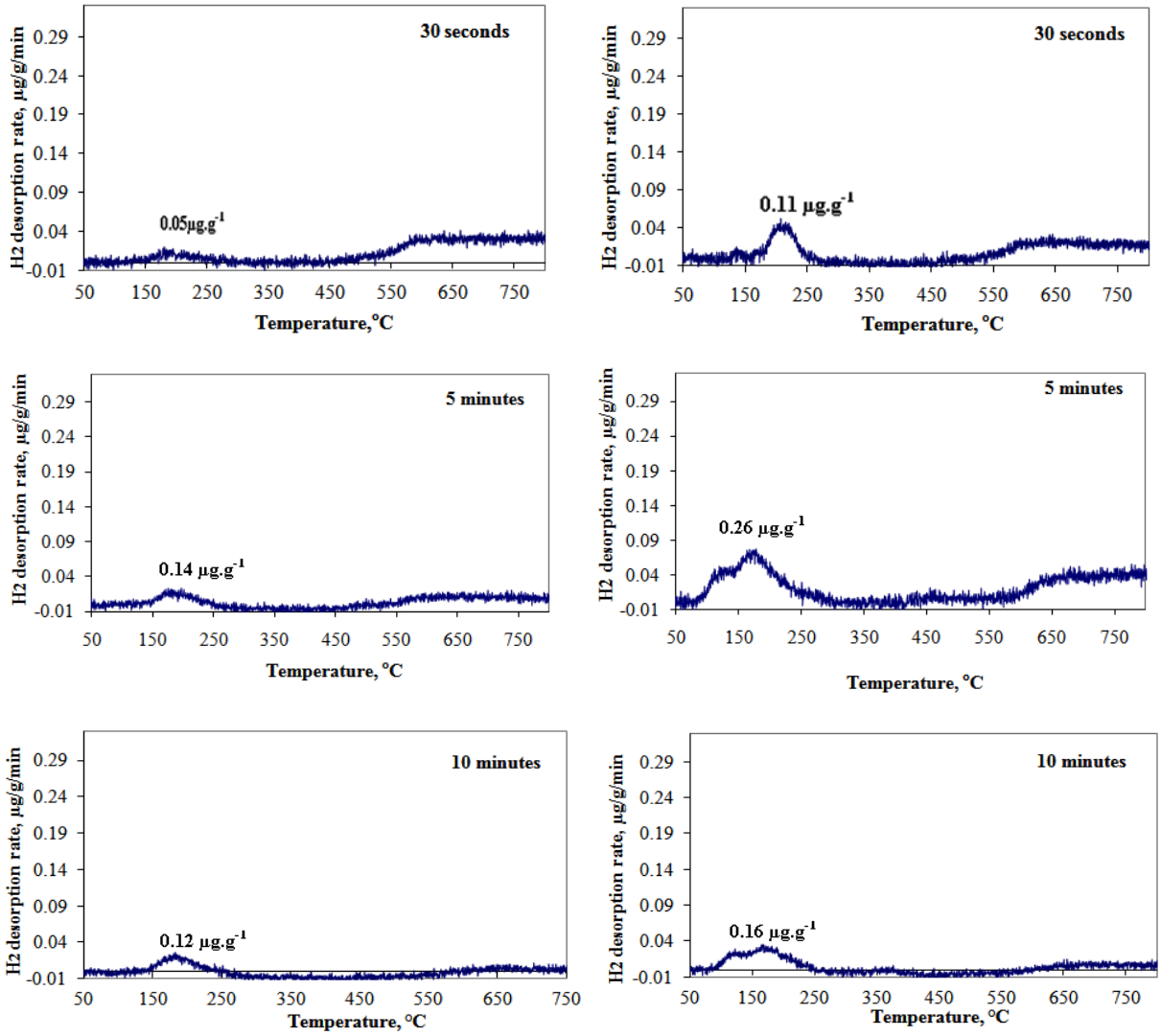

Figure 5-22: Dependance of desorption rate ($\mu g \cdot g^{-1}$/min) of diffusible H_2 on the temperature in HCT 780C samples that were etched with **(column1)** 16 % HCl in the presence of hexamethylenetetramine (inhibitor) and **(column 2)** without an inhibitor for 30 seconds, 5 minutes and 10 minutes.

The analysis of diffusible hydrogen was performed again by TDMS at the rate of 1200 °C/h in zinc coated sample, HCl (with inhibitor) and NAP etched samples to compare the influence of NAP and HCl on diffusible hydrogen concentration and desorption rate.

After one year the diffusible hydrogen was analysed in the same zinc coated, HCl and NAP etched samples. It is obvious (figure 5-23) that the diffusion of hydrogen out of the sample has occurred at room temperature. Hence low diffusible hydrogen concentrations were obtained compared to the results from last year (figure 5-21).

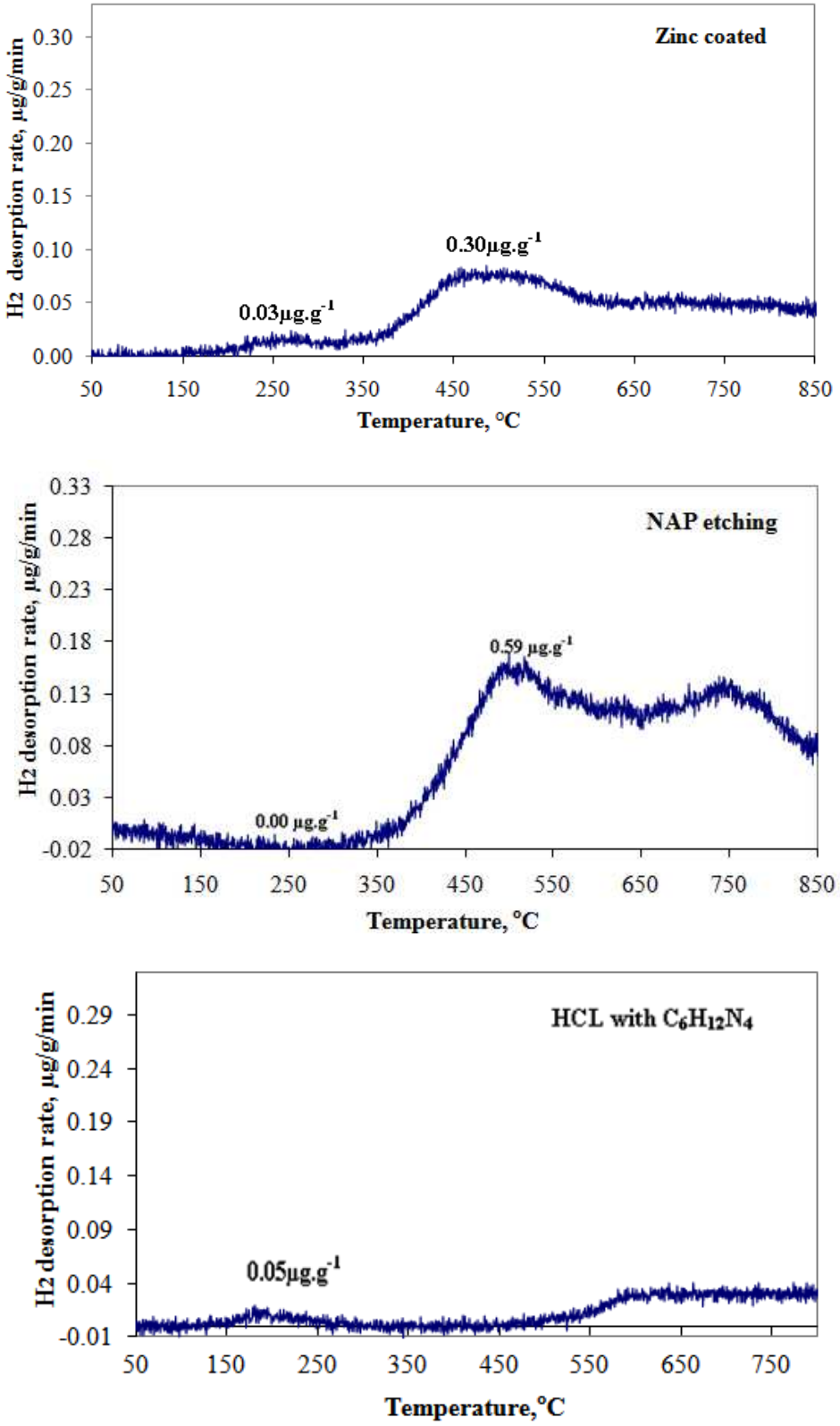

Figure 5-23: The desorption rate of hydrogen ($\mu g \cdot g^{-1}$/min) from HCT 780C sample which was **(a)** zinc coated, etched with **(b)** NAP and **(c)** HCl containing $C_6H_{12}N_4$.

5.4.2.2 Mechanical removal of zinc coating

To investigate a proper method for removal of zinc coating, the coating was also mechanically removed by scraping it off with fine grain silica carbide paper in HCT780C. The samples were also cleaned in dichloromethane for 5 minutes before analysis. The mechanical removal method of zinc coating was compared with the chemical removal of zinc using HCl.

The DSM 950 from Carl Zeiss Micromaging GmbH was used to observe the surface topography of the coated, filed (scraped) and etched steel surfaces (figure 5-24). The influence of the topography of the surface on the adsorption of impurities like hydroxides on it is probably high. The rough surfaces are more susceptible to hydrogen or impurity adsorption than the smooth surface [9, 74].

The surface condition of the sample plays a huge role during the analysis of hydrogen in steel samples because the interaction of hydrogen the depended mostly on the surface area. The coated sample (figure 5-24a) has a smooth surface area which indicated that the hydrogen concentrations will mostly likely result from sample contents only. Unlike in figure 5-24b, whereby the sample was scraped with silica carbide paper to remove zinc, the process left a large rough surface area for more water adsorption, hydroxides, carbides and other contaminants. While the etched sample in figure 5-24c showed semi smooth surface which could have less contaminants absorption ability due to the lower surface area.

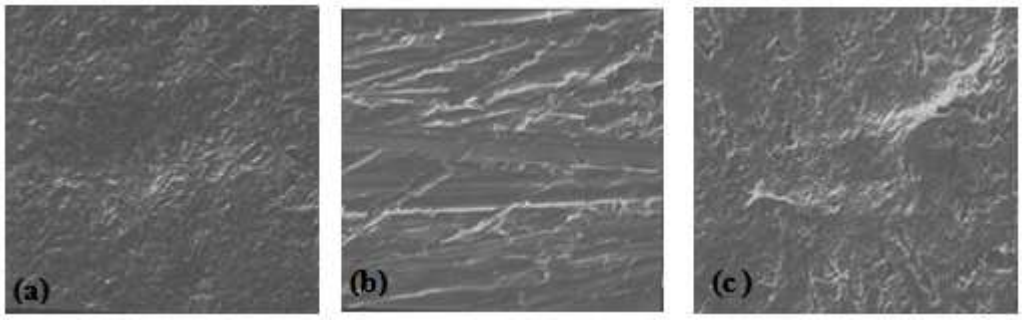

Figure 5-24: The pictures of the sample HCT780C used DEM **(a)** zinc coated surface, **(b)** scraped with fine grain paper **(c)** etched with 16 % HCl. The spot of 10µm was magnified to1000x.

The total amount of zinc in coated, filed and etched samples was determined by using ICP-OES from Thermo Fischer Scientific, Dreieich, Germany. The measurements were based on the determination of zinc concentration on different surfaces of the material. The investigations have been carried out in order to compare the variation of zinc concentration in zinc coated samples; acid etched samples and in paper scraped/filed samples. The zinc concentration was determined to observe if the zinc coating is totally removed so that the results will not be influenced by the hydrogen adsorbed on the zinc layer.

The coated sample contained 98 % Zn; the scraped had 0.72 % and the etched 0.0001 % Zn according to ICP-OES measurements.

Total hydrogen in coated, etched and paper scraped samples: The samples DC06 (A) and HCT 780C (C), were prepared in the same way as explained in figure 5-25 and sandblasting was also included during sample preparation. The analysis of total hydrogen in the above mentioned samples was conducted by melt extraction techniques and thermal conductivity detection.

The results in figure 5-25 showed higher hydrogen concentrations in both sample types which were scraped with silica carbide paper and sandblasted to remove zinc coating. It is highly possible that the high amount of hydrogen concentration was due to the contamination of the steel surface by silica carbide paper that introduced hydroxides. In case of sandblasting, the interferences could have resulted from the sand that was used.

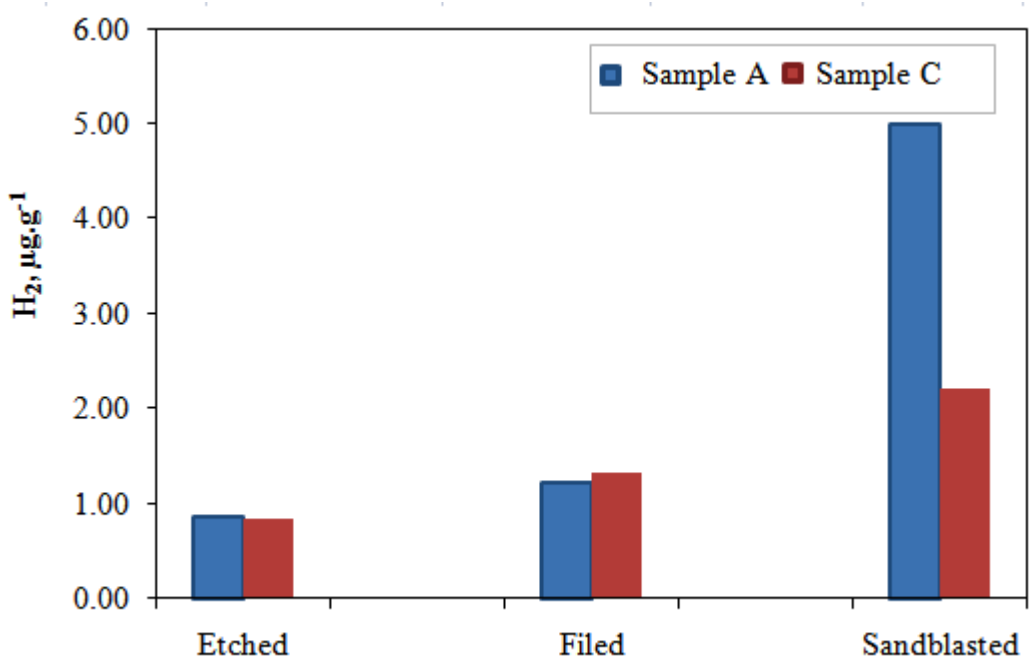

Figure 5-25: Determination of hydrogen concentration ($\mu g \cdot g^{-1}$) in sample A and C by TCD.

5.5 Influence of storage conditions on hydrogen concentrations

5.5.1 Reference materials

The stability of hydrogen in reference samples was determined by storing the sample pieces openly at 105 °C in the drier for three months and after the hydrogen determination was done by applying melt extraction method. Firstly, the samples were analysed before the storage process and both results are listed in table 5-11. But the measured hydrogen values in Leco 501-529 were higher than the certified reference value. This one of the biggest challenges that affect hydrogen content in reference materials during storage.

After the drier, the hydrogen content of Leco materials decreased by nearly half of the original values whereas the BS-HON-2 sample was very stable although the measured values were not representing the certified value.

The stability of the reference material seems to be a critical condition especially if the total hydrogen analyses depend completely on them for calibration.

Table 5-11: The influence of storage at 105 °C in the drier on the hydrogen concentration (n = 3).

Reference samples	Certified value ($\mu g \cdot g^{-1}$)	Measured values before drier ($\mu g \cdot g^{-1}$)	Measured values after the drier ($\mu g \cdot g^{-1}$)
Leco 762-747	1.80 ± 0.40	1.88 ± 0.12	1.09 ± 0.08
Leco 501-529	6.10 ± 0.30	7.95 ± 0.12	3.76 ± 0.10
BS-HON-2	1.70 ± 0.30	2.72 ± 0.12	2.84 ± 0.31

The remaining pieces of the samples from the drier were left at room temperature (22 °C) for another 3 months. Thereafter, the total hydrogen concentration was measured by the same method again. The difference in hydrogen content was not significant in all reference materials as illustrated in table 5-12. It is clear that desorption of hydrogen out of the reference material was enhanced by the temperature at 105°C because at 22 °C the hydrogen remained stable.

Table 5-12: The influence of storage at 22 °C at RT on hydrogen concentration (n=2).

Reference samples	Certified value ($\mu g \cdot g^{-1}$)	Measured values at RT ($\mu g \cdot g^{-1}$)
Leco 762-747	1.80 ± 0.40	1.20 ± 0.05
Leco 501-529	6.10 ± 0.30	3.41 ± 0.11
BS-HON-2	1.70 ± 0.30	2.45 ± 0.19

The hydrogen was also analysed in nickel alloyed and unalloyed reference material. These samples were also left at 105 °C in the oven for 7 days. After that, some of the samples were taken out to measure the concentration of diffusible and total hydrogen with TCD and the results are shown in figure 5-26. The same measurement was repeated after the next 14th day and this measurement continued in this pattern for a period of one month.

It was observed that the Ni alloyed steel had higher concentrations of both diffusible and total hydrogen although both concentrations decreased as the storage period increased. The hydrogen diffusion out of the sample could have taken place at this temperature just like in occurred in reference samples that were mentioned above. According to the theory, the nickel can dissolve in ferrite, non-metallic inclusions and in intermetallic compounds of the steel material. Hence it has the ability to attract more hydrogen within the steel [62].

Although, there is more interaction of hydrogen with Ni alloyed material the traps were reversible because more diffusible hydrogen concentration was obtained. Therefore, contents of the material have a huge influence on the hydrogen concentration distribution and they play a huge role in embrittlement. This point will be discussed more in chapter 5.7.

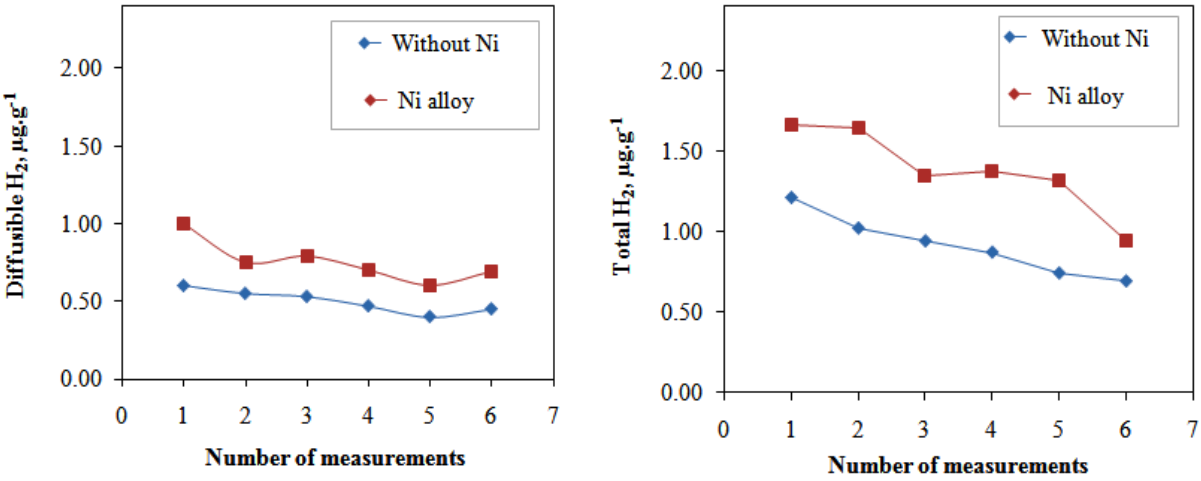

Figure 5-26: The total hydrogen concentration (µg·g^{-1}) analysed by thermal conductivity detector after completely melting the sample. The diffusible hydrogen (µg·g^{-1}) was measured by MS after solid extraction.

5.5.2 Hydrogen charged samples

To observe the content of hydrogen that can be absorbed by ferritic steels, it was a necessity to charge the samples with hydrogen from 6 % H_2SO_4 solution containing 0.05% As_2O_3 [79]. The sample was cut into strips of 1cm × 12 cm as the illustrated in figure 5-16 and wiped with acetone just before charging. Thereafter, some sample strips were cut into 0.5 × 0.5 cm and cleaned in dichloromethane for 5 minutes. They were quickly dried with air and weighed to 1 g to analyse total hydrogen by melt extraction.

The left over sample strips were stored at different conditions on steam ice, room temperature and drier at 105 °C. The same measurement of differently stored samples was repeated every sixth day during 24 days to monitor the change of hydrogen content with the time.

The first value of total hydrogen which was calculated to 38.04 µg·g^{-1} decreased in samples that were stored in the drier (105 °C), ice (-78 °C) and room temperature (22 °C) as shown in table 5-13 and figure 5-27. The hydrogen content in samples stored in the drier decreased drastically. The higher hydrogen amount could be observed in ice stored samples. This implied that cold conditions can delay dehydrogenation in ferritic steel samples.

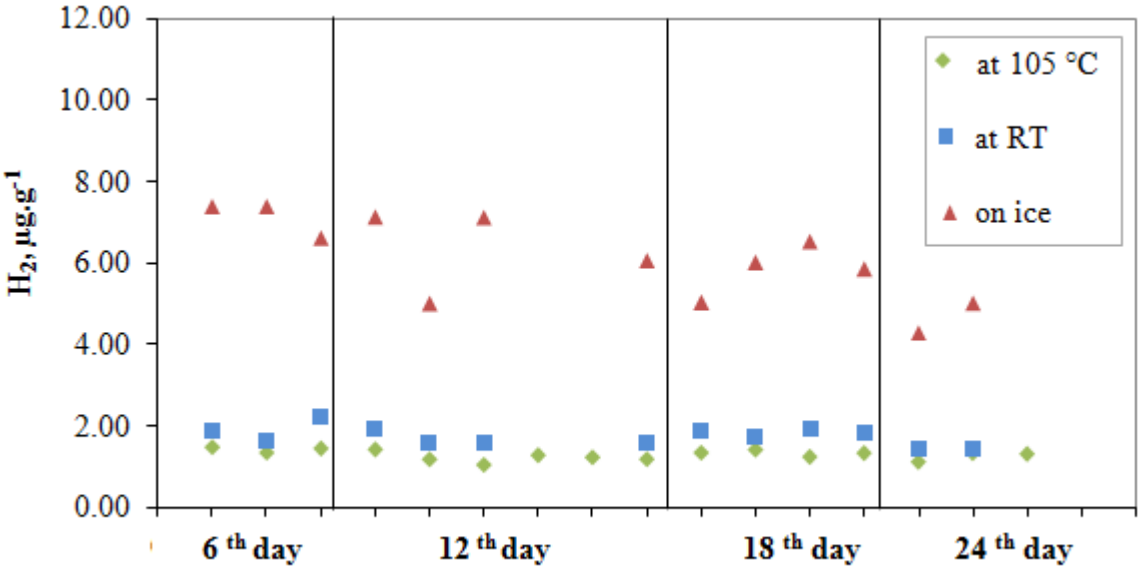

Figure 5-27: The total hydrogen concentration (µg·g^{-1}) in sample DC06 (E) that was stored at room temp. (22 °C), on dry ice (-78 °C) and in the oven at 105 °C.

Table 5-13: The total hydrogen concentration (µg·g^{-1}) measured in ferritic steel samples DC06 (E) samples.

Sampling days	Drier (105 °C)	RT (22 °C)	CO_2 dry ice (-78 °C)
6th	1.43 ± 0.07	1.92 ± 0.30	7.11 ± 0.44
12th	1.20 ± 0.10	1.59 ± 0.02	6.05 ± 1.50
18th	1.34 ± 0.09	1.84 ± 0.10	5.84 ± 0.80
24th	1.26 ± 0.12	1.43 ± 0.00	4.64 ± 0.52

The same sample (DC06) was charged as described in chapter 5.5.2 for 6, 18 and 20 hours. For diffusible hydrogen analysis, the pieces were cut to 1 cm × 2.5 cm. The measurement was done by heating the sample from 50 °C to 950 °C at a rate of 1200 °C/h using the TDMS.

According to the results shown in figure 5-28, the longest charging period (20hrs.) resulted in higher hydrogen concentration which was released at approx. 204 °C, during the 18 hrs. the hydrogen was desorbed at approx. 193 °C. The lowest hydrogen concentration was obtained from 6 hours charging period which released hydrogen at approx. 150 °C.

The shift of the maximum temperature of each peak could have been caused by the diffusion of hydrogen concentration over the distance within the sample. When the sample was charged for a short period, hydrogen can be quickly desorbed due to the distance it has diffused through the bulk. Hence 6 hours charging period released hydrogen at lower temperatures than 18 and 20 hours of hydrogen charging.

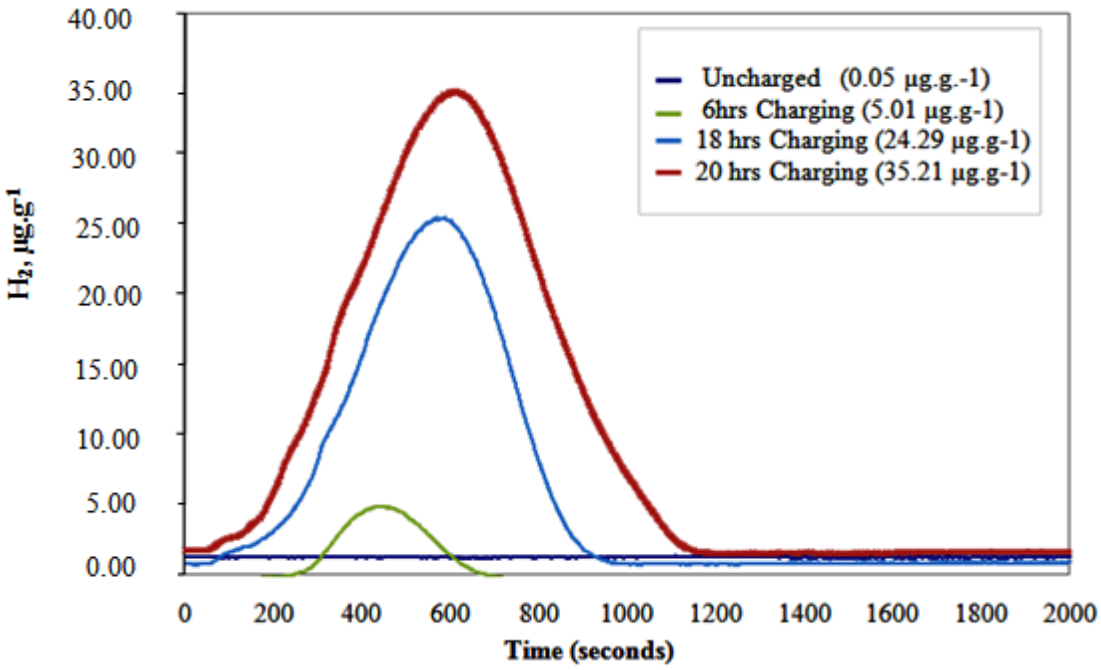

Figure 5-28: The diffusible hydrogen signal obtained for sample E by TDMS after charging with 6 % H_2SO4 in the presence of 0.05 % As_2O_3 for 6, 18 and 20 hours.

To test further the correlation between hydrogen charging period and the content of hydrogen, the ferritic steel samples were charged with hydrogen for 15 seconds, 2 minutes, 6 minutes and 12 minutes. This test was also aimed at observing the stability of the absorbed or adsorbed hydrogen within the material.

These samples were also stored in liquid nitrogen to keep the hydrogen in steel before diffusible and total hydrogen analysis. The total hydrogen was measured by melt extraction while diffusible hydrogen was determined by TDMS. The sample was cut in the similar way and cleaned with dichloromethane.

Before the measurement from each batch, the sample was left at room temperature (22 °C) for 15 minutes, then it was quickly analysed. The same sample was left for another 2 hours at RT before the second hydrogen determination and lastly it was kept for 5 hours before hydrogen determination.

The diffusible hydrogen decreased as the samples remained longer at room temperature according to the TDMS measurements in figure 5-29 and table 5-14.

The same trend was followed by the total hydrogen amount determined by melt extraction in the same samples under similar conditions as the results are shown in table 5-15. The hydrogen concentration increased simultaneously with the time of sample exposure to the acidic medium.

The blisters were observed after the hydrogen input on the metal surface. This confirmed the pressure expansion due to the theory of Zapffe and Sims [11]. It was stated that the hydrogen gas pressures generated in the internal micro cracks or micro voids force their way out by expansion which lead to metal deformation or plastic deformation. This occurs because the internal gas pressures attempt to reach a thermodynamic equilibrium with the large hydrogen activity developed by the charging medium.

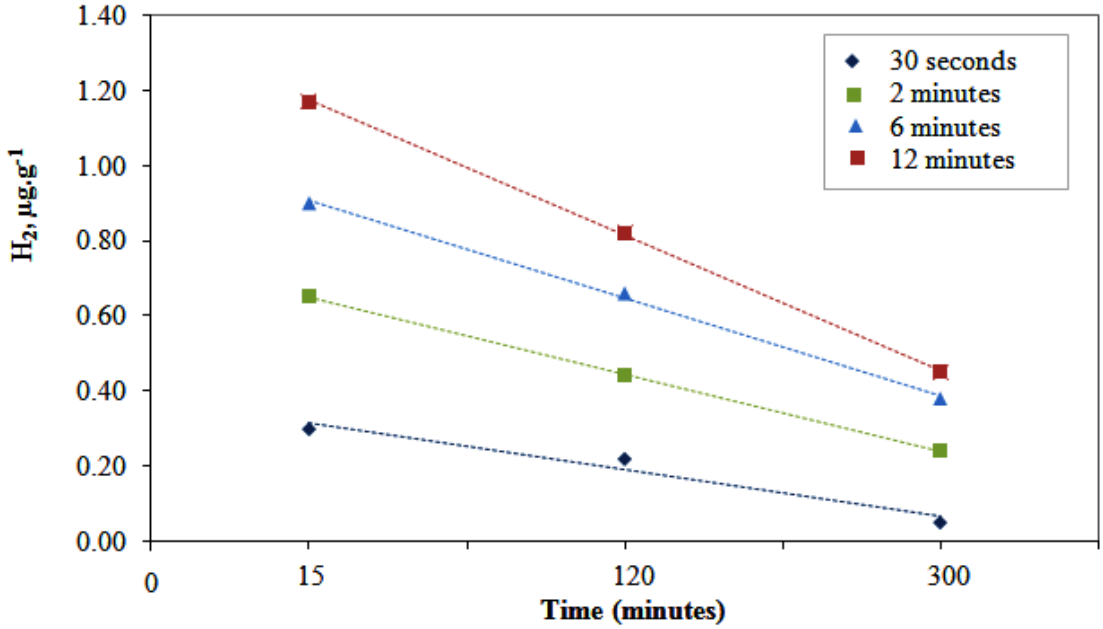

Figure 5-29: Diffusible hydrogen concentration (µg·g^{-1}) in ferritic steel samples charged with hydrogen; stored at room temperature for 15 min., 2 hours and 5 hrs and detection of diffusible hydrogen by TDMS.

Table 5-14: The diffusible hydrogen concentration ($\mu g \cdot g^{-1}$) of ferritic steel sample charged for 15 min, 2 hrs and 5 hrs.

	Total hydrogen concentration ($\mu g \cdot g^{-1}$)		
Storage period at RT	15 minutes	2 hours	5 hours
Charging time			
30 s	0.30	0.22	0.05
2 min	0.65	0.44	0.24
6 min	0.90	0.66	0.38
12 min	1.17	0.82	0.45

Table 5-15: The total hydrogen concentration ($\mu g \cdot g^{-1}$) in ferritic steel sample charged for 15 min, 2 hrs and 5 hrs.

	Total hydrogen concentration ($\mu g.g^{-1}$)		
Storage period at RT	15 minutes	2 hours	5 hours
Charging time			
30 s	1.54 ± 0.01	1.62±0.13	1.60 ± 0.19
2 min	1.39 ± 0.13	1.52±0.18	1.43 ± 0.07
6 min	1.55 ± 0.01	1.41±0.04	1.26 ± 0.04
12 min	1.93 ± 0.08	1.71±0.06	1.53 ± 0.04

5.5.2.1 Comparison electrolyte solutions for hydrogen charging

The presence of hydrogen in ferritic materials originates from various sources, therefore the contribution of below mentioned solution was determined:

1. 1N NaOH (alkaline) and 20 mg thiourea.
2. 5 % NaCl
3. 1N H_2SO_4 and 20 mg of thiourea.

After charging the samples for 10 min., 20 minutes and 30 minutes, the samples were stored in liquid nitrogen (-176°C). Before analysis they were cut to the standard size and quickly rinsed in acetone, then later in ethanol. They were dried by air to remove the solvent on the surface. It was observed that more damage of the metallic material occurred when charged with 1N H_2SO_4 with thiourea in figure 5-30 and the highest total hydrogen concentration was also obtained as indicated in figure 5-31.When the samples were charged with NaCl, the lowest hydrogen concentrations were analysed.

Thiourea can promote the adsorption and absorption of the hydrogen atoms into the material based on theory [79]. Therefore, more adsorption and diffusion of hydrogen into the steel bulk took place in the presence of the strong electrolyte solution (H_2SO_4).

It was confirmed again that the longer exposure time of the material to hydrogen concentrated environment (electrolyte solution) can result in more hydrogen absorption.

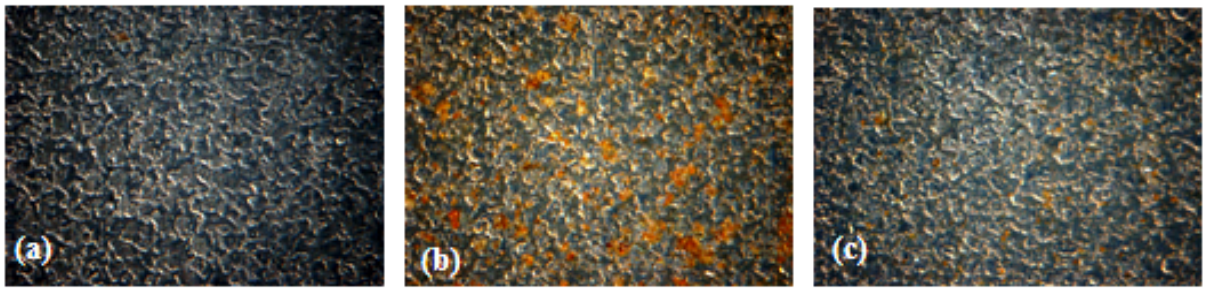

Figure 5-30: (a) The original ferritic steel sample, **(b)** charged with 1N H_2SO_4 with 20 mg thiourea and **(c)** with 1N NaOH with 20 mg thiourea.

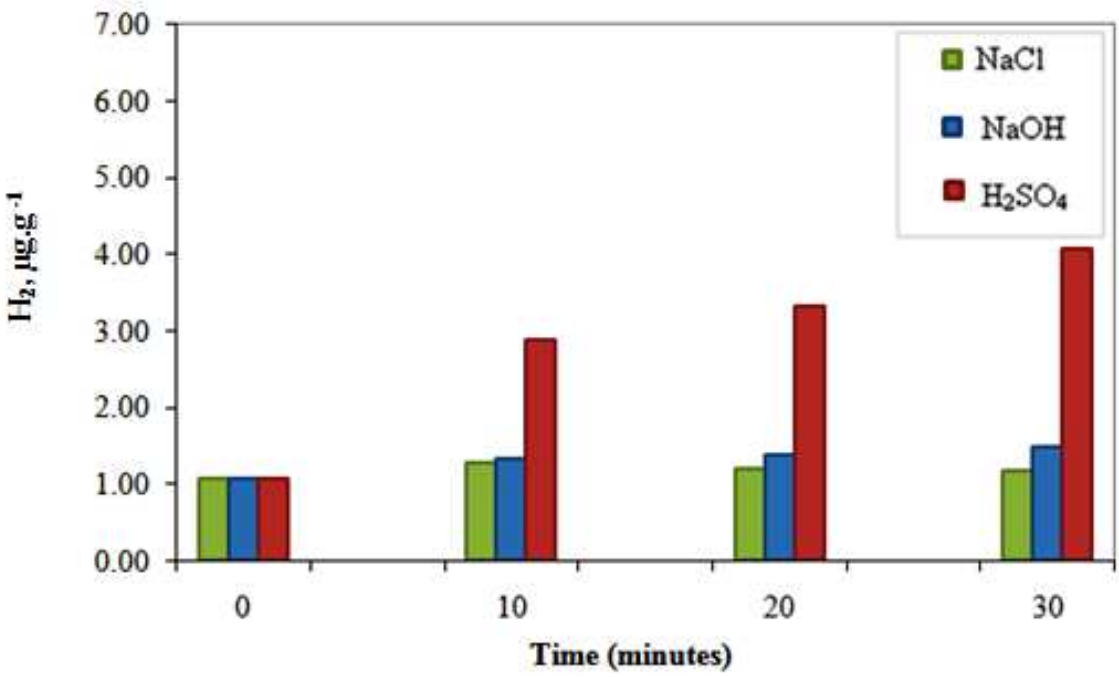

Figure 5-31: Influence on hydrogen concentration after charging the ferritic sample for 10, 20 and 30 minutes with H_2SO_4, NaOH and NaCl electrolytic solutions.

5.6 Molten steel sampling

This part of the work involved the detection of hydrogen in sample M6R56 at the production site from tundish and chill mould by Hydris system. The same material was sampled with quartz glass tube with an open end containing one way valve aspirator to produce pressure for withdrawing the molten steel. The first collection of samples were quickly quenched in iced water and stored in nitrogen. The second one was quenched in nitrogen and also stored in liquid nitrogen.

In order to determine hydrogen in the laboratory by melt extraction with Eltra ONH 2000 sytem, the glass rods in figure 5-32 (a) were broken and the long pin samples were cut by the scissors into 1g as shown in figure 5-32 (b). They were cleaned with dichloromethane for 5 minutes in ultrasonic and quickly dried with air.

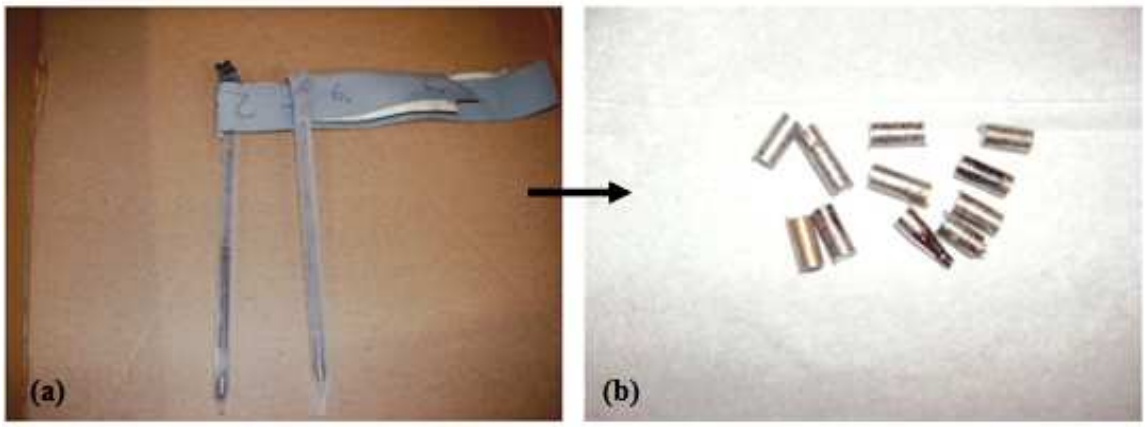

Figure 5-32: **(a)** The molten steel sampled in quartz glass tubes and **(b)** cut into 0.5 g pins before hydrogen analysis by melt extraction method in the laboratory.

There was a correlation in the total hydrogen values measured by Hydris with laboratory values from samples that were quenched in water after analysis by the Hydris system (figure 5-33). The lowest concentrations have been measured in the nitrogen quenched samples.

The same procedure was followed to analyse samples from the chill mould. The results illustrated in figure 5-34 were in agreement with the previous measurements. In this case also, the hydrogen amount analysed by Hydris system was comparable to the hydrogen values measured in the laboratory after the samples have been quenched with water. The nitrogen quenched samples were still containing the lowest hydrogen contents. This implied that quenching samples with water is vital for hydrogen determination. When quenching the samples with nitrogen, it is difficult to achieve a quick cooling rate. Therefore, the hydrogen diffusion out of the sample bulk can occur. This can be associated with role played by the heat capacity and Leidenfrost phenomenon of the liquid nitrogen.

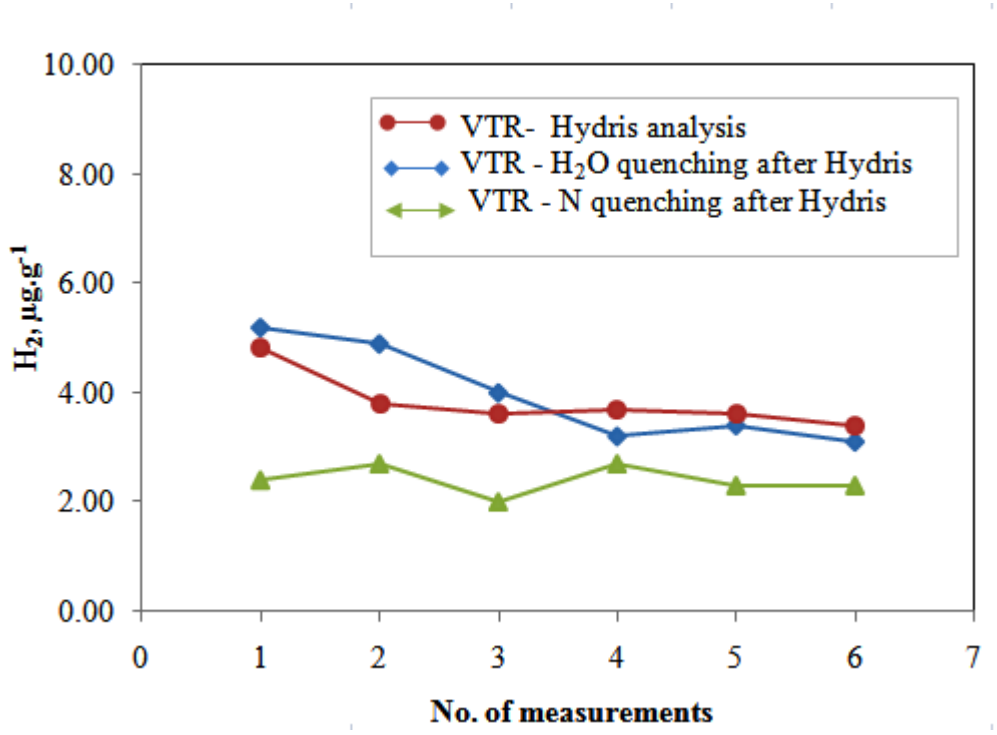

Figure 5-33: Comparison of the hydrogen concentration in molten steel contained in the tundish with the laboratory analysis after quenching the samples with water or nitrogen.

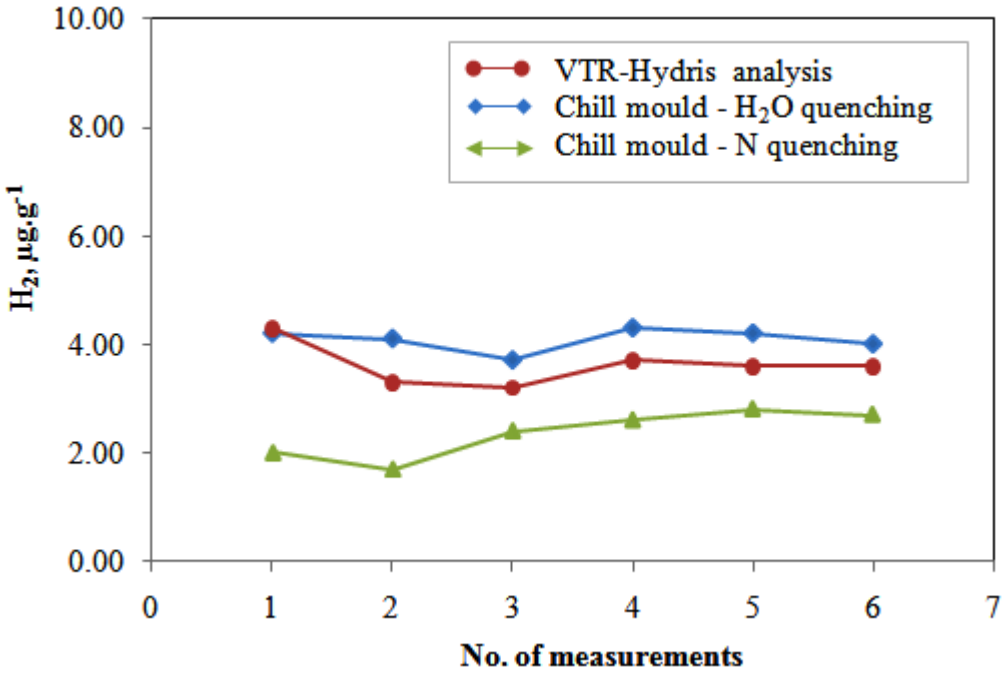

Figure 5-34: Comparison of the hydrogen concentration in molten steel contained in the chill mould with the laboratory analysis after quenching the samples with water or nitrogen.

5.7 Influence of alloys on hydrogen distribution in steel

5.7.1 Effect of a cooling medium on hydrogen concentration in pure iron

To investigate the influence of different alloying elements on hydrogen amounts, steel samples were melted at the laboratory scale on the base of highly pure iron matrix (99.99% Fe). At first the influence of the melting process on pure iron in the form of chips was investigated. The sample containers were ceramic crucibles which were purified by being baked at 1200 °C. Then, 60 g of iron chips was weighed into ceramic crucibles and melted in the high frequency electric furnace (Himmel SGS 02, NETZ, current at 1 A). After depositing the iron mould into the copper blocks, the samples were cooled either with nitrogen or water.

The melted round sample disks were cut into 1 g pieces and analysed by melt extraction method using the Eltra OHN 2000 system as shown in figure 5-35.

The hydrogen amounts in water and nitrogen cooled samples were compared to the pure Fe block from real production line in table 5-16. The precision of hydrogen concentration values in nitrogen cooled samples was not uniform in comparison to the water cooled samples. Therefore water is recommended as the metal cooling substance.

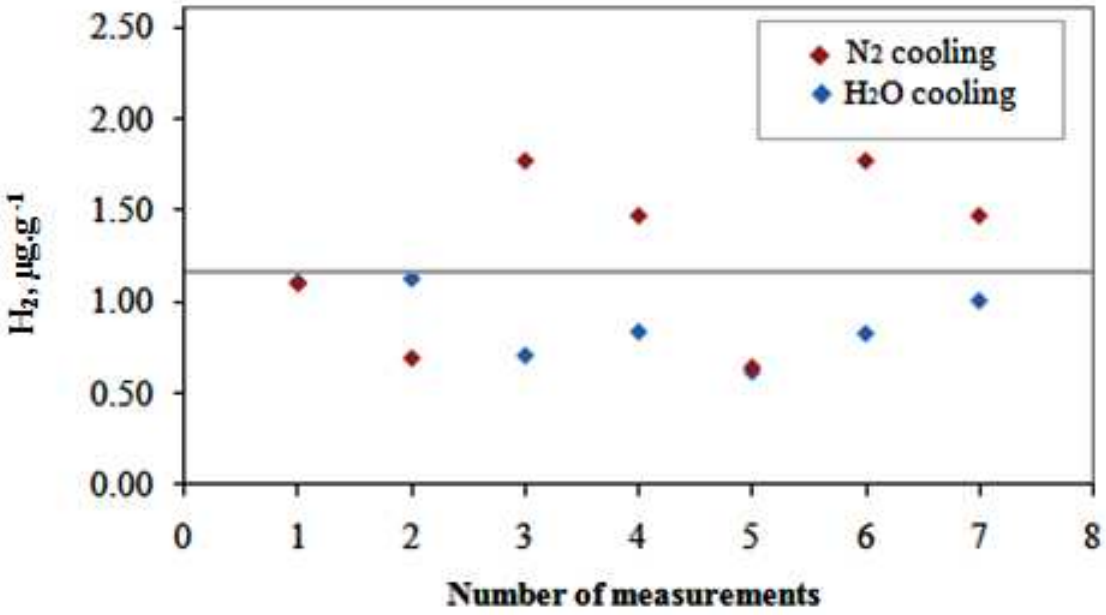

Figure 5-35: The total hydrogen concentration (µg·g^{-1}) determined by TCD in samples cooled by water and nitrogen.

Table 5-16: The total hydrogen concentration ($\mu g \cdot g^{-1}$) in melted pure Fe grains.

Iron blocks (production site) H_2 ($\mu g \cdot g^{-1}$)	Iron chips melted in high frequency furnace (laboratory) H_2 ($\mu g \cdot g^{-1}$)	
	Cooled with water	Cooled with liquid nitrogen
1.01 ± 0.1	0.89 ± 0.20	1.27 ± 0.47

To research further on the influences of alloying elements, 1 % of the elements: titanium, vanadium, silicon and carbon were also melted with Fe as a base according to the mentioned procedure. They were cooled with water, cut to 1g for total hydrogen determination by melt extraction and 2 g for diffusible hydrogen analysis with TDMS.

Before hydrogen determination, the concentration of the steel alloying elements in the samples (w/w %) was confirmed by using spark ablation optical emission spectroscopy. The results are listed in table 5-17.

Table 5-17: The contents (w/w %.) of steel alloying elements that were measured by spark ablation optical emission spectroscopy.

(%)	FeC rough	FeC fine	FeMn	FeVC	FeSiC	FeTiC	FeSiTiVC	FeV	FeSi	FeTi	FeSiTiV	FeTiMnV
C	0.92	0.53		0.53	0.79	0.80	0.82					
Mn			0.72									0.96
V				0.82			0.83	0.73			0.82	0.84
Si					0.90		0.95		0.87		0.97	
Ti						0.83	0.85			0.43	0.69	0.65

5.7.2 Effect of carbon grain size on diffusible and total hydrogen

The carbon was added to the Fe grains in a rough grain and fine powdered form. The hydrogen concentrations obtained are listed in table 5-18. The TDMS measurement (1200 °C/h) in figure 5-36 showed no diffusible hydrogen in pure iron, but upon the addition of carbon, there was a distribution of hydrogen in the sample due to the presence of carbides in the crystalline structure. In FeC with rough carbon grains, 0.08 $\mu g \cdot g^{-1}$ of diffusible hydrogen concentration was released at low temperatures between 200 and 300 °C. This confirmed the presence of reversible traps.

In FeC with fine carbon powder, no hydrogen was released at temperatures below 400 °C. Therefore stronger hydrogen trapping tendencies existed. Above 400 °C the hydrogen desorption peaks were incompletely separated and that implied the difficulty of hydrogen escape from traps within the sample when insufficient heat energy was applied.

Between 400 °C and 600 °C the diffusible hydrogen concentration was calculated to 0.41 $\mu g \cdot g^{-1}$. It was decided to use the rough carbon grains for alloying samples in chapter 5.7.3.

The same pattern was obtained from total hydrogen measurements.

Table 5-18: Hydrogen content in samples with fine and rough carbon grains.

Hydrogen ($\mu g \cdot g^{-1}$)	Fe (pure, 99.99 %)	FeC (rough grains)	FeC (fine powder)
Total	0.89 ± 0.20	1.01 ± 0.25 $\mu g \cdot g^{-1}$	1.34 ± 0.18 $\mu g \cdot g^{-1}$
Diffusible	< 0.05	0.08	0.41

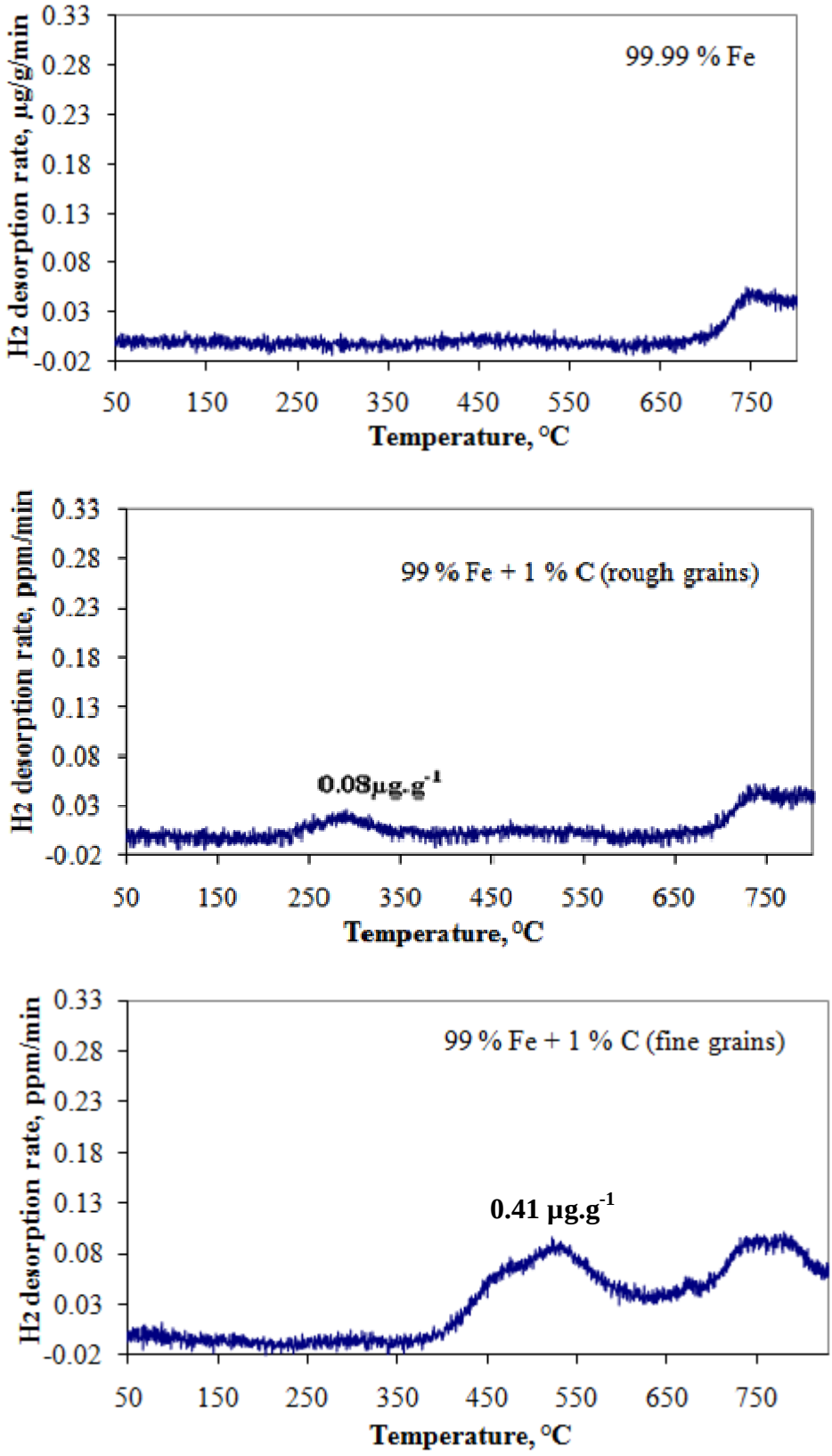

Figure 5-36: Hydrogen desorption at 1200 °C/h from **(a)** Fe **(b)** FeC with rough carbon grains, **(c)** FeC with fine carbon powder

5.7.3 Influence of Ti, Si and V alloys on diffusible and total hydrogen in steel

These elements were firstly alloyed with Fe and the hydrogen analysis took place. Thereafter carbon with rough grains was added to the ferroalloys to compare the results. According to results in table 5-19 and figure 5-37 to 5-40, the diffusible and total hydrogen concentration increased after the addition of carbon by a factor of approx. 2 to 2.5.

In ferroalloys (FeTi, FeSi, FeV) the hydrogen concentration was almost equal to the concentration of hydrogen in pure iron which was 1 $\mu g \cdot g^{-1}$ in table 5-18.

In FeTiC, FeSiC and FeVC, the diffusible hydrogen was mostly released at low temperatures between 100 °C to 350°C which indicated the presence of reversible traps. When comparing the hydrogen desorbed from other elements, V seemed to have increased the diffusible hydrogen content in the temperature range of up to 350 °C. In FeTiSiVC, an additional hydrogen desorption peak appeared at the temperature range of 500 °C to 800 °C which also can be an indication of stronger trapping tendencies.

Table 5-19: The diffusible and total hydrogen ($\mu g \cdot g^{-1}$) in metals alloyed with and without carbon.

Alloy	Diffusible (µg·g-1)	Total hydrogen (µg·g-1)
Fe	0.00	0.89 ± 0.20
FeC	0.08	1.01 ± 0.00
FeV	0.25	0.86 ± 0.14
FeVC	0.83	1.53 ± 0.15
FeTi	< 0.05	0.82 ± 0.06
FeTiC	0.77	2.68 ± 0.04
FeSi	< 0.05	0.6 ± 0.03
FeSiC	0.42	2.24 ± 0.00
FeVSiTi	0.17	0.87 ± 0.05
FeVSiTiC	0.40	1.97 ± 0.26

*Heating rate at 1200 °C/h, hydrogen peaks were desorbed between 100 °C and 400 °C.

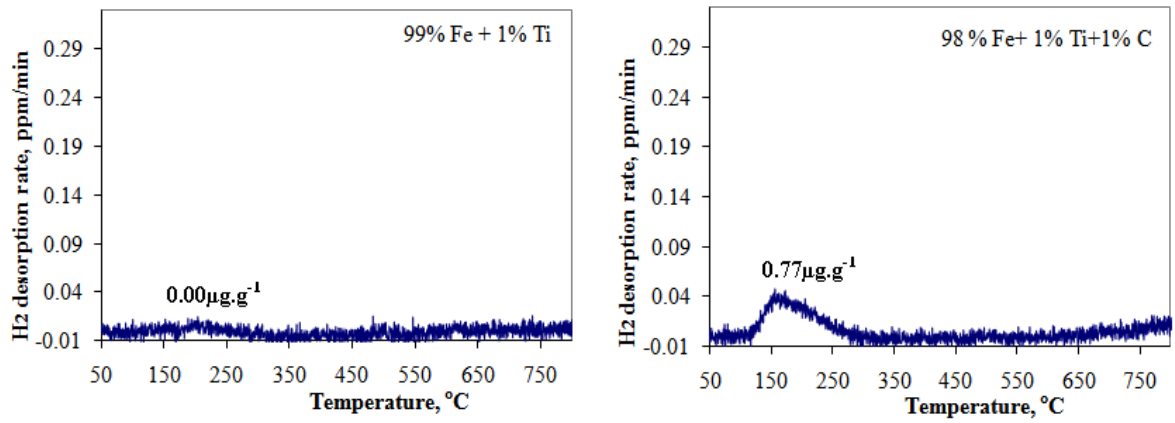

Figure 5-37: Diffusible H_2 concentration in FeTi and in FeTiC.

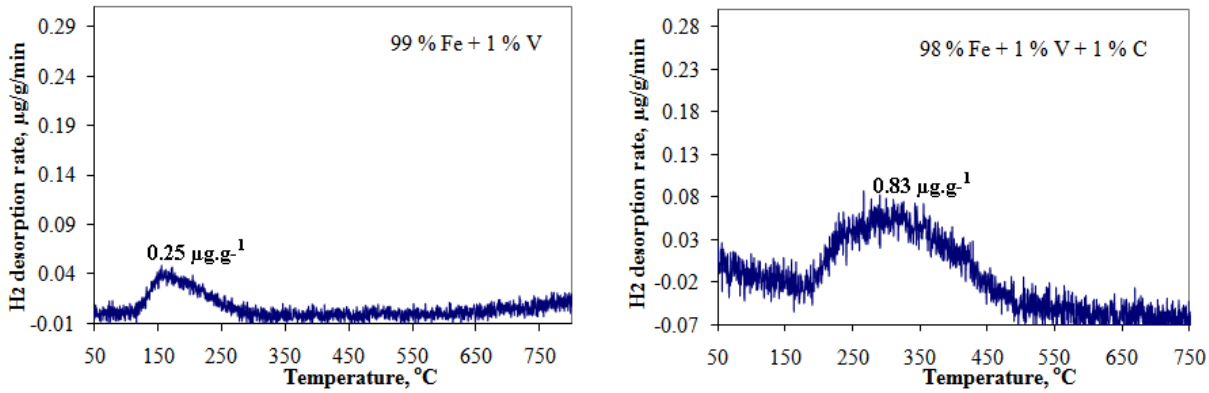

Figure 5-38: Diffusible H_2 concentration in FeV and in FeVC.

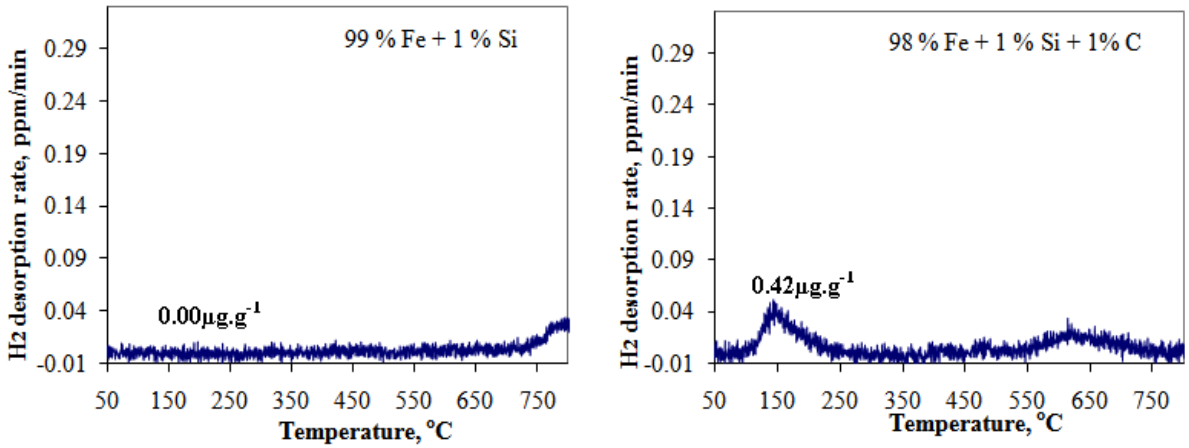

Figure 5-39: Diffusible H_2 concentration in FeSi and in FeSiC.

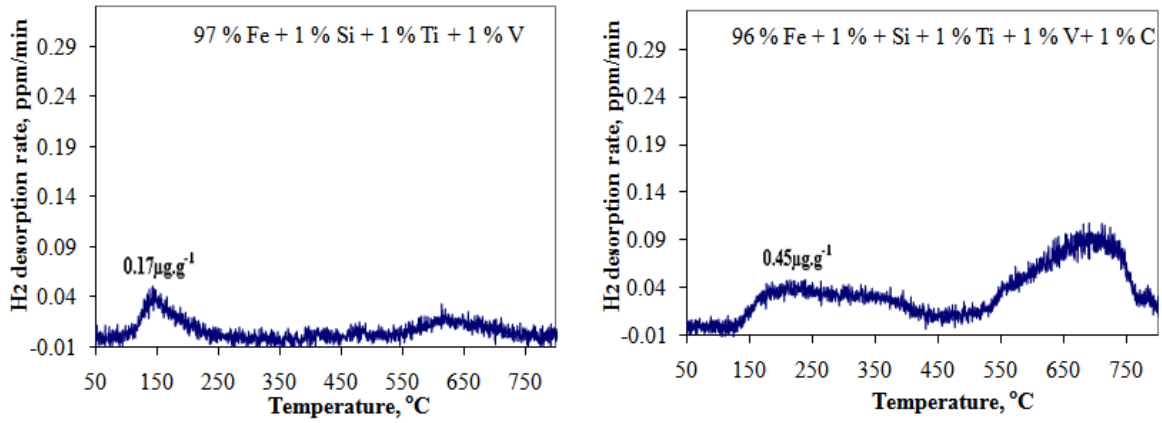

Figure 5-40: Diffusible H_2 concentration in FeTiSiV and in FeTiSiVC.

5.7.4 Qualitative analysis of alloys microstructure

The above mentioned alloys in figures 5-37 to 5-40 were qualitatively analysed by optical microscope and energy dispersive x-ray spectroscopy (LEO with Zeiss Axiocam).The resulting structures are in figure 5-41 to 5-44.

In FeTi, FeSi, FeV, the ferrite structure was obtained. Whereas in alloys that contained carbon (FeTiC, FeSiC and FeVC), the pearlite structure dominated with some parts showing bainite and martensite structures. Therefore, the pearlite microstructure influenced the higher total and diffusible hydrogen concentrations in carbon alloys.

In case of FeSiTiVC the residual austenite seemed to have enhanced the irreversibility of traps at higher temperatures. EDX analysis was summarized in table 5-20 and there are no significant reasonable interpretations. The element Al that was found in some samples could be a contaminant of the sample holder during melting in the oven.

Because these samples were prepared at the laboratory scale, they did not really resemble the real steel characteristics. Therefore, a well defined production program with optimized heating and cooling parameters is still required for producing normal samples in order to characterize the microstructure.

Table 5-20: Impurities found in alloyed steel samples.

Alloyed sample	Impurity phases, inclusions
FeSi	Nonmetallic inclusions (Al,Si,O), sporadic
FeTi	TiN, often; spinal (Ti, Al, O), sporadic
FeV	VN, often; mixed oxide (Al, Si, V,O), sporadic
FeSiTiV	(Ti,V)N, often; Ti (C,N) often
FeSiC	SiO, O, often
FeTiC	Ti (C,N), often; mixed carbides (Ti, Al, C), often
FeVC	VN, often; (Al, V) O, often

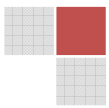

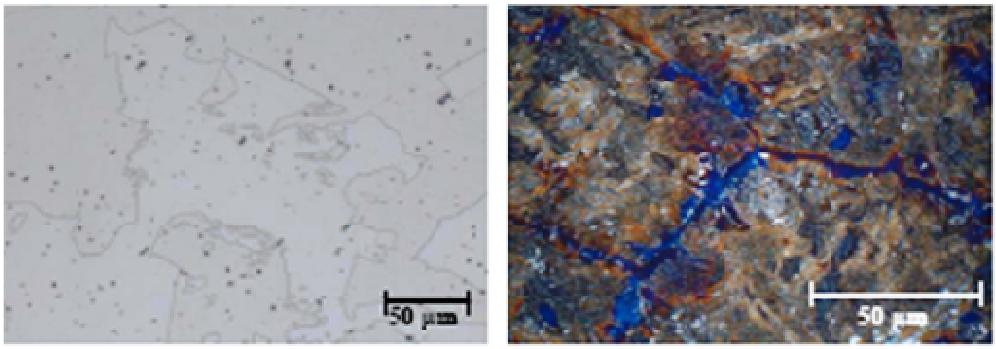

Figure 5-41: The microstructure of **(a)** FeV and **(b)** FeVC.

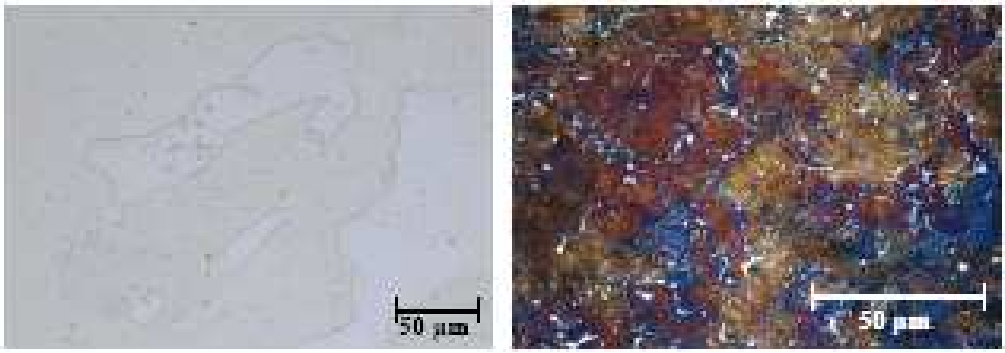

Figure 5-42: The microstructure of **(a)** FeTi and **(b)** FeTiC.

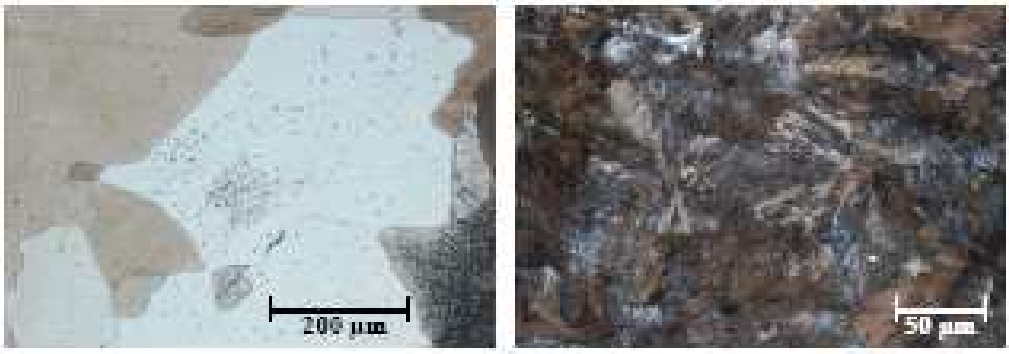

Figure 5-43: The microstructure of **(a)** FeSi and **(b)** FeSiC.

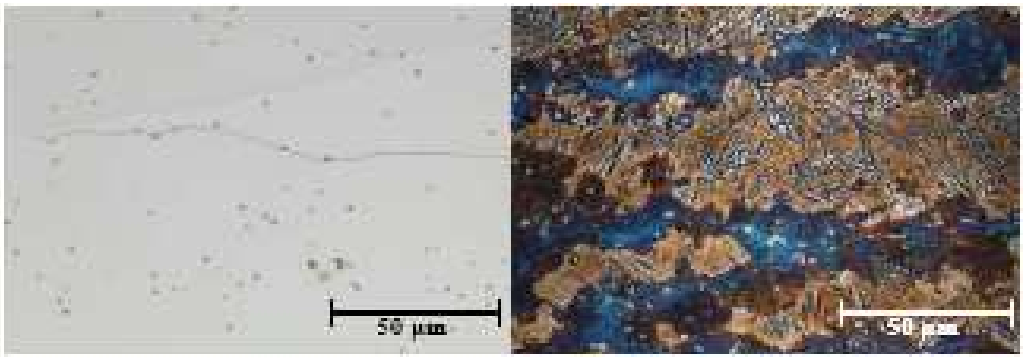

Figure 5-44: The microstructure of **(a)** FeSiTiV and **(b)** FeSiTiVC

5.7.5 Comparison of carbon to boron alloys

After observing the increase of diffusible and total hydrogen amount due to addition of carbon in chapter 5.7.3, boron was suggested as a substitute because of its similar hardening properties like carbon.

The first exploratory analysis to test the influence of boron was done by alloying 1 % of B with pure Fe, then with FeTi and FeV. The contents of the alloying elements (w/w %) after melting them were measured with ICP-OES (Thermo Fischer Scientific. The results illustrated in table 5-21 indicated that during sample melting in the furnace, most of the boron was lost in FeB; either by evaporation due to high temperature or it remained on the walls of the crucible.

A higher diffusible and total hydrogen amount in FeB than FeC has been observed according to the results shown in table 5-22 and figure 5-45. The diffusible hydrogen in FeB released at 250°C was almost equal to the total hydrogen in FeC which is approx. 1 $\mu g \cdot g^{-1}$. Therefore, it seemed that the traps formed by boron alloy were reversible. Hence high diffusible hydrogen concentrations were obtained.

Upon the addition of vanadium to both alloys FeB and FeC the diffusible hydrogen concentration decreased in FeB alloy from 1.00 $\mu g \cdot g^{-1}$ to 0.49$\mu g \cdot g^{-1}$. Vanadium could have trapped some of the hydrogen in FeBV alloy. But vanadium addition in FeC increased the diffusible hydrogen concentration from 0.08$\mu g \cdot g^{-1}$ to 0.83$\mu g \cdot g^{-1}$. This effect of vanadium on the hydrogen concentration in FeC and FeB could not be explained. Therefore, micro structural analysis is necessary to identify this effect.

In FeC, low diffusible hydrogen concentration was released at 280°C which confirmed the strong trapping character of carbon than boron. But more information based on activation energies will be able to identify whether boron or carbon has less reversible traps to inhibit the mobility of hydrogen in chapter 5.8.3.

Table 5-21: The boron contents (w/w %) in different alloys.

Boron content (%)		
FeB	FeTiB	FeVB
0.29 ± 0.16	0.57 ± 0.11	0.82

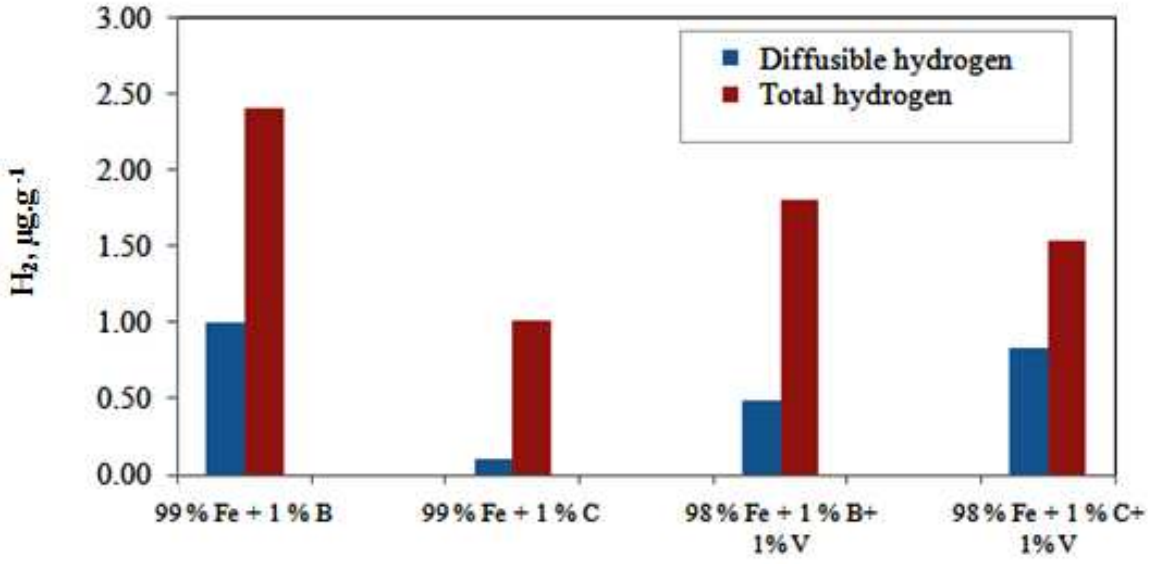

Figure 5-45: The comparison of diffusible and total hydrogen concentration in FeB, FeBV, FeC and FeCV alloys.

Table 5-22: The diffusible and total hydrogen concentration (µg·g$^{-1)}$ in boron and carbon alloys.

Alloy	Diffusible H_2	Total H_2
FeB	1.00	2.40 ± 0.42
FeC	0.08	1.01 ± 0.00
FeBV	0.49	1.84 ± 0.12
FeCV	0.83	1.53 ± 0.15

5.8 Characterization of diffusible hydrogen activation energy in traps.

5.8.1 Mathematical model for calculating desorption energies

Thermal desorption spectrometry has been used together with the application of mathematical procedure for calculating the hydrogen desorption process and the energy required by hydrogen to leave the traps (activation energy). The first hydrogen desorption/adsorption models were proposed by Choo and Lee [31] illustrated in figure 5-46.

$$\boxed{H}_{trap} \rightleftarrows \square_{trap} + H_{(in\ lattice)} \qquad (12)$$

The lowest energy level in desorption process is the trap. The difference between the trap and the lattice energy level is the binding energy between the trap and the hydrogen (Eb). The trap activation energy (Ea) is then the sum of the binding energy and the saddle point energy around the trap (Es). Finally, there is the diffusion energy (Ed), which is not considered by this model.

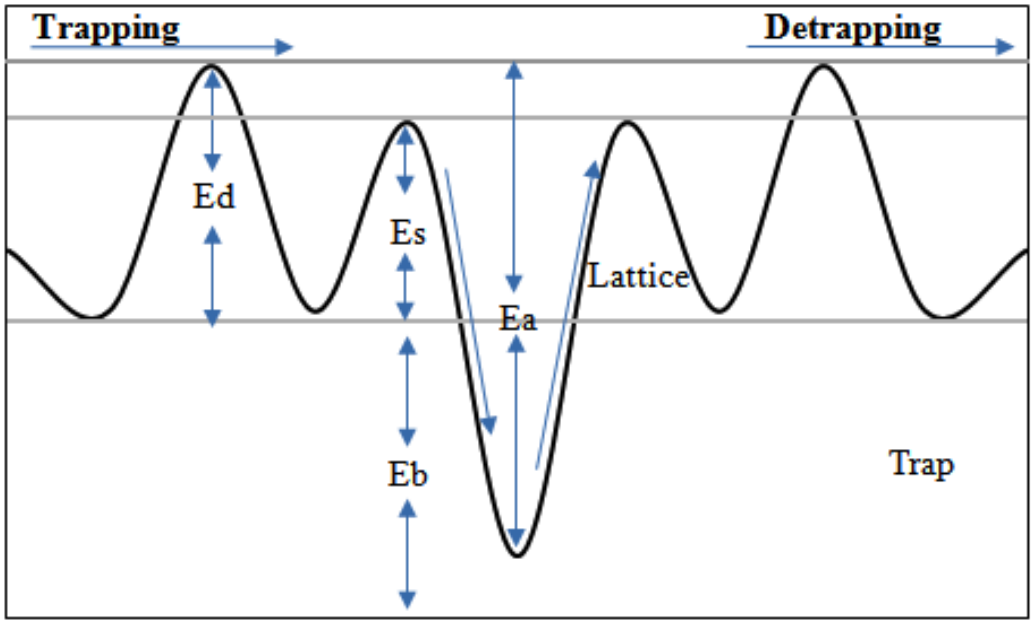

Figure 5-46: Energy levels of hydrogen trapping / detrapping mechanisms in steel.

A hydrogen escape rate can be derived from the Polanyi-Wigner equation, which involves a desorption rate of nth order and a rate constant described by the *Arrhenius* equation as shown below:

$$r_{des} = \frac{d\Theta}{dt} = \nu_n \cdot \exp\left(-\frac{\Delta E_{des}}{R \cdot T}\right) \cdot \Theta^n \qquad (13)$$

Where

r_{des}: desorption rate

Θ: surface coverage or trap occupation

ν_n: frequency factor

ΔE_{des}: desorption activation energy

n: order of the desorption rate

R: gas constant

T: absolute temperature (°C)

Supposing at first order desorption rate, the Polanyi-Wigner equation can be written as following:

$$dt = \frac{1}{\phi} \cdot dT \tag{14}$$

$$\frac{d\Theta}{dT} = -\frac{1}{\phi} \cdot \nu_n \cdot \exp\left(-\frac{E_a}{R \cdot T}\right) \cdot \Theta^n ,$$

Where:

Φ: heating rate

The maximum escape rate at the temperature Tp is given by the following relation:

$$0 = \frac{d^2\Theta}{dT^2}\Big|_{Tp} = n \cdot \Theta^{n-1} \cdot \frac{d\Theta}{dT} + \Theta^n \cdot \frac{E_a}{R \cdot T^2} \tag{15}$$

Where

Tp: is the maximum peak temperature

Thus, yielding:

$$\frac{Ea}{R \cdot T_p^{\,2}} = -\frac{1}{\phi} \cdot \nu_n \cdot n \cdot \Theta^{n-1} \exp\left(-\frac{Ea}{R \cdot T_p}\right) \tag{16}$$

If the 1st order desorption is assumed (n=1), then the peak temperature (Tp) is only dependent on the heating rate (Φ) as shown below:

$$\frac{Ea}{R \cdot T_p^{\,2}} = -\frac{1}{\phi} \cdot \nu_1 \cdot \exp\left(-\frac{Ea}{R \cdot T_p}\right)$$

By taking the logarithm and rearrangement, a linear version of the above equation can be written as follows:

$$\ln\left(-\frac{\Phi}{T_p^{\,2}}\right) = -\frac{E_a}{R \cdot T_P} + \ln\left(\frac{E_a}{\nu_1 \cdot R}\right)$$

Desorption activation energy can calculated from the gradient of the above equation:

$$\frac{\partial \ln\left(\frac{\Phi}{T_p^{\,2}}\right)}{\partial\left(\frac{1}{T_p}\right)} = -\frac{E_a}{R} \qquad (17)$$

This formulation leads to the most commonly applied method for the determination of the activation energy, which is to measure thermal desorption spectra of the same sample at different heating rates to determine E_a from the shift of the peak temperature.

A single steel material has usually several kinds of traps and lattice sites, in which hydrogen can reside. That means, a thermal desorption spectrum usually presents not only one, but several desorption peaks, which have to be individually characterized.

Due to the overlapping of the peaks, a deconvolution of the desorption spectrum is usually necessary in order to characterize a material with multiple traps. The hydrogen released from the trap is believed to have a *Gaussian* distribution [31, 93] which is systematic peak represented by equation 18 and figure 5-47.

$$I(x) = y_0 + A \cdot \exp\left(\frac{-(x-C)^2}{2 \cdot B^2}\right) \qquad (18)$$

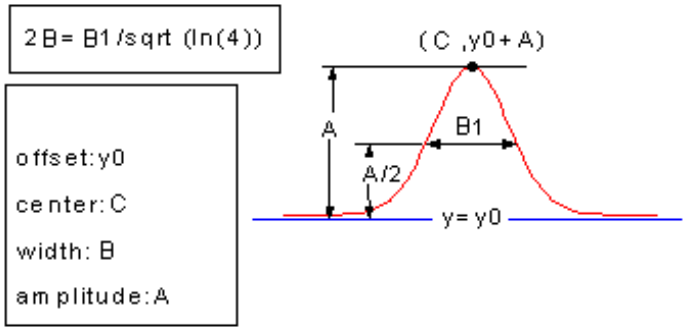

Figure 5-47: Gaussian peak

Interpretation o f the model and equations: The whole spectrum is then interpolated by the sum of a given number of *Gaussian* peaks, each representing an absorption site in the steel. By increasing the heating rate, desorption peaks shift to higher temperatures. Thus, activation energy can be calculated for each *Gaussian* peak through the slope of the *Arrhenius* plots:

$$\ln\left(\frac{\Phi}{T_p^{\,2}}\right) \quad \text{versus} \quad \left(\frac{1}{T_p}\right)$$

1. The diffusion of hydrogen from the interior to the surface of the material, as well as the surface impendence is not considered to be rate controlling processes.
2. The traps are sparsely distributed, so that there is no interaction between them.
3. The retrapping of hydrogen is neglected.

These simplifications imply that there are some limitations concerning the sample size and geometry, surface characteristics, heating rate and hydrogen concentration. In order to minimize the influence of the diffusion, e.g. the diameter of a cylindrical sample should be small as possible. Furthermore, an appropriate surface treatment is required in order to avoid the influence of surface impedance, recombination kinetics and retrapping events. The heating rates must be low as possible so that desorption is the only rate controlling process. High hydrogen concentration can also increase the interaction between traps but it is not considered by this model.

5.8.2 Certified reference material

The trapping and desorption characteristics of hydrogen were studied by measuring the amount of thermally desorbed hydrogen from Leco 501-061 with certified hydrogen concentration of 2.19 ± 0.35 $\mu g \cdot g^{-1}$. The sample was in a cylindrical pin form that weighed about 5g. The sample was analysed by applying different heating rates from 0.1 to 1 K/s and the spectra is illustrated in figure 5-48.

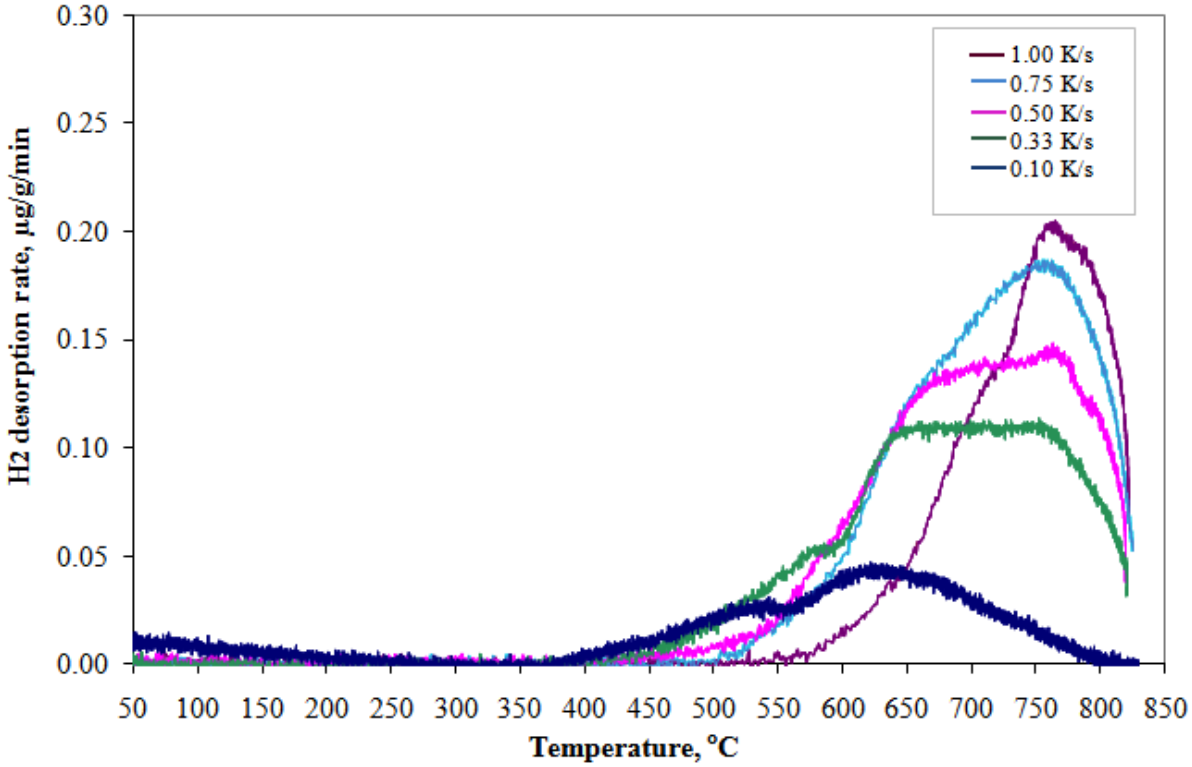

Figure 5-48: Thermal-desorption spectrum of Leco 502-061 analysed by TDMS at different heating rates.

At lower heating rates the maxima of the desorption curves shifted to lower temperatures. In each peak, different hydrogen desorption at particular temperatures were noticed. To identify the sufficiently resolution peaks, the *Gaussian* curves were fitted as shown in figure 5-49.

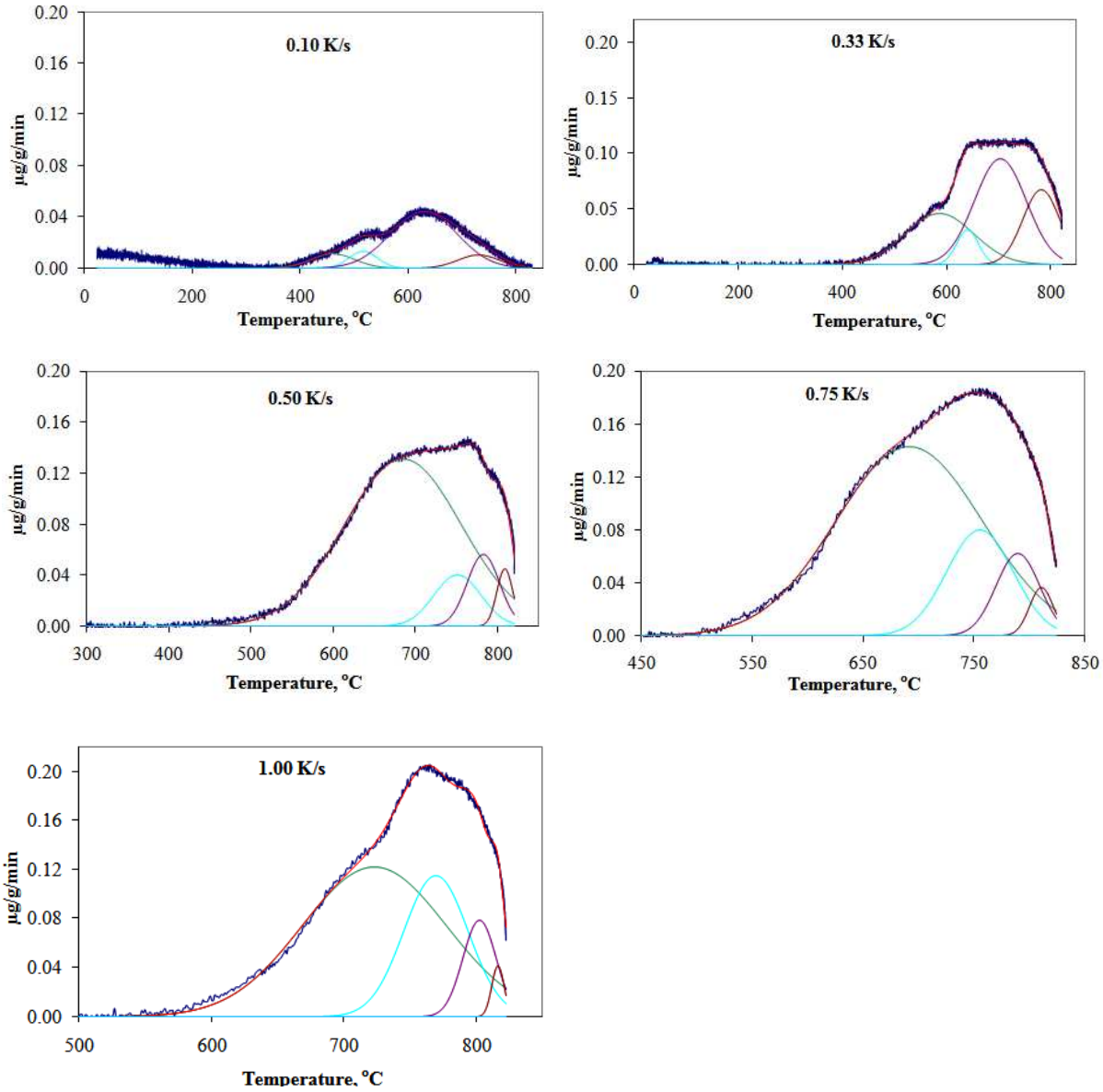

Figure 5-49: Peak deconvolution of thermal desorption spectra.

The sum of diffusible hydrogen concentration (1.89 ± 0.15 $\mu g \cdot g^{-1}$) from different heating rates was determined by obtaining the integral value under the interpolated curves. This TDMS measurement was also compared to TCD measurement at 1040 °C with the resistance furnace (chapter 5.1.4) and 1.73 ± 0.20 $\mu g \cdot g^{-1}$ of hydrogen concentration was obtained.

The TDMS does not only quantify diffusible hydrogen but it also provides information on diffusibility at various temperatures. There are publications which describe both theoretical and experimental thermodynamic kinetics of diffusion and desorption processes in table 5-23.

Table 5-23: Hydrogen desorption activation energies of hydrogen in traps determined by various research groups.

Source	Material	Trap	Ea (kJ/mol)
[2]	Pure iron	Grain boundary	17.2
		Dislocation	26.8
		Microvoid	35.15
[66]	Austenitic stainless steel	Grain boundary	180
		CrC	96
			87
			73
[100]	-	Impurities, precipitates	86.8
[101]	Fe-Ti-C	Grain boundary	93.6
		TiC	25.8
		Dislocation	23.9
		Ti subst. atom	25.8
		α-Fe	7.6
[102]	Ti-added steel	Grain boundary	21.9
			32
		Incoherent TiC	85.7
			68 – 116
		Coherent TiC	46 – 54
[103]	High-strength steel	Complex sites, lower energy	23.4
		Ferrite / Fe_3C interface (strained, dislocation)	65
[31]	V-added steel	VC	33-35
[94]	-	TiC	86.9
[104]	-	α-Fe	6.85

Choo and Lee [31] used experimental data to calculate the desorption activation energies of traps in steel (figure 5-46) and the same model was used to calculate activation energies according to equation 17 in reference material (Leco 502-062) which was analysed by applying heat from 50 °C to 950 °C at the rate of 0.1 to1 K/s. The resulting activation energies of hydrogen with steel traps are plotted in figure 5-50 and the distribution percentages are listed in table 5-24.

The *Arrhenius* plots from equation 17 were relatively linear and the activation energies seem to be consistent with values found in the literature in table 5-23 which range from about 10 to180 kJ/mol.

The traps with the lowest activation energies (38.78 and 45.24 kJ/mol) are probably related to coherent carbides. Activation energies of 33-35 and 46-54 kJ/mol were related by prior works to vanadium and titanium carbides, respectively. The third located trap with activation energy of 86.59 kJ/mol is most probably related to incoherent carbides, since values ranging from 85.7 to 87 kJ/mol are related to this trap type by many publications. The strongest trap was 221.43kJ/mol and could not be associated to any trap found in the available literature. This implies that there are still undiscovered traps in this material, therefore metallurgical characterization of the material must be applied to discover the particles in the metallic lattice that are responsible for strong trapping of hydrogen. The highest activation energy found in the literature in table 5-23 was 180 kJ/mol which is related to the grain boundary of an austenitic stainless steel.

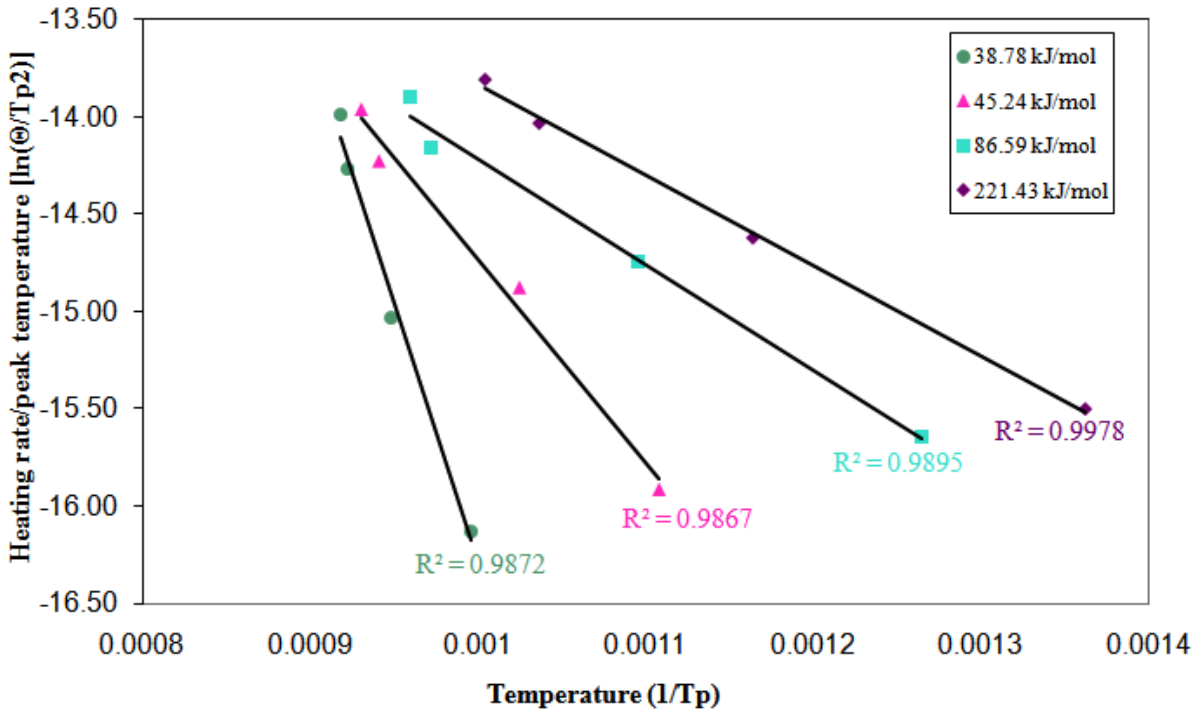

Figure 5-50: Arrhenius plot of Leco 502-061 for calculating activation energy of hydrogen interaction with traps.

Table 5-24: Distribution of hydrogen (%) in the traps at different heating rates

	0.10 K/s	0.33 K/s	0.75 K/s	1.00 K/s
Trap 1	9.38 %	22.53 %	52.69 %	38.51 %
Trap 2	7.69 %	5.24 %	21.51 %	25.85 %
Trap 3	70.97 %	46.47 %	19.31 %	19.62 %
Trap 4	11.96 %	41.12 %	11.03 %	8.69 %

5.8.3 High Strength Steel

Three high strength steel materials (HS-1, HS-2 and HS-3) with similar properties were analysed with TDMS in order to determine desorption activation energies and the concentrations of diffusible hydrogen to eventually characterize the resistance of materials against hydrogen embrittlement. The heating rates were ranging from 0.1 to 0.75 K/s. The hydrogen appeared to be released from a single desorption site, although some spectra especially at higher heating rates were not correlated well by a single Gaussian peak. The Arrhenius plot based on the single trap assumption yielded a better linearity and consistent activation energy as shown in figure 5-51, 5-52 and 5-53.

In sample HS-1, the activation energy of 42.22 KJ/mol could be related to coherent carbides in table 5-22. The diffusible hydrogen obtained from the spectra was 0.63 ± 0.13 $\mu g \cdot g^{-1}$ while the total hydrogen measured by melt extraction was 2.71±0.15 $\mu g \cdot g^{-1}$. The diffusible hydrogen of 1.02 ± 0.2 $\mu g \cdot g^{-1}$ was determined by solid extraction in the resistance furnace (1040 °C) by using TCD

It is assumed that in such high strength steels, hydrogen is located in strong irreversible traps which could not be detected by TDMS because the hydrogen concentrations obtained by MS were lower than those obtained by TCD value.

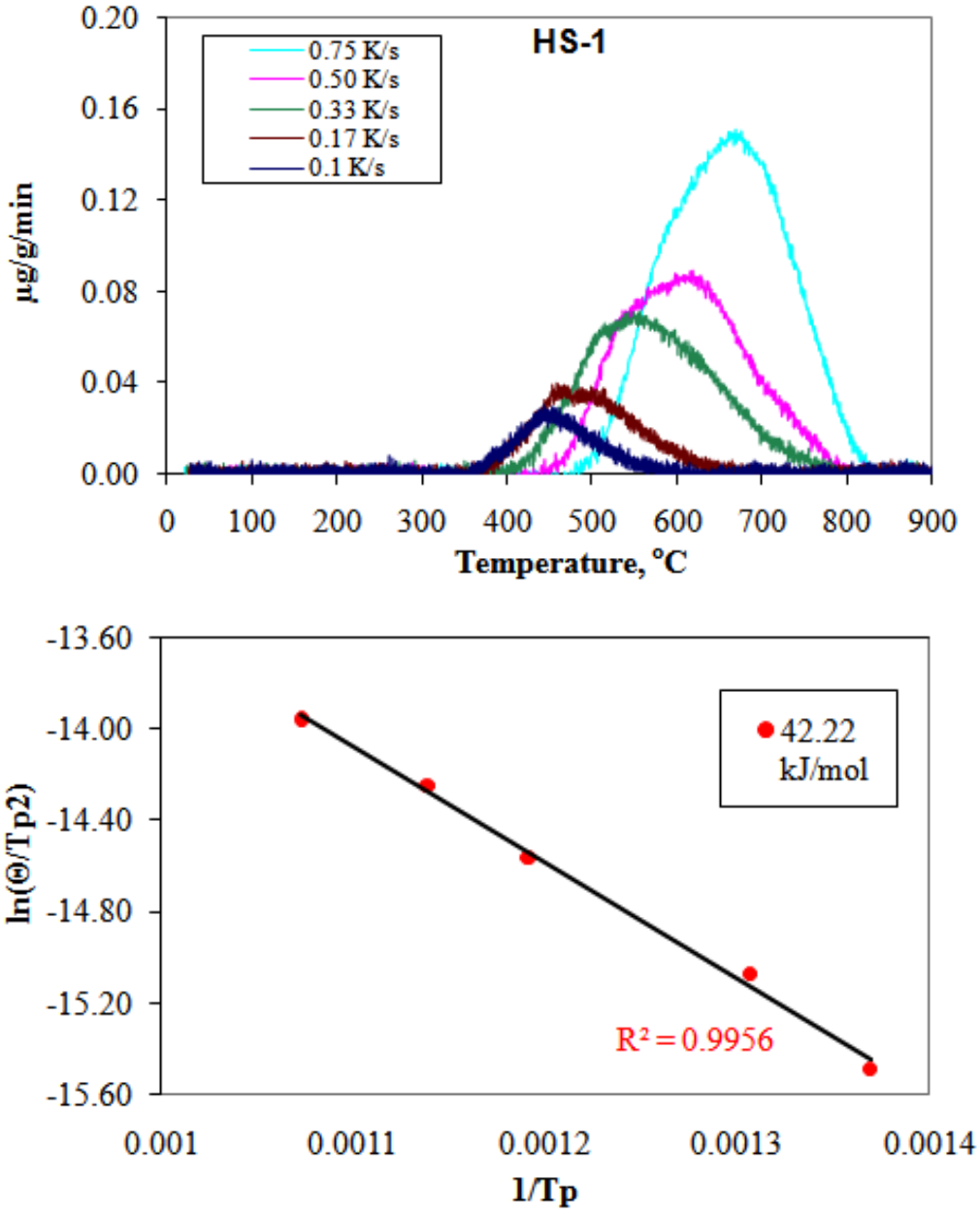

Figure 5-51: (a) Thermal desorption spectra of sample HS-1 and **(b)** *Arrhenius* plots of activation energy.

A single hydrogen trap was also detected in HS-2 which presented similar properties to HS-1 but with lower hydrogen concentration and slightly stronger trapping tendencies in figure 5-52. The activation energy of 48.55 KJ/mol was also on the same level and related to coherent carbides in table 5-23. The slightly higher value can be explained by the presence of a different type of carbide resulting from different alloy. The diffusible concentration was 0.39 ± 0.05 $\mu g \cdot g^{-1}$ which was lower than the bulk hydrogen concentration of 2.78 $\mu g \cdot g^{-1}$. Analysing the sample HS-2 higher diffusible hydrogen concentrations of 1.07 $\mu g \cdot g^{-1}$ was obtained from the same isothermal extraction method at 1040 °C.

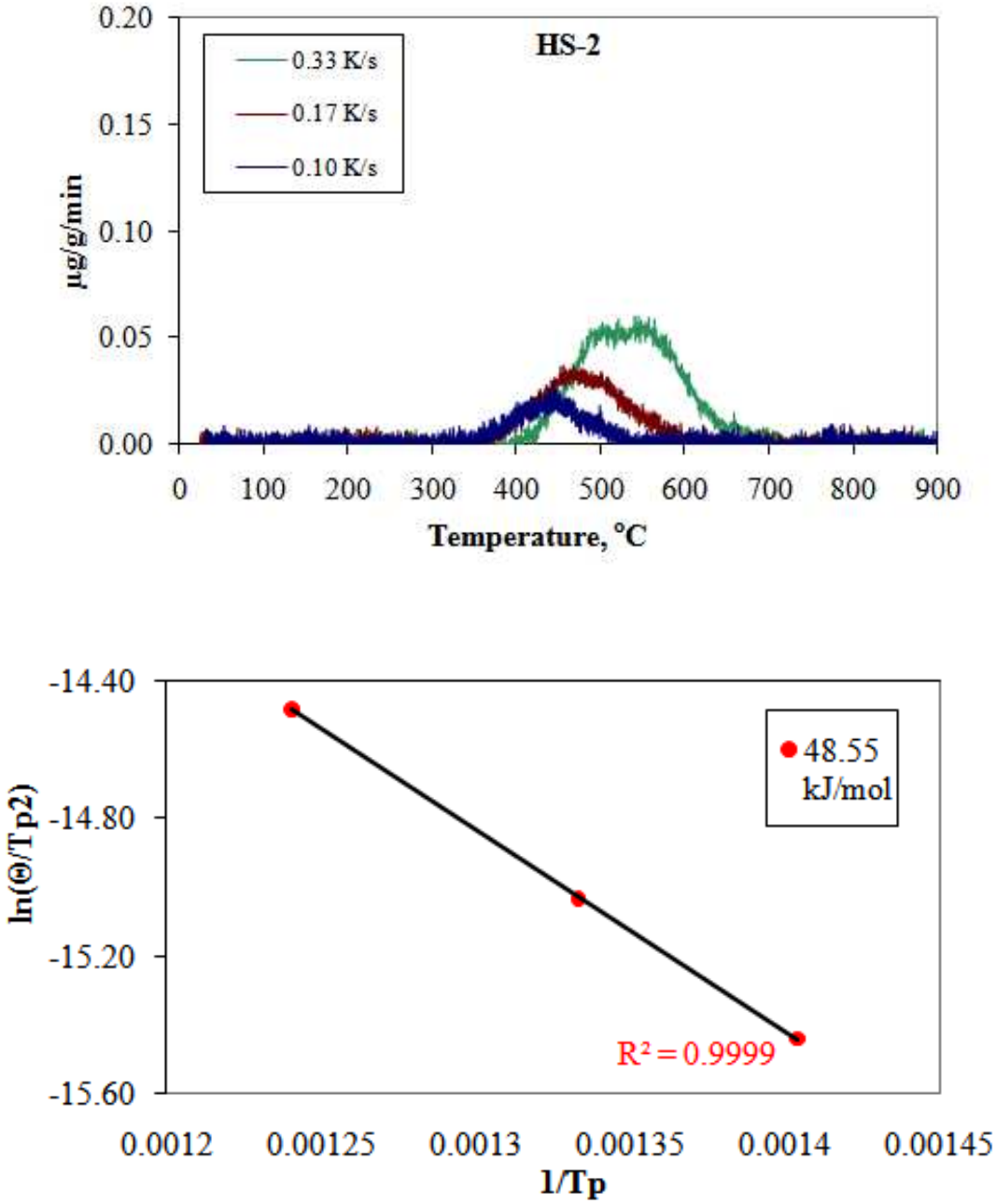

Figure 5-52: (a) Thermal desorption spectra of sample HS-2 and **(b)** Arrhenius plots of activation energy.

In the last sample HS-3, higher diffusible hydrogen concentration of 1.34 ±0.41 $\mu g \cdot g^{-1}$ was recovered from TDMS analysis while the bulk concentration was 6.13$\mu g \cdot g^{-1}$ from melt extraction. The isothermal extraction leads to higher concentrations (3.25$\mu g \cdot g^{-1}$). The investigations of sample HS-3 showed the weakest trap with the activation energy 31.68 KJ/mol.

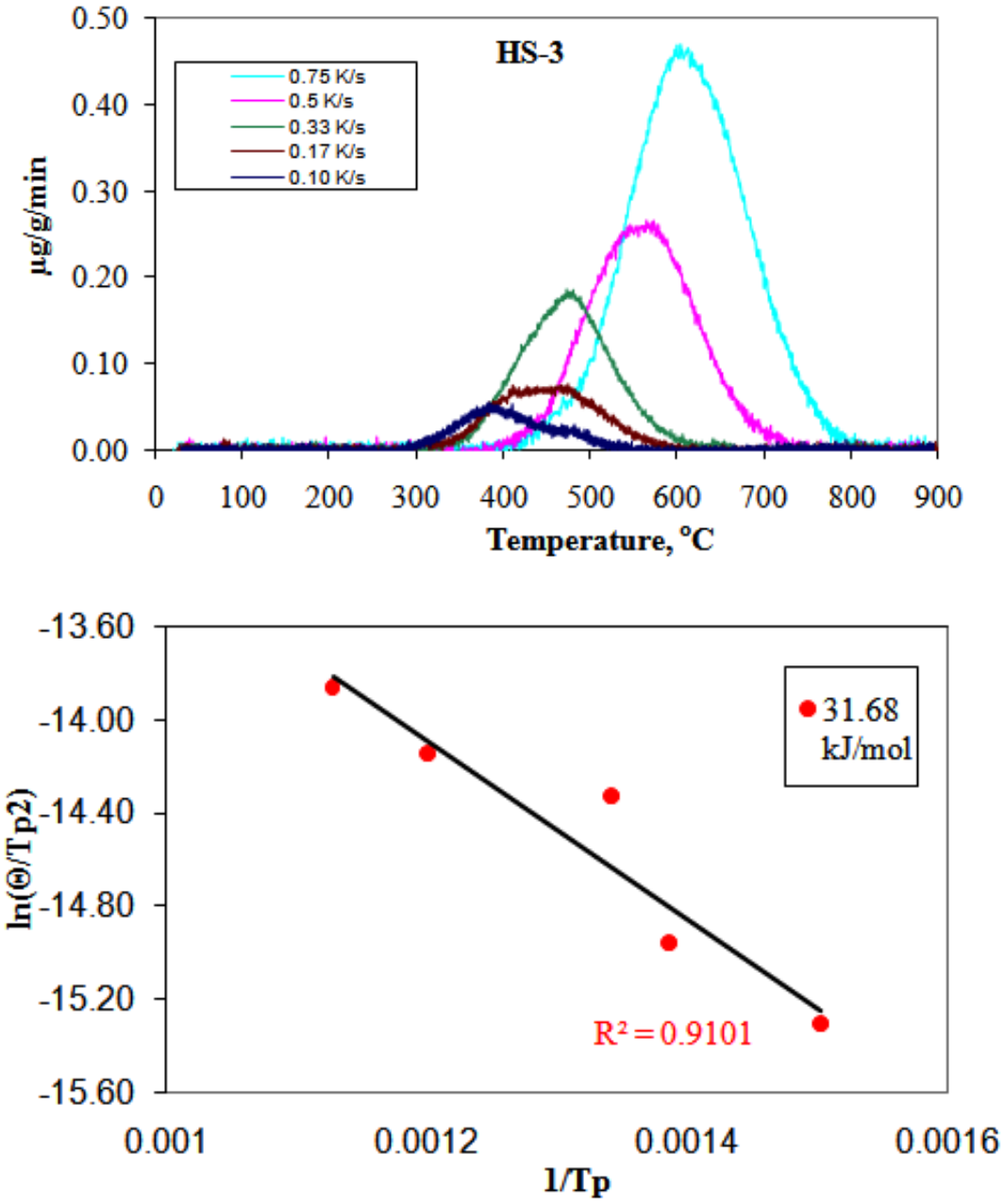

Figure 5-53: (a) Thermal desorption spectra of sample HS-3 and **(b)** Arrhenius plots of activation energy.

The amount of the diffusible hydrogen was lower than the amount of total hydrogen in all three samples. This implied that these high strength steels have irreversible hydrogen traps within the microstructure. The highest value of activation energy was calculated for HS-2. This is related to the strongest traps. Therefore, it is reasonable to conclude that it cannot be easily embrittled.

In contrast, sample HS-3 had the lowest activation energy (weakest trap). Hence higher diffusible hydrogen values were obtained and this means that there is a high possibility of hydrogen embrittlement.

It was also observed that as the heating rate increased, the concentration of hydrogen also increased. Therefore, the dependence of diffusible hydrogen concentration determined by TDMS on heating rate could be related to a possible phase transformations occurring during the heating process. These phase transformations could also influence the activation energy determination. Here more research can clear this point.

Applying isothermal extraction the sample heating takes place very fast (3 min), from room temperature to 1040 °C which could induce changes in the microstructure of the steel and decrease the amount of reversible traps. Hence higher diffusible hydrogen concentrations were obtained.

5.8.4 Hydrogen traps in carbon and boron alloys

The trapping characteristics of FeTiC and FeTiB were also quantified by an application of *Arrhenius* plots in equation 17 using the same method in 5.8.1 and 5.8.2 and the results are in figure 5-54 and 5-55.

The FeTiC sample contained 35.91 kJ/mol of activation energy and it was referred to as the grain boundary which was found at 32 kJ/mol [94]. The activation energy of 29.56 kJ/mol corresponded to TiC with 25.8 kJ/mol activation energy or with Ti that acted as the substitution atom [31]. There was also 42.29 kJ/mol of hydrogen activation energy in FeTiC that could have been released from coherent TiC traps with desorption activation energy of 46-54 kJ/mol [94].

The FeTiB samples were having very low activation energies from 10-13 kJ/mol which were not associated with any energy in literature listed in table 5-23. In this case also more characterisation on trapping particles in FeTiB is required for tracing the origin of hydrogen activation energy values.

Obviously in FeTiC, there are fewer possibilities for embrittlement occurrence due to higher activation energies while FeTiB has the lowest activation energies which implied that it can be easily embrittled.

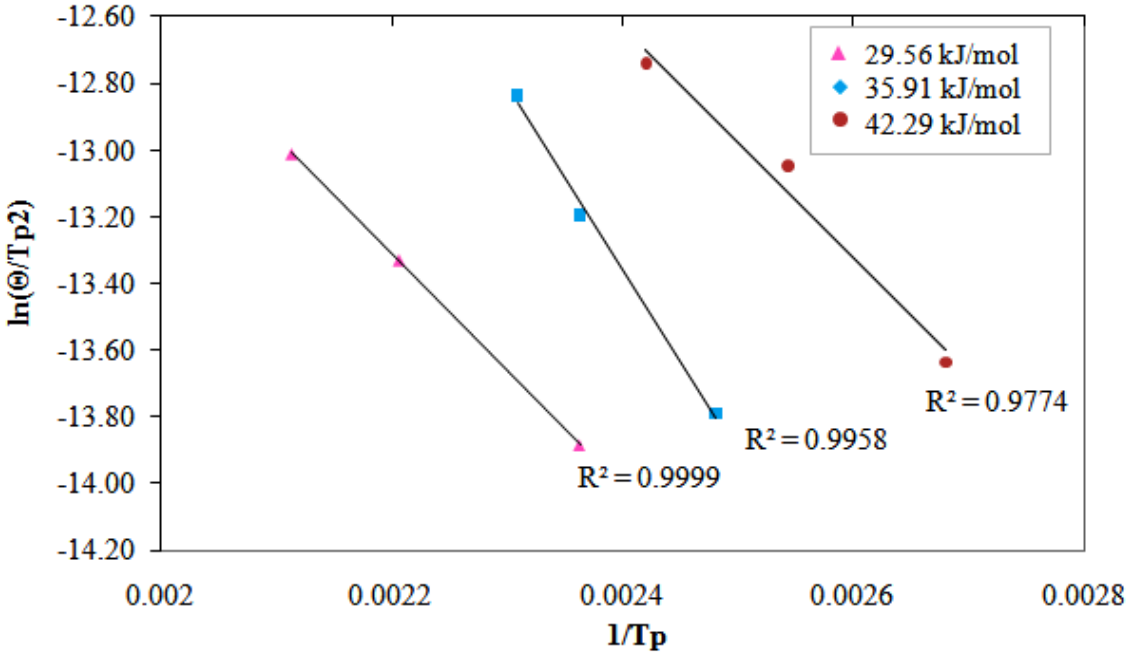

Figure 5-54: The activation energies (kJ/mol) in FeTiC.

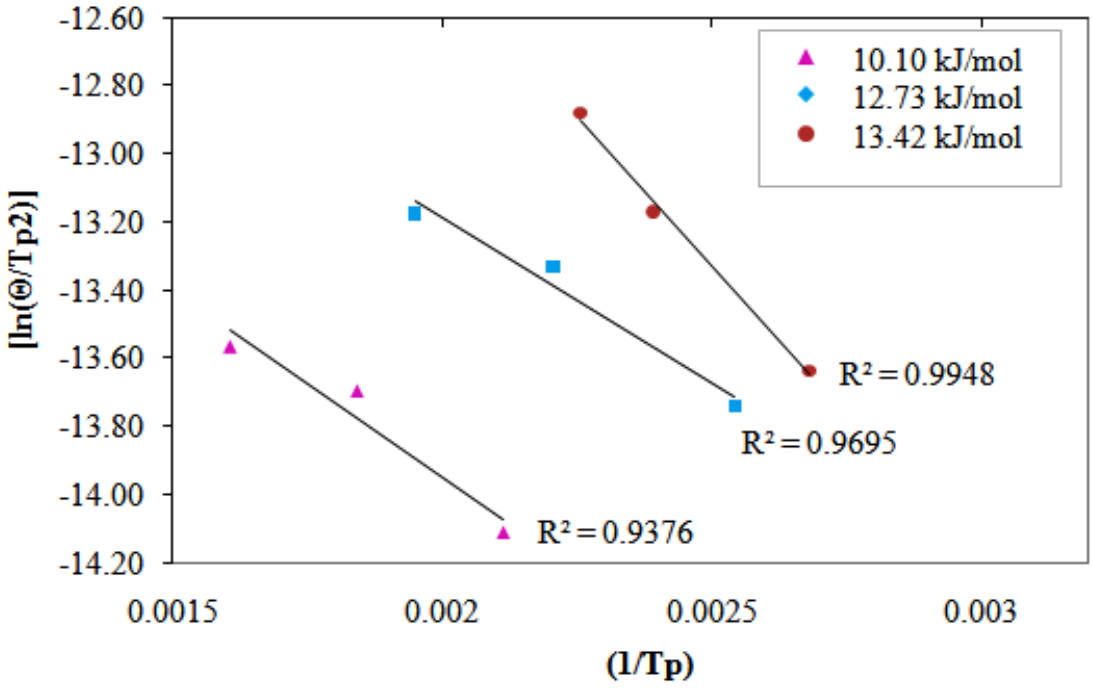

Figure 5-55: The characterisation of activation energies (kJ/mol) in FeTiB.

6. VALIDATION OF THE APPLIED METHODS

Limit of detection (table 6-1): It is crucial to evaluate the efficiency of the methods applied for diffusible and total hydrogen analysis. The lowest possible value that can be detected by an instrument is considered to play an important role because it indicates the noise within the measurement. This is possible by calculating the limit of detection for each method according to the following formula:

$$(LOD = \bar{x}_b + 3 \cdot s_b) \qquad (22)$$

x_b: mean blind value

s_b: standard deviation of the blind values

The limit of detection in melt extraction method was measured by analyzing an empty pyrocoated graphite crucible with an inner smaller crucible for 10 times. The limit of detection with TCD was 0.17 $\mu g \cdot g^{-1}$ and with IR 0.43 $\mu g \cdot g^{-1}$ was obtained.

In TDMS the LOD was determined through the blind value method, “white samples” with very low amounts of hydrogen (<0.1 ppm) were used, in order to better simulate the conditions of an actual analysis. 10 pure iron samples of 1g were measured in two different days, yielding a LOD of 0.13 $\mu g \cdot g^{-1}$.

The sensitivity of the analysis does not relate directly to the concentration of hydrogen in the sample ($\mu g \cdot g^{-1}$) but to the absolute amount (μg) of released hydrogen. Therefore, it should be noted that the detection limit expressed in $\mu g \cdot g^{-1}$ by this validation relates only to a 1g sample.

Samples with higher mass and the same concentration of diffusible hydrogen release a higher absolute amount of the analyte. In relation to typically used sample weights of 2 to 8 g the LOD is approximately 0.02 to 0.01$\mu g \cdot g^{-1}$.

Sensitivity of the measurement: the sensitivity gives an idea about the variation of the signal. It can be obtained by the following equation:

$$\text{Sensitivity} = S_{b/g} \qquad (23)$$

s_b: standard deviation of blank values

g: gradient of the calibration curve from reference material

The sensitivity in melt extraction methods depends on the mass of the sample than the concentration of hydrogen. It was observed that the samples that weighed below 1g had higher hydrogen concentrations than those that weigh above 1g.

These results indicated that the analysis time and temperature had a huge influence on recovering the certified values of hydrogen in Leco reference material and in normal steel samples.

The sensitivity of the isothermal extraction does not directly relate to the concentration of hydrogen in the sample ($\mu g \cdot g^{-1}$) but the absolute amount of the hydrogen released from the sample (μg).

Therefore, the stated validation in limit of detection relates to the 1g sample in isothermal extraction. Samples with a higher mass and the same concentration of diffusible hydrogen release higher amounts of the analyte. Thus the sensitivity of the instrument is increased. Therefore, the sensitivity in isothermal extraction is related to the hydrogen desorption rate ($\mu g \cdot g^{-1}$/min) from the sample and not to the concentration of the hydrogen in the sample. The hydrogen desorption rate depends upon the heating rate, sample composition, baseline drift etc. Hence there are no norms and conventional methods to accomplish the sensitivity of TDS.

Table 6-1: The limit of detection for bulk and diffusible hydrogen ($\mu g \cdot g^{-1}$) analysis in 1g sample.

Measuring technique	Melt extraction	Melt extraction	Hot extraction
Blank detection	TCD	IR	MS
L.O.D= X+ 3Sb	0.17	0.43	0.13

The methods applied for hydrogen analysis in this work managed to characterize hydrogen in steel using a carrier gas system. The melt extraction methods provided only quantities of hydrogen concentrations in metallic materials. Hence it is a necessity to complement them with solid extraction methods which determine the content of diffusible hydrogen. To make the hydrogen analysis more informative based on steel quality, MS was coupled to solid extraction system to analyse hydrogen desorption rate, desorption temperatures and calculation of activation energies of hydrogen in traps.

The methods were calibrated with gas but the stability in between measurements was tested by analyzing reference materials in melt extraction techniques. In solid extraction method there were no reference materials containing certified diffusible hydrogen. Further research needs to be conducted to produce reference material for certified diffusible hydrogen. Besides the fact that TDMS analysis was very slow e.g. each analysis took approx. 20 minutes, this technique is a promising tool in investigating quantities of diffusible hydrogen and its interactions with metallic materials.

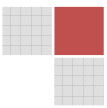

Therefore, melt and solid extraction techniques were combined during the analysis for quantitative and qualitative analysis of hydrogen in steel. The advantages and limitations of the applied techniques are listed in table 6-2.

Table 6-2: Overview on Hydrogen Determination Methods.

Analytical method	**Hydrogen detection**	**Hydrogen analysis**	**Limitations**
Melt extraction	TCD, IR	Total/bulk H_2	Destructive to the sample
Hot/solid extraction	TCD	Diffusible H_2	No information on hydrogen desorption rate Lack of reference material
Hot/solid extraction	MS	Diffusible H_2 (Activation energy) (Desorption rate and temperature)	Long analysis period Lack of reference material

7. SUMMARY OF DISCUSSION

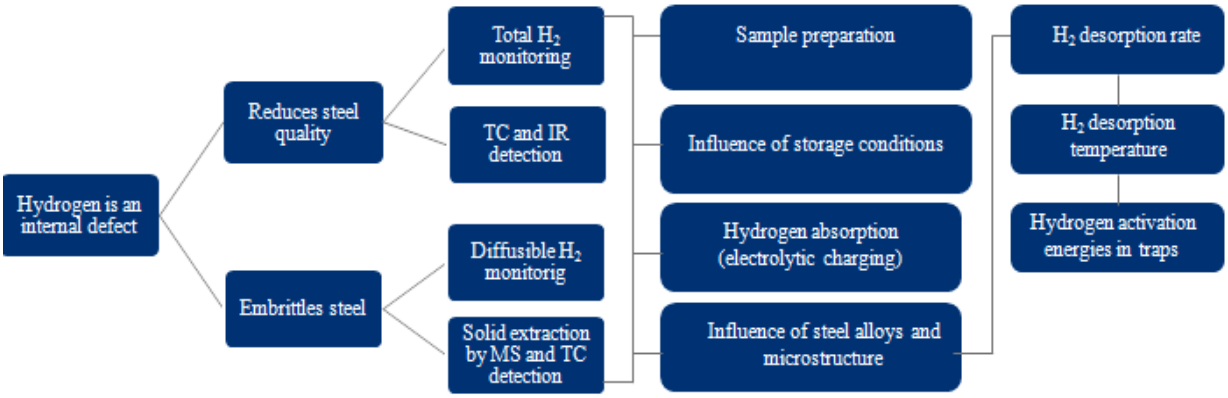

Figure 7-1: The experimental steps performed in the present work during hydrogen analysis in steel.

The hydrogen entrance into the metallic materials has been proven to be a huge problem that brought embrittlement and unreliable quality of solid metallic products as indicated by figure 1-8. The hydrogen resides in lattice sites like grain boundaries, precipitates and inclusions in a solubilised form (immobile) [9, 10, 11]. But due to pressure, temperature, stress etc. that product experiences during production, transportation and storage, some quantity of hydrogen diffuses within the structure or it can allocate itself in traps and interstitial sites. The main issue is that the mobile hydrogen can damage the products internally by deforming the metallographic structure before any defect can be manifested by crack formation on the outside. To quantify the total hydrogen, the melt extraction methods were applied while the diffusible hydrogen was determined by isothermal and thermal desorption techniques. The monitoring process of hydrogen in metallic materials is summarized in figure 7-1 and in the following paragraphs.

The carrier gas melt extraction method for quantifying total hydrogen with TCD was successfully optimised by gas calibration which showed high reproducibility. The Leco reference materials were also applied as drift indicators in-between the measurements.

The determination of diffusible hydrogen concentrations was conducted by hot extraction analyser H-mat 221 (Bruker Elemental) which used TCD for hydrogen measurement (chapter 5.1.4). But there was still missing information based on the desorption rate, desorption temperature and the interacting activation energy of hydrogen localised in traps. This was achieved by coupling the hot extraction analyser with mass spectrometer by using a steel capillary which compensated for the pressure difference between the MS and the hot extraction analyser. This connection was done to avoid suspicions on carrier gas interferences and for more characterisation of hydrogen, e.g. hydrogen desorption rates, desorption temperatures (chapter 5.1.5) and activation energies in traps (chapter 5.8).

Compared to ultra high vacuum systems, TDMS with carrier gas system is less expensive, more compact, can be applied for qualitative and quantitative analysis of diffusible hydrogen. The L.O.D was calculated to 0.13 $\mu g \cdot g^{-1}$ of hydrogen in the sample that weighed 1g. It is possible to analyze relatively large samples of up to 30 g. Typical sample weights of 2 to 8 g were used in this work. The developed instrument is able to determine extremely low concentrations in steel and inherently low hydrogen desorption rates.

Furthermore, by comparing the analysis of total hydrogen certified reference materials with different instruments and detectors it became clear that the concentration of diffusible hydrogen can be consistently determined through mass spectrometric detection from both isothermal and thermal desorption analysis.

Although the accuracy and sensitivity of the mass spectrometric detection was very satisfactory for most of the analysis, some constructive and parametric optimization could still enhance the efficiency of the developed TDMS-instrument:

- By changing the stainless steel capillary by a quartz capillary, the interaction between the hydrogen and the steel material could be avoided, thus improving the quality of the analysis;
- The T-junction between the carrier gas system and the MS could be improved by eliminating the dead-volume between the MS capillary and the carrier gas system, bringing the capillary's tip directly into the carrier gas stream;
- A more efficient turbo-molecular pump could decrease background drift and memory effect;
- The sensitivity of the mass spectrometric detection could be enhanced by optimizing the standard parameters of the ion source.

In order to quantify hydrogen, the operating parameters must be well optimised because the extraction of hydrogen from solid or molten metal is highly governed by the diffusion phenomenon according to *Ficks* law in equation 3.

Therefore, it is crucial to record the variation of sample temperature versus time to measure at the maximum temperature to be reached so that the kinetics of dehydrogenation is quick enough to occur. To ensure that accurate analysis was performed, the following parameters were optimised:

Calibration: Correlation between the melting temperature and the hydrogen content detected was firstly established by setting up a two point gas calibration (chapter 5.2.1 and 5.3.1) in melt extraction method (TC detection).

In total hydrogen analysis technique, there was another possibility of calibrating with reference material but due to the experiments performed in this work lead to more favouritism towards gas calibration. For instance in chapter 5.5.1 there was reference material from which the measured hydrogen concentration did not agree with the certified values. This could have been due to storage effect during packaging or transportation of the products. Therefore in melt extraction method, the reference materials were used as drift indicators in between the measurements while the gas calibration was applied as the major calibrating method.

In case of diffusible hydrogen analysis a 5-point-calibration was conducted by using a pure hydrogen gas that was carried by nitrogen first to the TCD, then to the MS.

Operating parameters: The sample mass influence in total hydrogen analysis was observed during melt extraction (thermal conductivity detection). Although the Leco reference materials were already weighing approx.1g, it was noticed that using the Eltra OHN 2000 system, the smaller samples gave rise to higher hydrogen concentrations due to the easy contamination of smaller signals hence in all measurements 1 g was the standard mass (figure 5-12). The variety of sample shapes and forms such as chips, pins, blocks (cubes) and balls can be analysed by melt extraction methods. But for hydrogen analysis the pins and block forms were mostly preferred because they represented the concentration that was in certified reference materials.

The temperatures for melting samples at identical operating conditions were setup by analysing various reference materials. The Leco materials showed the highest stability (table 5-3). It is crucial to remember that during bulk hydrogen analysis, the transfer times of the analyte between the detector and temperature depended mostly on the components of the material (figure 5-13).

Although these melt extraction methods were able to analyse total hydrogen, there are still challenges like getter effects from the graphite crucibles which yield lower hydrogen concentrations in comparison to the certified values and sample matrix which required manual cleaning of the furnace after every few measurements. It would be better if the TCD system can have a closed self-cleaning system in the furnace.

The influential parameter in TDMS was the heating rate, because at slower heating rates the hydrogen desorption occurred at low temperatures while the opposite occurred when higher temperatures were applied (figure 5-48.)

Sample preparation: In order to characterise correctly the metallic material, sample preparation has to be taken into great consideration because the quality cannot be based on precision achieved by analytical results. The originality of the material plays a huge role. The feedback concerning the analyte concentrations should be based on sample preparation, analytical method and finally up to the calculation of the results.

The segregation of gases e.g. H_2 in metals occurs especially during cutting with a saw because of heat introduction, H_2 can diffuse out of the sample. Hence in the present work all the flat steel samples were cut by using a plate shear.

Before any hydrogen analysis, the ferritic steel samples in table 5-7 were freed from surface contaminants like the oils and oxides by cleaning them with dichloromethane for 5 minutes in ultrasonic bath for accurate hydrogen analysis because it is a polar solvent with a high volatility which makes it as an ideal solvent for removing grease and other contaminants from steel surfaces.

In order to monitor hydrogen in zinc coated samples, the coating was removed by paper filing/scraping, sandblasting and acid etching to indicate the dependence of hydrogen concentration on sample preparation. Paper filing and sandblasting introduced impurities e.g. oxides, water vapour into the sample surface that caused an increase in hydrogen concentration due to carbon oxides contaminants [figure 5-25].

To analyse the hydrogen in the steel bulk, the zinc coating was chemically etched with 16 % HCl containing 5g/l hexamethylenetetramine (recombination reaction inhibitor) which was mostly preferred to NAP etching and mechanical removal by paper filing and sandblasting. The presence of chemical species (inhibitors) on the sample surface has a crucial role because they inhibit the hydrogen dissociation processes which can lead to hydrogen absorption. In contrast to that, chemical etching with NAP resulted in less hydrogen contents due to the recombination reactions that had taken place on the sample surface and resulted in dehydrogenation.

The total hydrogen concentration in zinc coated sample (HCT780C) was higher than in uncoated samples. This indicated that the hydrogen is distributed in the coating which makes zinc a metal that reduces the risk of embrittlement. Less contents of diffusible hydrogen were measured in the zinc coated sample which showed that zinc can slow down the rate of hydrogen diffusion.

The non diffusible hydrogen in the ferritic material was higher than the diffusible hydrogen which makes them less susceptible to embrittlement.

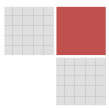

Storage conditions: The sample storage conditions are a quite a challenging issue during hydrogen measurement. For example some of the reference materials were not in agreement with the certified values (table 5-3). The Leco 762-747 and Alpha 546 were considered to be more stable. To simulate the long time stability of the materials, they were stored in a drier at 105° C. A drastic decrease in the amount of hydrogen of the Leco standards was observed. That confirmed that desorption of hydrogen took place at this low temperatures (table 5-11). The BS-HON-2 showed a great stability in hydrogen content although the measured value was not in agreement with the certified one but the precision was satisfactory.

To measure the content of hydrogen that can be absorbed by ferritic steel, the materials were charged with various electrolytic solutions. It was observed that when the material was exposed to more acidic solutions for longer periods, hydrogen diffusion into the sample was greatly enhanced (figure 5-28) and higher concentrations of hydrogen were obtained. But after hydrogen charging and leaving the samples at room temperature, hydrogen desorption occurred. Hence the samples were stored on dry ice or liquid nitrogen (figure 5-27). Dehydrogenation at room temperature (22 °C) confirmed that the hydrogen was located in reversible traps (figure 5-29).

The influence of sample storage conditions and sample cooling mediums on total hydrogen concentration could also be observed by analysing the molten steel at the production site. On one hand the material was cooled with iced water and on the other hand with liquid nitrogen. Afterwards the samples were analysed with melt extraction method in laboratory. (chapter 5.1.3). The onsite hydrogen values, measured by hydris system, were comparable to the hydrogen content in samples that were quenched with water. The rate of sample cooling by water was more appropriate for hydrogen sampling. When the samples were cooled with liquid nitrogen, more hydrogen diffused out. Therefore liquid nitrogen is not appropriate for cooling molten steel but well recognised as a better sample storage medium.

In any case the molten steel sampling method applied in this work does not quite satisfy the proper standard because of the hydrogen mobility and the complications that resulted during quartz rod sampling. For an example some of the rod shaped samples had holes inside them that contained black carbide material whereby in such cases extremely high, scattered values of total hydrogen concentrations were obtained in laboratory measurements. Therefore, direct sampling of the steel by using quartz rods for hydrogen analysis requires more attention to be paid towards the quality of quartz glass used, sampling temperatures and quenching and cooling time e.g. with iced water first and later the sample can be stored in nitrogen.

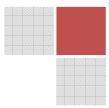

The steel alloying experiments in this work were representing steel at a very simple level without being properly worked on like at the production site. Steel alloying is a very critical process which required great attention to be paid towards the concentrations of the elements involved and their texture in order to form homogeneous alloyed products (chapter 5.7). It has been mentioned before that in this work laboratory alloying experiments were done to study the hydrogen concentrations in differently alloyed steel. During alloying in the high frequency furnace (Himmel oven), the outgassing, melting temperature and the time for taking the sample out, must be well optimised to avoid combustion interferences in the oven because various compounds were also alloyed in the same oven.

After the sample has been baked, rapid or slow cooling must be taken into great consideration because it affects the analyte (hydrogen). For instance in the recent work, Fe was alloyed with C (FeC). It was discovered that the precision of water cooled samples was uniform while the nitrogen cooled samples had scattered values (chapter 5.7.1). Hence water was mostly preferred as the cooling agent after these tests.

The influence of carbon grain size in hydrogen distribution was observed. The rough grain carbon in FeC had lower hydrogen concentration than the powdered carbon in FeC (chapter 5.7.2). Therefore, rough grain carbon was mostly used in carbon alloyed steels in this work.

The influence of steel alloys on hydrogen concentrations was studied by analysis of diffusible and total hydrogen to observe their potential input on embrittlement (chapter 5.7.3). There was no diffusible hydrogen detected by TDMS from FeSi and FeTi which implied that they could have formed irreversible traps while the total hydrogen was around $1 \mu g \cdot g^{-1}$. They inhibited the hydrogen mobility by solubilising it in strong traps and this makes them less susceptible to embrittlement.

But after the carbon addition to the alloys (FeSiC, FeTiC; FeVC), more diffusible and total hydrogen concentrations was measured. Although carbon is very recognised for its hardening characteristics in steel industry but it can also contribute a lot towards higher hydrogen concentrations in alloyed steel.

To characterise further the interaction of hydrogen with traps in metallic materials, Polanyi Wigner equation (13) was applied to characterise desorption rates and temperatures by applying different heating rates from 0.1 to 1 K/s. From this data, the activation energy was characterised by using *Arrhenius* plots in equation (17).

Both Leco reference materials and some high strength steels were analysed. In the reference material Leco 501-061, the measured activation energies were comparable to the literature values in table 5-23. One value was unknown at 221.43 KJ/mol.

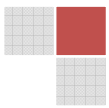

The same method was applied to high strength steels (chapter 5.8.2) and it was also observed that they contained different activation energies. Sample HS-3 had the lowest one which makes the material to have less quality than the other two (HS-1 and HS-2).

The analysis of newly developed high-strength steels with TDMS is in fact very interesting to the steel industry, as it is able to provide valuable information about the susceptibility of the steel to hydrogen embrittlement and also to individually locate and characterize hydrogen traps added to the base-alloy of HS-steels.

Different alloys with the appropriate thermo-mechanical treatment can be efficiently compared by TDMS, characterizing the most efficient trapping sites and contributing to the development of more reliable materials.

Due to the unknown activation energy values more work needs to be done on structural characterisation by metallurgical methods in order to identify the unknown source of activation energy.

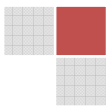

8. CONCLUSION AND FUTURE SUGGESTIONS

This work was performed to quantify the total and diffusible hydrogen in metallic materials for providing information based on the susceptibility towards embrittlement. The total hydrogen determined did not exhibit enough information based on embrittlement. Hence diffusible hydrogen was measured to identify hydrogen desorption rates, desorption temperatures and activation energies in traps of differently prepared samples. Since the internal embrittlement cannot be foreseen, the concentrations of diffusible hydrogen work as indicators.

The optimizations of the operating parameters lead to more information on characterizing hydrogen in steel. Based on this data, more future investigations can be performed on newly developed materials.

In both melt extraction and solid extraction techniques gas calibration was discovered to be more reliable and stable in routine analysis.

Sample preparation has a major influence on hydrogen concentration in metallic materials. The evaluation of hydrogen content in both coated and uncoated samples requires the cleaning of the surface with a proper solvent for accurate analysis.

When dealing with zinc coated samples it is strongly suggested to remove the coating by chemical etching method which includes hydrogen desorption inhibitor in order to avoid the loss of the analyte (H_2) and more hydrogen absorption from the solution.

In this work dry ice and liquid nitrogen were storage mediums for samples. But more comparison on hydrogen concentration in samples stored on liquid nitrogen and dry ice still needs to be performed to identify the best storage method.

Water was recognized as the better cooling medium than liquid nitrogen during molten steel sampling.

More studies based on microstructures of carbon alloys and alloys without carbon need to be done in detail to identify the particles that can contribute towards hydrogen irreversible traps in order to improve the quality. Steel alloying should involve strict measures on the concentration of alloys, melting temperature, cooling medium and sample storage because they can highly influence the hydrogen concentration in the final product hence this part of the work needs to be intensively investigated in future. Here also, water was the better sample cooling method because the concentration data had a better precision than the samples that were cooled with liquid nitrogen.

The determination of desorption activation energies from the Polanyi-Wigner equation with the assumption of a first order desorption rate yielded to in most cases satisfactory results.

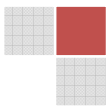

There are several aspects involved in the determination of the activation energies, which are still need to be more deeply explored, such as the effects of sample geometry and surface treatment and hydrogen amount, the influence of tailing in the deconvolution with *Gaussian* peaks and the effects of background drift and polynomial normalization in the quality of the analysis.

The analysis of activation energy in Leco reference material, high strength steels and ferroalloys showed the great potential of TDMS in quality evaluation of the materials. Different alloys with the appropriate thermo-mechanical treatment can be efficiently compared by TDMS, characterizing the most efficient trapping sites and contributing to the development of more reliable materials. The measured values could be compared with those found in literature (table 5-23).

The quantitative determination of diffusible hydrogen through TDMS is still to be more deeply evaluated. The effects of phase transformation during the heating process should be taken into consideration in future research, as it could influence the determination of the effective concentration of diffusible hydrogen in steel, which is the one actually relevant to the evaluation of the susceptibility to hydrogen embrittlement. The diffusivity of hydrogen in steel is the greatest threat in steel producers because it leads to an unpredictable internal embrittlement.

Throughout the experiments it was noticed that the non diffusible hydrogen was higher than the diffusible hydrogen in most samples. In reality, the saturation of hydrogen in metallic materials cannot be totally avoided but the concentration should not exceed a certain limit otherwise the mobility of hydrogen throughout the material will occur which compromises the quality of steel by internal deformation of the structure. But this all depends on the processes that influence hydrogen during production, transportation, storage and use of the materials.

It was observed that heating the sample at low temperatures for long periods can enhance the dehydrogenation process. But there was no certainty if the properties of the material were still the same after heating it e.g. properties like tensile strength, malleability ductility etc.

This work showed the promising way to evaluate the total and diffusible hydrogen contents in metallic materials by setting up proper sample preparation methods, investigating better ways of sample storage, determining conditions that lead to absorption and desorption of hydrogen. The influence of the microstructure alloys and trapping tendencies of hydrogen were also characterised.

The concept of analysing total and diffusible hydrogen contributes towards the susceptibility of the material to embrittlement. The analysis of hydrogen desorption rates and activation energies provides more tangible information based on the interaction of hydrogen with the material, the quality and the suitability of the material for a particular application.

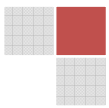

Therefore analytical methods applied in this work; melt and solid extraction (TDMS) have a great potential in proving valuable information towards the improvement of metallic materials.

.

9. REFERENCES

[1]	Richardson, F.D.; Jeffers, J.H.E. *Journal of Iron and Steel Industry*, **1948**, *160*, 261
[2]	Stone, R.P.; Plessers, J.; Turkdogan: *Stahl and Eisen* **,1990**, 110(11),65-74
[3]	Hurst, C.R.; Vergauwens, M. Haraeus Electro-Nite International N.V. Annual Australian Foundry Institute Conference **2004**, 185-208.
[4]	*International Journal of H_2 energy*, **1998**, *23 (7),* 593-598.
[5]	Oriani, R; Hirth, J; Smialowski, M. Hydrogen degradation of ferrous alloys, 215-250, Noyes, **1985**.
[6]	Weber, J.*Galvanotechnik*, **1980**, *71*, 1082-1089.
[7]	McBreen, J; Gernshaw, M.A. *Elsevier*, Proc.Int.Symp. on SSC, Nace, Houston, **1967**
[8]	Albrecht, J.; Birmes, W.; Büchel, E.; Meyer, L.**1971**, 19(*3*), 21-25.
[9]	Rogers, H.C. *Science*, **1968**, *159 (3819),* 1057-1064.
[10]	Wie, F.G.; Hara, T.; Tsuzaki, K. *Metal Trans. B*, **2004**, *35B*, 597.
[11]	Zapffe, C.; Sims, C. *Trans.AIME*, **1941**, *145*, 225-59.
[12]	Kehr, K.W.; JÜL Bericht JÜL-1211 (Kernforschungsanlage Jülich **1975**)
[13]	Kawasaki Steel JFE 21st century foundation, **2003**, (http://www.jfe-21st-cf.or.jp/chapter_2/2a html.
[14]	Johnson , E.W.; Hill, M.L. *Trans. AIME,* **1960**, *218*, 1104-1112
[15]	Beke, D.L.; Szabo, I.A. *Scitec*, **1995**,*5*, 23-31,
[16]	Pressouyre, G.M.; Interrante C.G. International Conference of Current Solutions to Hydrogen Problems in Steel, *American Society for Metals* Washington, DC, **1982**, 3-8.
[17]	Darken, L.S.; R.P. Smith, R.P. **1949**, 5, 1-16.
[18]	Astaf``ev, A.A. *TsNIITMASH*, **1991**, *2*, 5-8.
[19]	Crank, J., The Mathematics of Diffusion, 2nd edition, Oxford, **1989**
[20]	Oriani, R.A. *Phys.Chem.***1972**, *76*, 848-857.
[21]	Oriani, R.A.; Josephic, P.H. *Acta Metall*. **1977**, *25*, 88-979
[22]	Bastein, P.; Azou, Proc.*ASM*, **1951**, 535-552
[23]	Petch, N.J.*Phil.Mag*, **1956**, *1*, 331-335

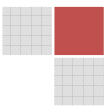

[24]	Sil`man, G.I., Zhukov, A.A. *Metallovedenie I Termicheskaya Obrabotka Metallov*, **1978**, *7*, 28-31
[25]	Kuznetsov, V.V.; Subbotina, N.I.; Khaldeev, G.V. *Material Science,***1972**, *10 (3)*, 323-325
[26]	Zikeev, V.N.; Serebryanaya, E.B. *Metallovedenie I Termicheskaya Obrabotka Metallov*, **1984**, *12*, 23-25.
[27]	Yu, H.Y.; Li, J.C.M. In Proc. Conf. Computer Simulation for Materials Applications, Gaithersburg, 1976, ed. Arsenault, R.J.; Beeler, Simmons, Jr., J.A.81-872.
[28]	Pressouyre, G.M. *Met.Trans.*, **1979**, 10A, 1571-1579.
[29]	Thomas, R.L.S; Scully, J.R.; Gangloff, R.P. *Metall.Mater.Trans.A,* **2003**, *34*, 327-344
[30]	Bernstein, I.M.; Pressouyre, G.M.;. ibid, 1978, 9A, 1571
[31]	Choo, W.Y.; Lee, J.Y.*Metal Trans*.A **1982**, *13A*, 135.
[32]	Huang, Y,; Nakajima, A; Nishikata, A; Tsuru, T. *ISIJ International*, **2003**, *43*, 548-554
[33]	Sklyuev, P.V. Hydrogen and Flakes in Large Forgings, Mashgiz, Moscow, 1963.
[34]	Paatsch, W.; Hodoroaba, V.D. 4th Kurt Schwabe Corrosion Symposium, **2004** Finland
[35]	Troiano, A.R. *Trans.Am.Soc.Metall.* **1960**, *52*, 54-80
[36]	Troiano, A.R. *Trans.ASM.***1960**, *52*, 25-259.
[37]	Troiano, A.R.; Steigerwald, E.A.; Schaller, F.W. *Trans. AIME*, **1959**, 1048.
[38]	Indranil Chattoraj, *National Metallurgical*, **1995**, *20(1),* 199-211
[39]	Beachem, C.D. Met.Trans. 1972, 3(2), 437-451
[40]	Westlake, D.G. *Trans.ASM*, **1969**, *62*, 1000-1006
[41]	Tien, J.K.; Nair, S.V.; Jensen, R.R. *Met.Soc. of AIME*, **1980**, 37-56
[42]	Kawasaki Steel JFE 21st century foundation, **2003**,http://www.jfe-21st-cf.or.jp/chapter_2/2a html
[43]	Lee, J.Y; Lee, J.L.; Choo, W.Y. First International Conference on Current Solutions to Hydrogen Problems in Steel, **1982**, Washington.
[44]	Huang, C.; Li, J.; Wang, Y.; Chu, W. Journal *of Chinese Society for Corrosion and protection,* **1997**, *17(2)*, 129-134.
[45]	Birrnbaum, H.K.; Shih, D.S.; Robertson, I.M. *Acta.Met*. **1988**, *36*, 111-124
[46]	Fourlaris, G.; Baker, A.J.; Papadimitriou, G.D. *Acta etal.mater.***1995**, *43(10)*, 3733-3742.

[47]	Coudreuse, L. *Corrosion sous contrainte*, **1990**, 397-424
[48]	Perng, T.P.; Altstetter, C.J. *Metal Trans.* **1988**, *A19*, 145
[49]	Hanninnen, H.; Hakarainer, T. *Corrosion*, **1980**, *36*, 47
[50]	Zackay, V.F.; Parker, E.R.; Fahr, D.; Busch, R. *ASTM*. **1967**, *60*, 59-252
[51]	Rees, W.P.; Hopkins, B.E. and Tipler, H.R. *Journal of the Iron and Steel Institute*, **1961**, *169*, 157.
[52]	http://www.wipo.int/pctdb/ja/ia.jsp?ia=EP2009%2F001276&IA=EP2009001276&DI
[53]	http://www.msm.cam.ac.uk/phase-trans/2001/shingo/img6.htm
[54]	Tang, Z. Phase Transformations in Metals and their Alloys, University of Pretoria etd.**2007**.
[55]	US Patent 6669789 – Method for producing titanium-bearing micro alloyed high-strength low-alloy steel
[56]	Kuznetsov, V.V.; Subbotina, N.I.; Khaldeev, G.V. *Material Science*,**1972**, *10 (3)*, 323-325
[57]	Zhu, L.J.; Wu, D.; Zhao, X.M. *Acta Metallurgica Sinica*, **2008**, *21(3),* 163-168
[58]	Shvartsbart, YA.S. *Metallov*, **1960**, *HB5312 (2),* 11-13.
[59]	Sil`man, G.I., Zhukov, A.A. *Metallovedenie I Termicheskaya Obrabotka Metallov*, **1978**, *7*, 28-31
[60]	Takagi, S.; Inoue,T.; Hara,T. Hayakawa,M.; Tsuzaki,K.; Takashi,T.; Tsetsu_to-Hagané, **2000**, *86 (10),* 49-56
[61]	Berns, H; Theisen, W. Eisenwerkstoffe Stahl und Gusseisen, Springer Verlag: Heidelberg, 2008.
[62]	Wright, E.C.; Mumma, P.F. *AIME Iron and Steel Div*.**1933,** *496*, 11
[63]	Tetelman, A.S. Robertson, W.D. *Acta Metall.Soc*.**1963**, 11, 26-415
[64]	de Kazinsky, F.J. *J.Iron Steel*, **1954**, *177*, 85-92
[65]	Etzold, U.; Mohr, K.P.; Hulser, P. CSSP Symposium, **1999**, 201-210.
[66]	International Organization for Standardization: *Steel and iron* **1996**, ISO 14284, Switzerland.
[67]	Plessers, J.; Maes,R., Vangelooven, E.V. *Stahl &Eisen*, **1988,** *108(9)*, 451-455.
[68]	Kim, D.H.; Ho, H.G. *Punsok Hwahak*, **1980**, *1*, 8; *Chem.Abstr.* 1980, 93, 153994x
[69]	Am.Soc. Test Mater, *Unpublished Committee* E-3 Task *Force Report*, **1969**

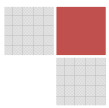

[70]	Berkowitz, B.J.; Preece B.J.; Strozier, J.A. *Scr. Metall,* **1975**, *9*, 803, *Chem.Abstr.***1975**, *83*, 187887y.
[71]	Martin, J.F.; Jakaes, R.C.; Melnick , L.M. *Trans.Metall.Soc. AIME*, **1964** *203*, 107.
[72]	Sugiyama, T.; Yamamoto S.; Yamada, M.; Sugino, M. *Trends Steel Consumables Weld. Int. Conf.* 1979, *1*, 299; *Chem. Abstr.* **1980**, *92*, 62757k.
[73]	Strobel, H.A.; Heineman, W.R. Chemical Instrumentation: Systematic Approach Third Edition, Wiley-Interscience, New York, p.15, 1989.
[74]	Hayashi, M.Horiba Ltd. Technical Note, EMGA 27 Japan
[75]	Degreve, F.; Jardin, C. *N.Met.Trans*.B, **1975**, *6B*, 545-550.
[76]	Sastri, V.S. *Talanta*, **1987**, *34(5)*, 489-493.
[77]	Nishifuji, M.; Ono A.; Chiba K. *Anal.Chem.* **1996**, *68*, 3300-3303.
[78]	Westerberg, L.; Hjörvarsson B.; Wallen, E. and Mathewson A. *Elsevier Science* Ltd. **1997**, *48 (7-9)*, 771-773.
[79]	Berman, D.A.; Agarwala, V.S. The Barnacle Electrode Method to Determine Diffusible Hydrogen in Steels, in Hydrogen Embrittlement Prevention and Control, ASTM STP 962, L. Raymond, American Society for Testing and Materials, p.98-104, 1988.
[80]	Macher, A.; de Krenk, W.; Schoonman, J. The Barnacle Electrode Method to Determine Diffusible Hydrogen in Steels, in Hydrogen Embrittlement Prevention and Control, ASTM STP 962, L. Raymond, American Society for Testing and Materials, p.90-97, 1988.
[81]	Pressouyre, G.M.; Faure, F.M. *ibid*, Quantitative Analysis of Critical Concentrations for Hydrogen Induced Cracking.
[82]	Price, D.L.; Skold, K. *Academic Press*, 1987, *23 (B),* 131-186.
[83]	William H.; Kumar, A.; Meyer, W. *Journal of Nondestructive Evaluation*, **1991**. 10(4), 151-158.
[84]	Angelic J.; Haselgrübler K.; Achammer E.M.; *Springer Verlag* **1993**, *A, 4031*,
[85]	Adriaens, A., VanVaeck, L., and Adams, F., 1999, *Material Science Applications*, *18*, p. 48-81.
[86]	Pocklington, D.N.; Cheyne, T. *ISSM*, 1986, *11 (6),* 319-323
[87]	Corporation: ELTRA-OHN-2000 catalogue, **2006**
[88]	Corporation: TCH-600 catalogue, **2006**
[89]	http://www.physics.upenn.edu/balloon/phototube.html
[90]	Yamaguchi, T.; Nagumo, M. *ISIJ International* **2003**, *43*, 514-519

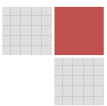

[91]	Thomas, R.L.S; Scully, J.R.; Gangloff, R.P. *Metall Mater.Trans.A*, **2003**, *34*, 327-344.
[92]	Nagumo,M.; Nakamura,M.; Takai,K.Met and *Mat.Trans.A*, **2001**, 339-347.
[93]	Juwe Laborgeräte GmbH: Katalog H-Mat 221, **2004**.
[94]	Mizuno, M.; Anzai, H.; Aoyama, T.; Suzuki T.*Metal. Trans*.**1994** 35 (10), 703.
[95]	Budzikiewics, H. Massenspectrometrie-Eine Einführung, vierte Auflage, Wiley VCH Verlag, Weinheim, **1996**, 9-55.
[96]	Skoog, D.A.; Holler, F.J.; Nieman, T.A. Principles of Instrumental Analysis, 5th edition, Saunders, **1997**.
[97]	http://www.chemguide.co.uk/analysis/masspec/howitworks.html
[98]	Netzch-Laborgeräte, Katalog TA-QMS Kopplung
[99]	M. Zheng, M.; Zhen, X. *Metall. Mater. Trans. B,* **1993**, *24B*, 789-794
[100]	Budzikiewicz, H. Massenspektrometrie-Eine Auflage, Wiley-VCH Verlag Switzerland, 1998
[101]	Hoffmann, E.; Stroobant, V. Mass spectrometry-Principles and Applications, 3rd edition, Wiley, **2007**.
[102]	Mc Lafferty, F.W.; Turecek, F. Interpretation von Messenspecktren, *Spektrum Akademischer Verlag*,**1995**, 1-25, 37-43,
[103]	Balzers AG; Omnistar / Thermostar Betriebsanleitung, GSD 300 O/T, 1997
[104]	Yoshida, N.; Ashizuka, N.; Fujiwara, T.; Kurita; T.; and Muroga, T., *J.Nucl. Mater*. 1988, 155-157, 775.

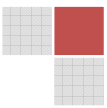

10.APPENDIX

Appendix A: Diffusible hydrogen concentration, desorption rate and temperature

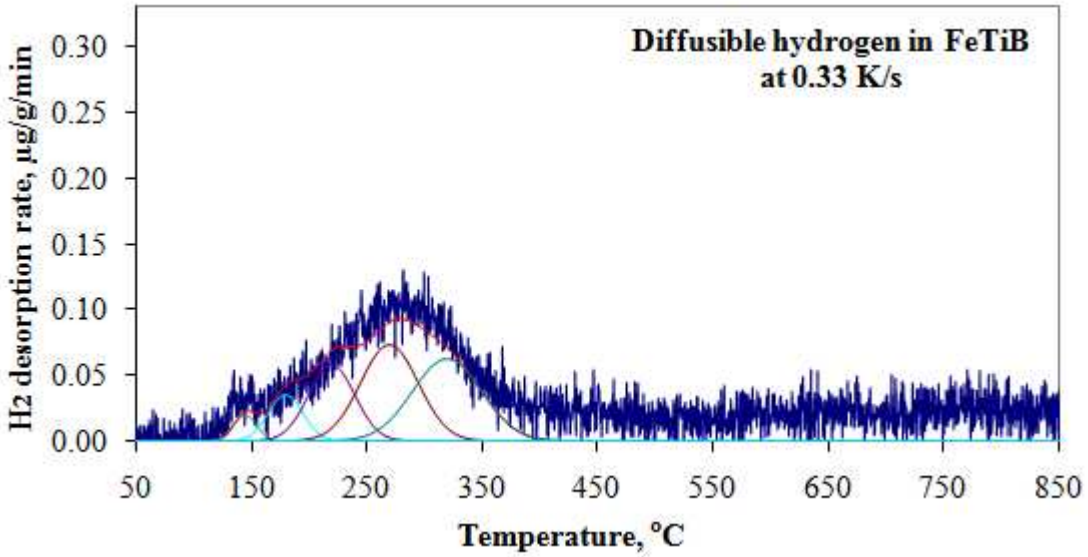

Figure 1A: The Gaussian curves fitted into the FeTiB hydrogen desorption rate signal plotted against the temperature during hot extraction by TDMS.

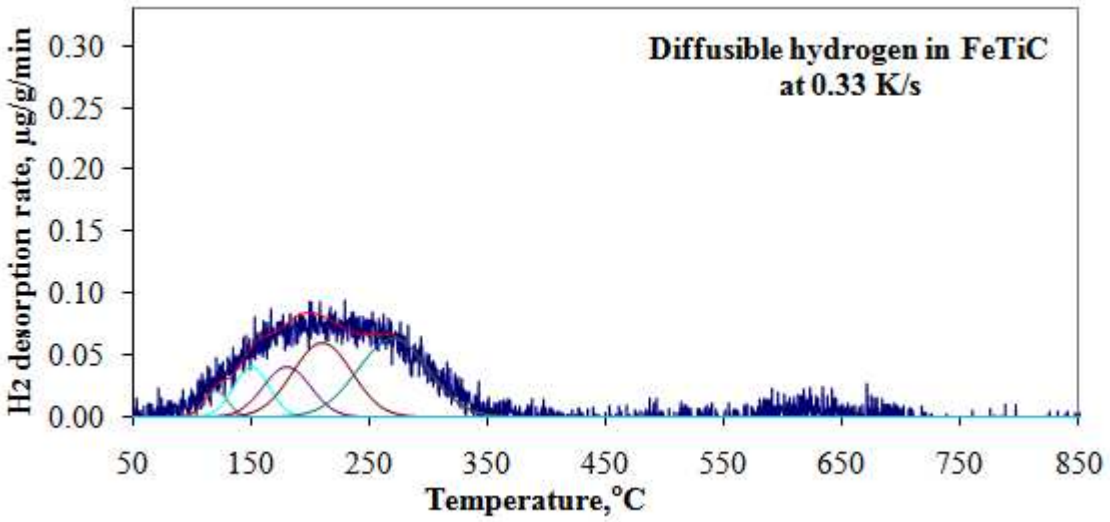

Figure 2A: The Gaussian curves fitted into the FeTiC hydrogen desorption rate signal plotted against the temperature during hot extraction by TDMS.

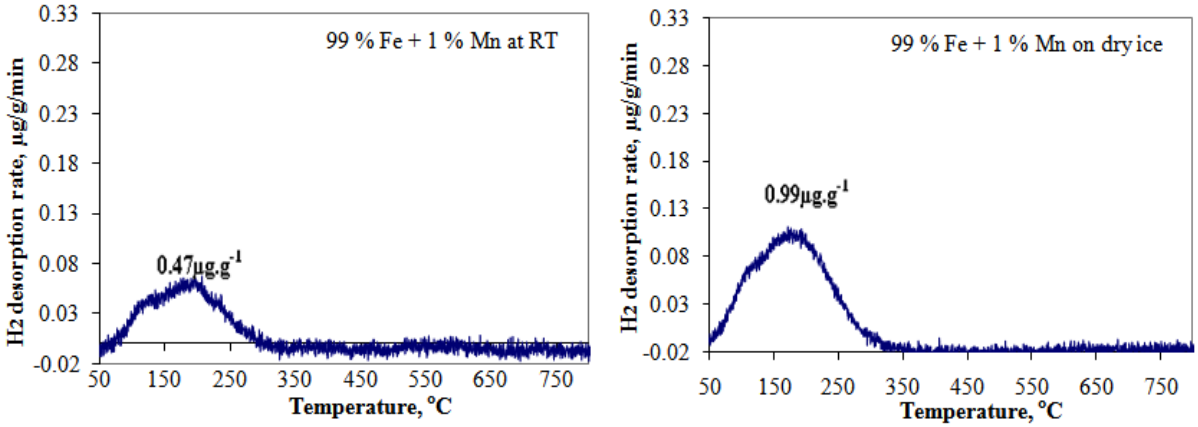

Figure 3A: Hydrogen desorption in FeMn alloy stored on ice and at room temperature.

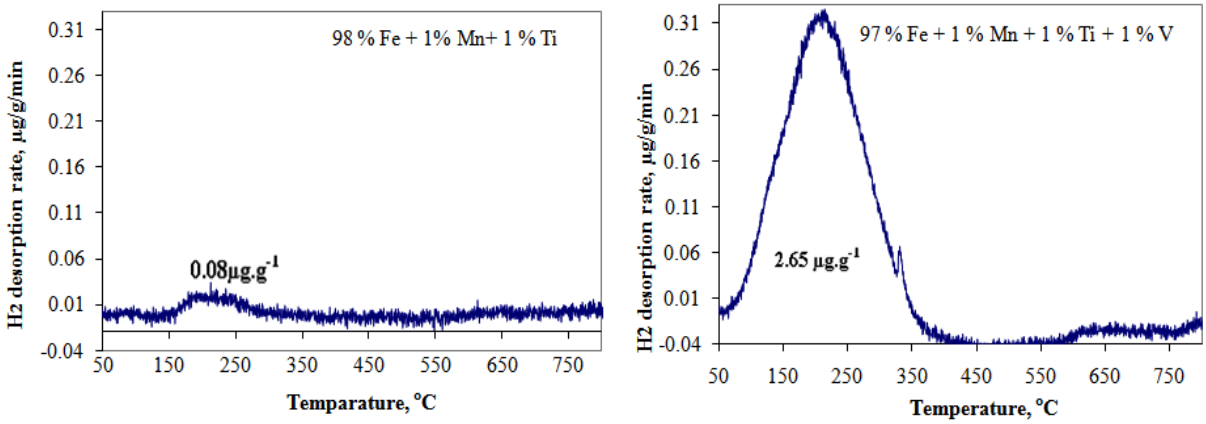

Figure 4A: Hydrogen desorption in FeMnTi and FeMnTiV

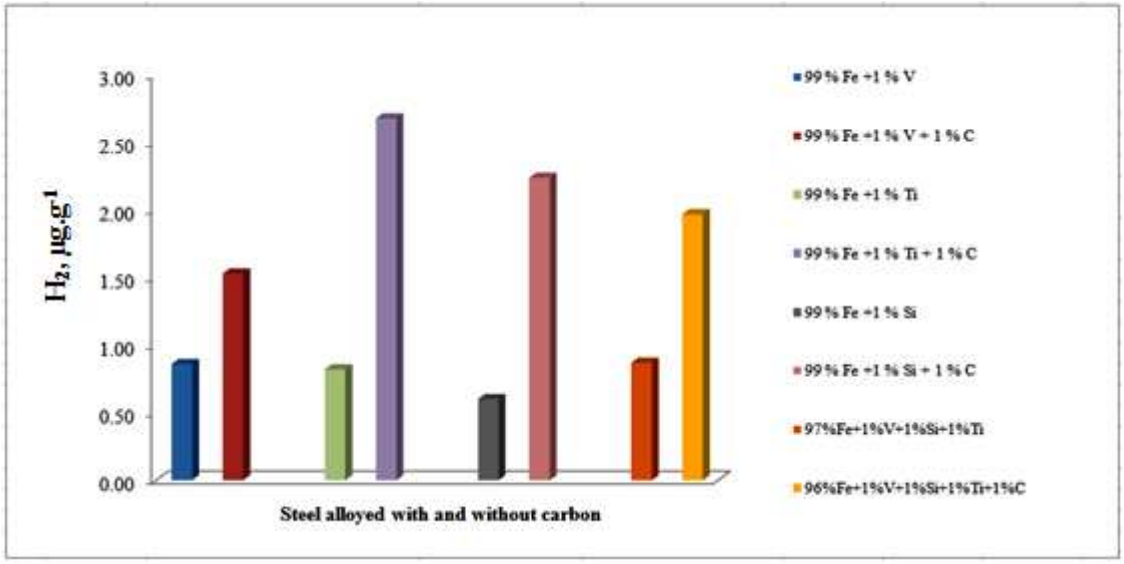

Figure 5A: The total hydrogen in ferro-alloys measured by TCD.

Appendix B: Microstructures of steel alloys

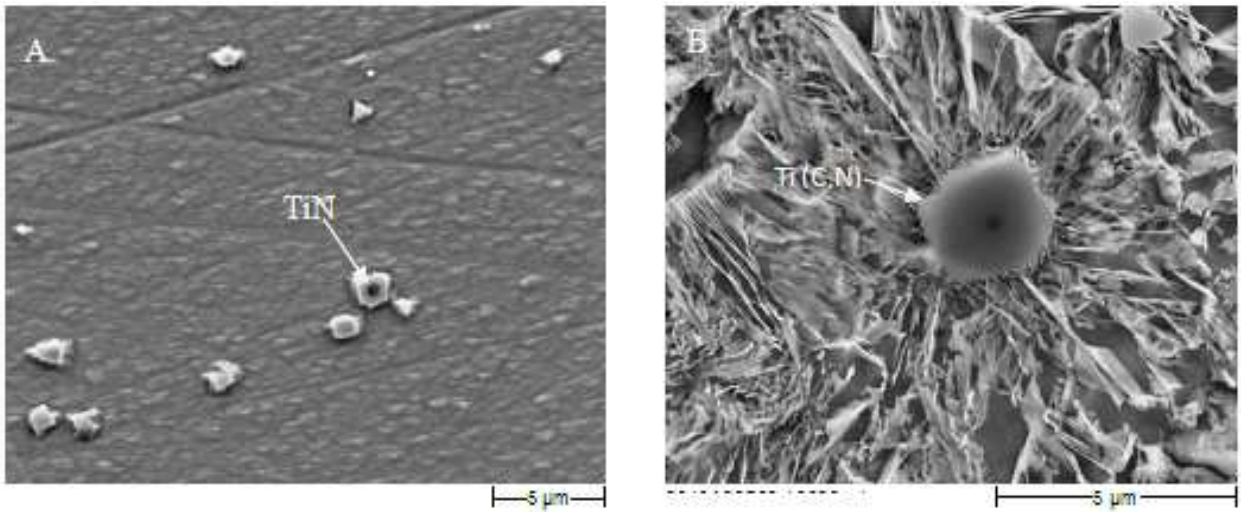

Figure 1B: The microstructure of (a) FeTi and (b) FeTiC.

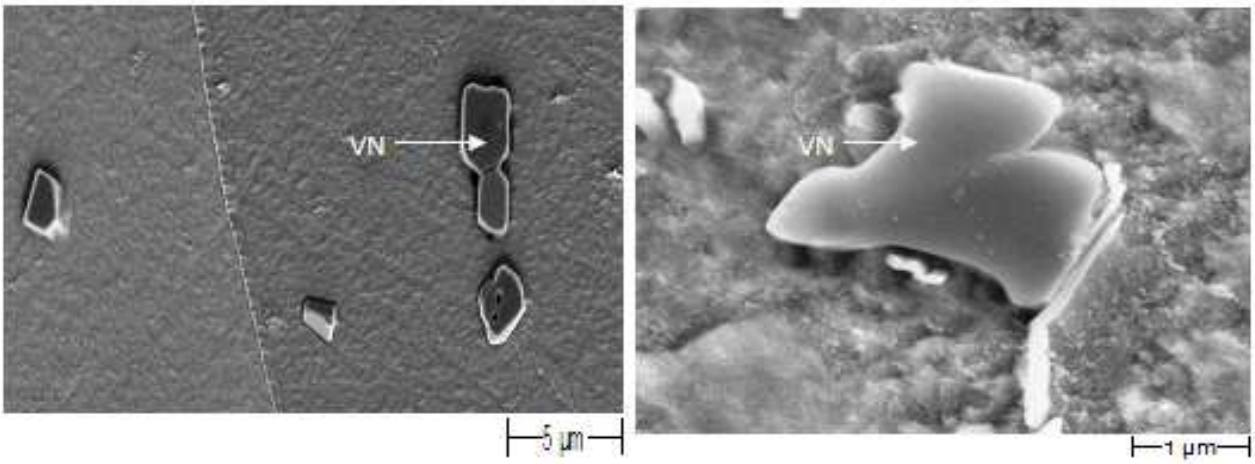

Figure 2B: The microstructure of (a) FeV and (b) FeVC.

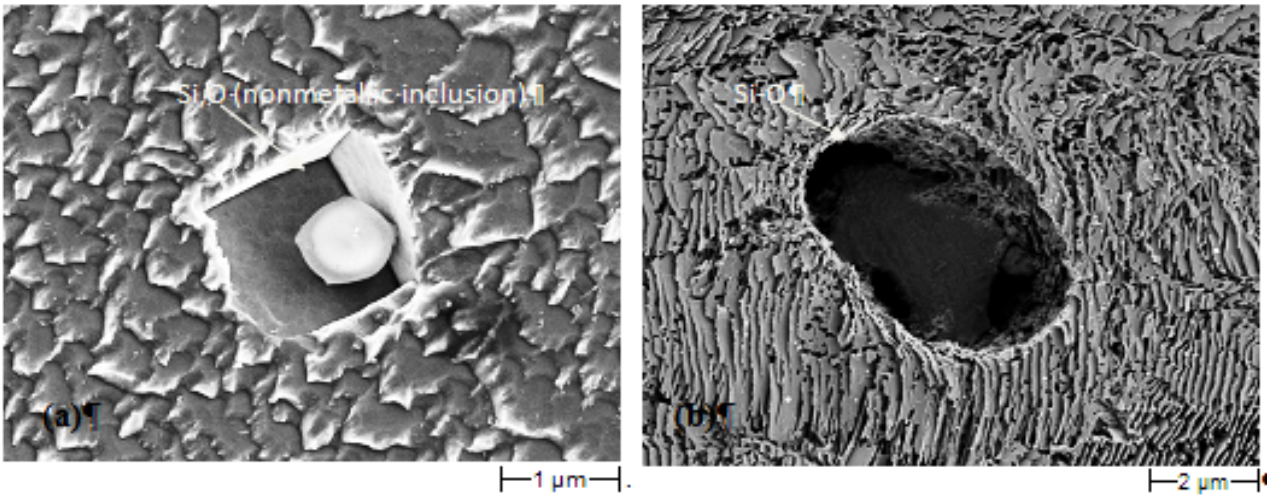

Figure 3B: The microstructure of (a) FeSi and (b) FeSiC.

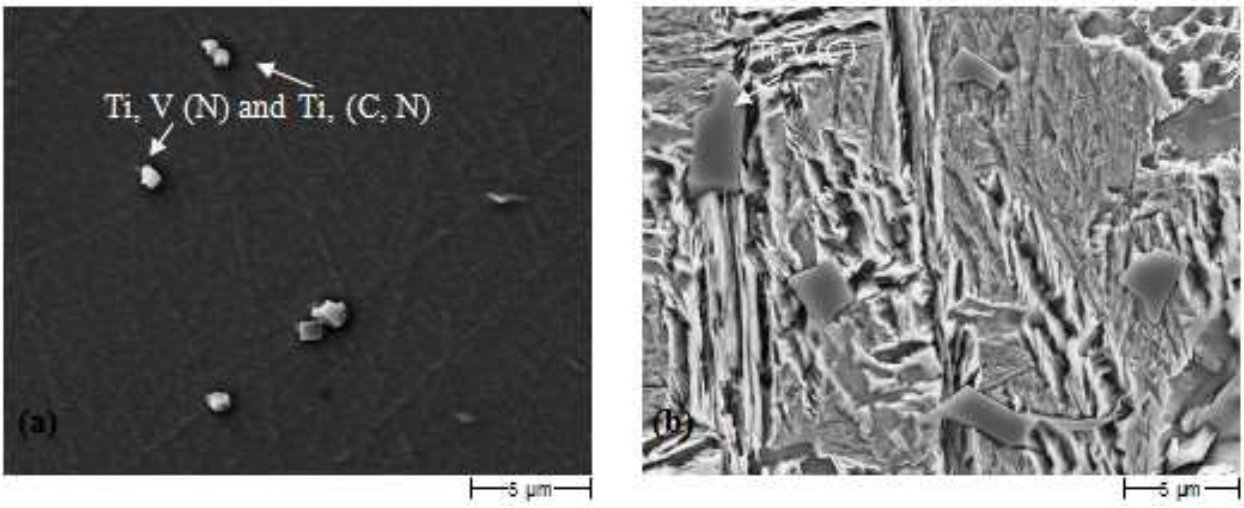

Figure 3B: The microstructure of (a) FeTiSiV and (b) FeTiSiVC.

Appendix C: Hydrogen absorption by charging steel with hydrogen

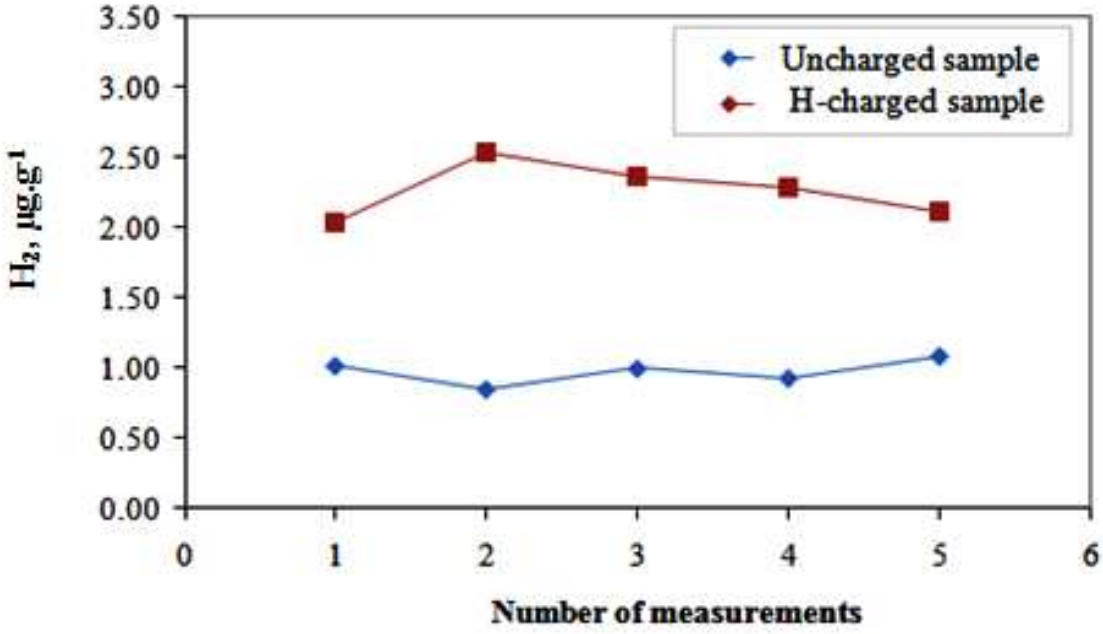

Figure 1C: FeC sample electrolytically charged with hydrogen by using a solution of 6 % H_2SO_4 containing 0.05 % As_2O_3.

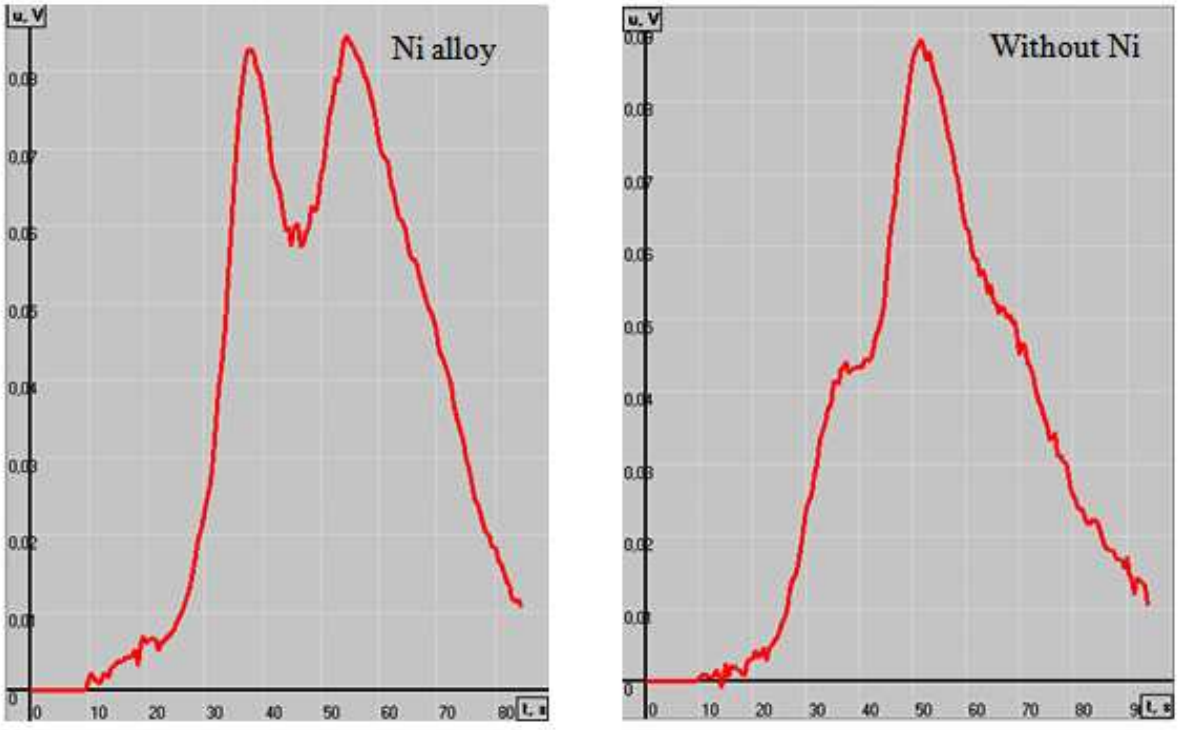

Figure 2C: The total hydrogen signals measured by TCD in Nickel alloyed and unalloyed reference material.

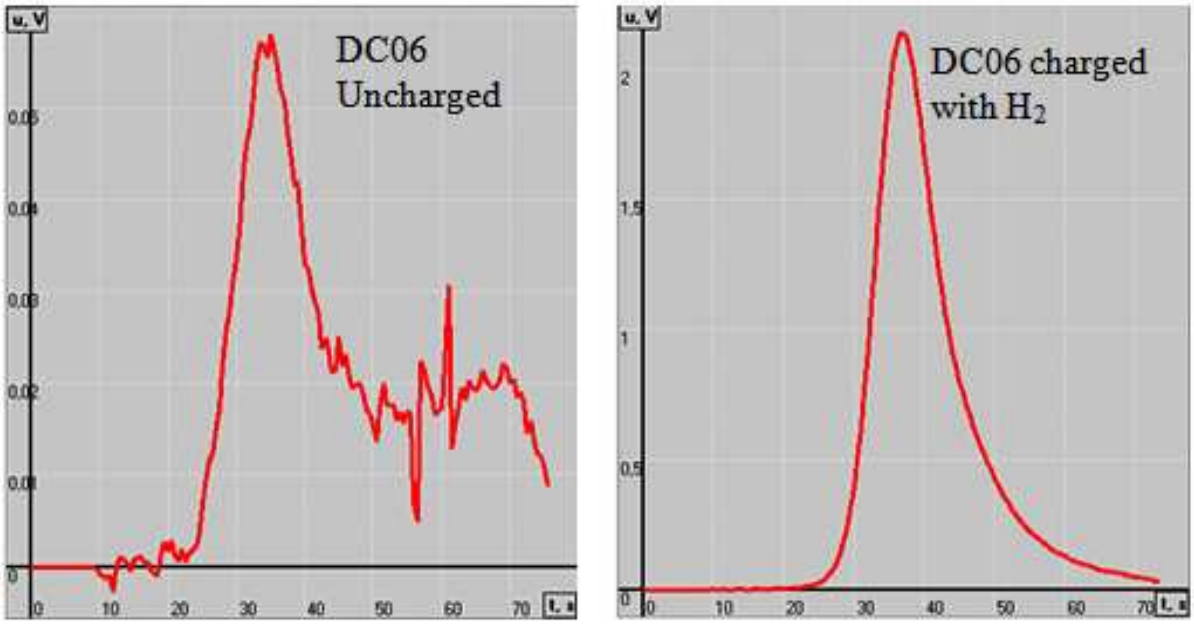

Figure 3C: The total hydrogen signal from TCD in uncoated DC06 sample and after charging the sample with hydrogen from the solution of 6 % H_2SO_4 with As_2O_4.

Appendix D: Sample preparation

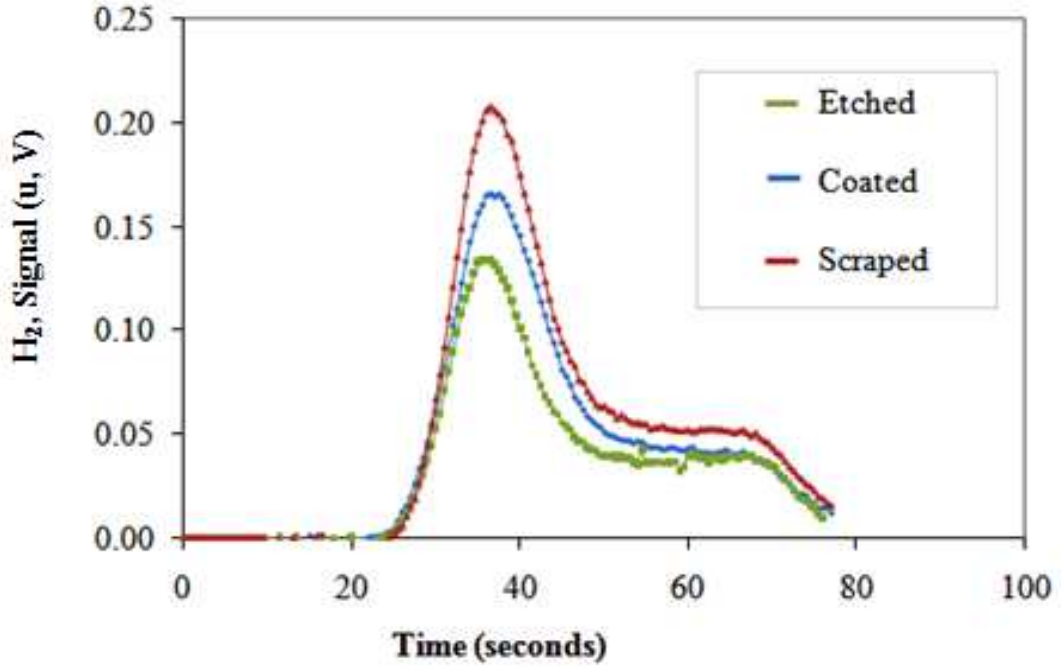

Figure 1D: The comparison hydrogen signal analysed by TCD in DC06 when the zinc coating was chemically and mechanically removed.

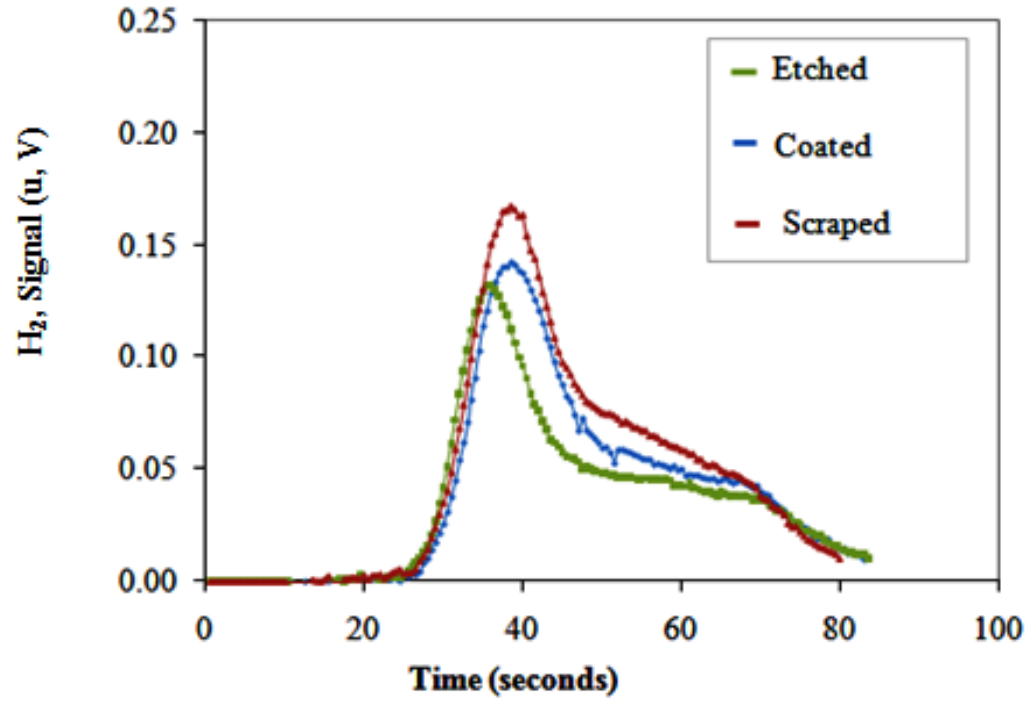

Figure 2D: The comparison hydrogen signal in HCT780C measured by TCD when the zinc coating was chemically and mechanically removed.

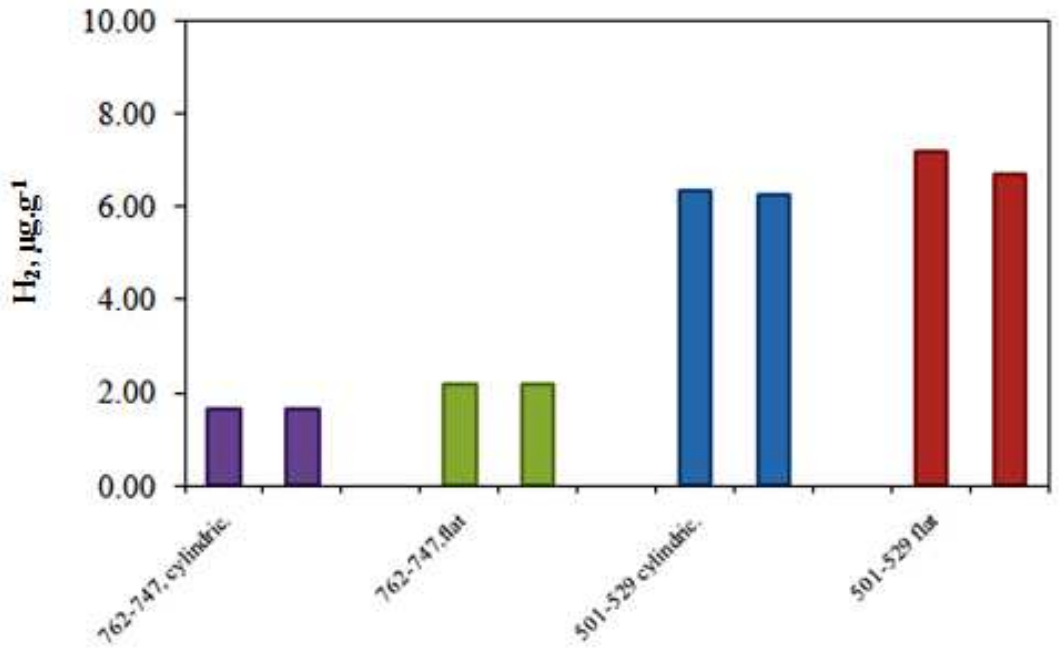

Figure 3D: The influence of sample shape on total hydrogen in 762-747 (1.8±0.2µg.g^{-1}) and 501-529 (6.0 ±0.2µg.g^{-1}) Leco reference materials.

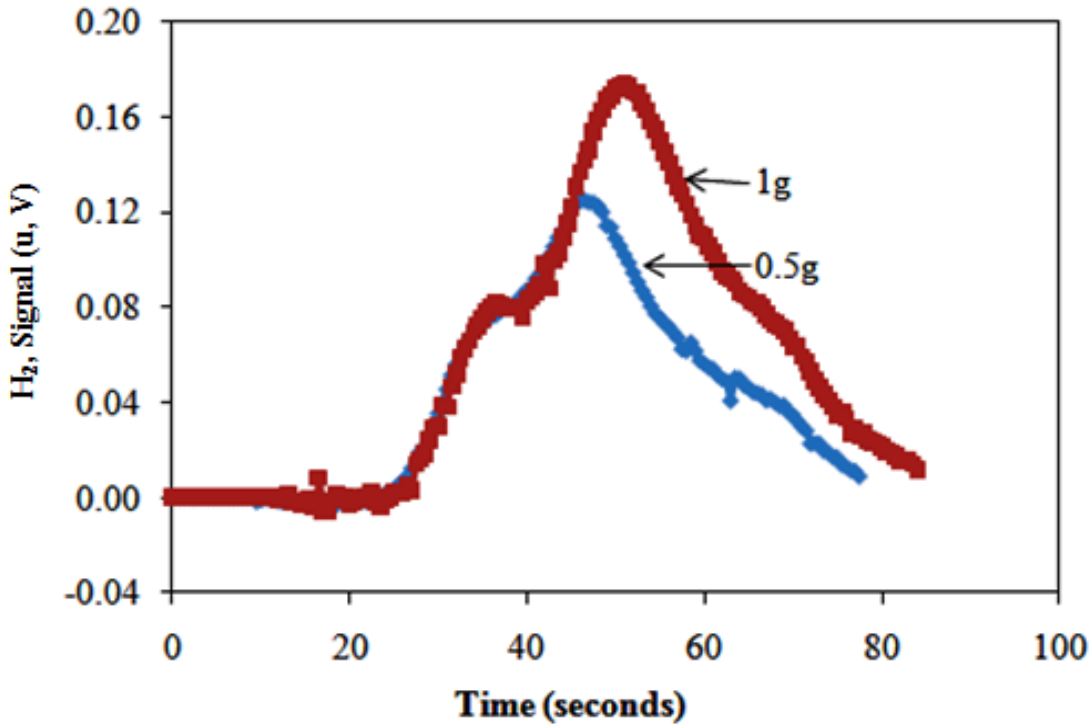

Figure 4D: The mass influence on total hydrogen concentration in Leco 762-747 (1.8 ±0.2) µg.g^{-1} reference material.

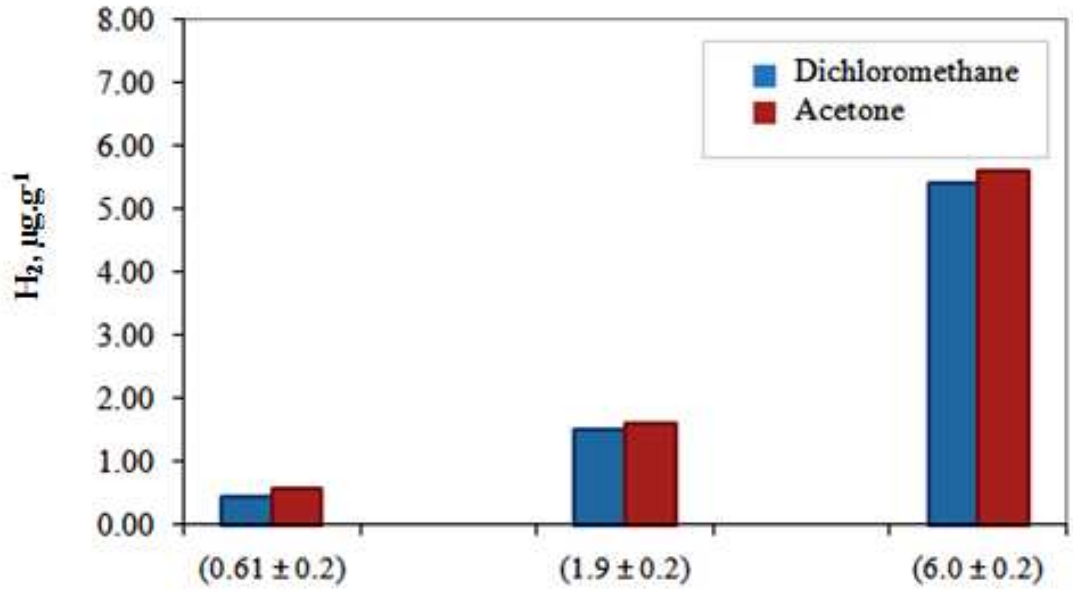

Figure 5D: The total hydrogen in reference material cleaned with acetone and dichloromethane.

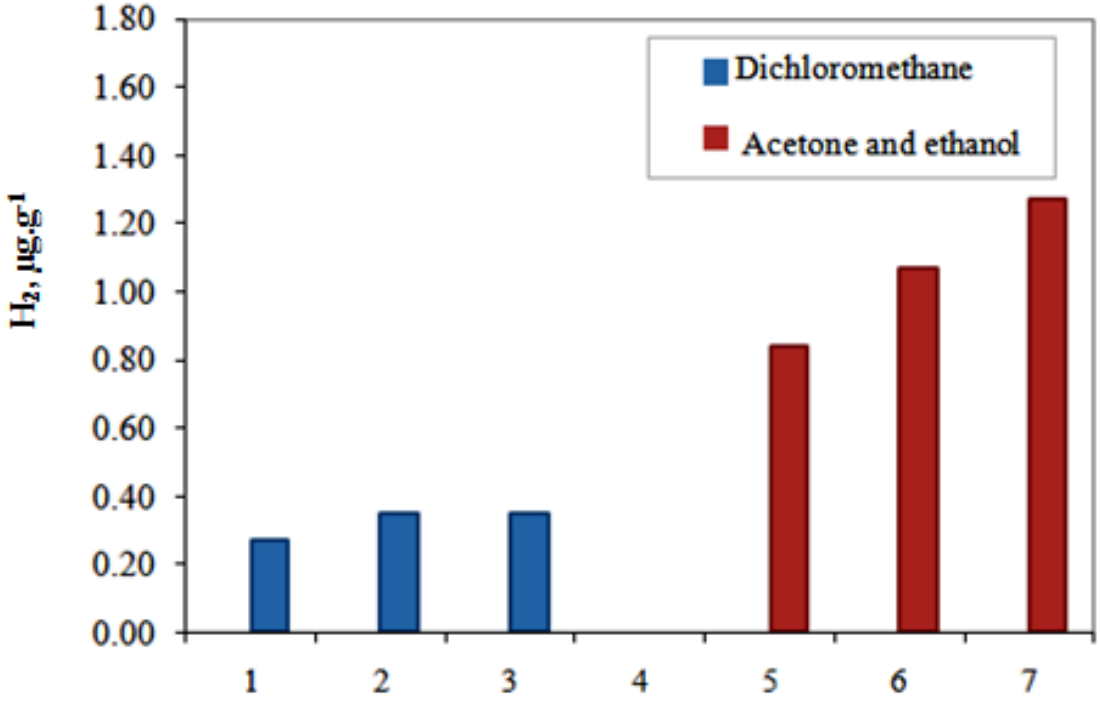

Figure 6D: The total hydrogen in DC06 samples cleaned with dichloromethane and acetone with ethanol.

Table 1D: The total hydrogen concentration in different masses of Leco reference material 501-529.

Sample identity	[H] $\mu g \cdot g^{-1}$ in 200 mg	[H] $\mu g \cdot g^{-1}$ in 400mg	[H] $\mu g \cdot g^{-1}$ in 1000mg
501-529 (6.0± 0.2 $\mu g \cdot g^{-1}$)	6.77	5.72	5.60
	6.48	5.65	5.56
	6.21	6.07	5.72
	6.48	5.81	5.62
Mean and Std. deviation	**6.49 ± 0.23**	**5.81± 0.18**	**5.63 ± 0.07**

Table 2D: The total hydrogen concentration measured by TCD after Zn coating removal with NAP and rinsing the samples with dichloromethane and methanol.

Sample	Cleaning solvent	Weight (g)	[H] $\mu g \cdot g^{-1}$	Mean ($\mu g \cdot g^{-1}$)	
DC06 Zn coated	Dichloromethane				
		2.32 2.17	1.94 2.00	2.25	0.04
		6.09 6.27	1.17 1.22	6.18	0.04
		1.04 1.03	0.99 0.83	1.03	0.11
Etching (N.A.P)	Methanol	5.92 5.87	0.80 0.83	5.80	0.02
		9.42 9.64	0.64 0.70	9.53	0.04
		1.08 1.08	0.67 0.48	1.08	0.13

Table 3D: The total hydrogen in FeCr with fine and rough grains**.**

FeCr	Form	TC detector ($\mu g \cdot g^{-1}$)	IR detector ($\mu g \cdot g^{-1}$)
1	Fine grains	4.46 4.94 4.78	4.90 5.10 5.20
	Rough grains	2.56 3.10 2.64	2.20 4.10 6.30
2	Fine grains	11.90 11.88 11.59	19.00 17.70 18.30
	Rough grains	24.27	0.70 9.40 23.00

APPENDIX E: Influence of sample storage on hydrogen desorption

Table 1E: The total H_2 in certified reference material that was stored at 105°C for 3 months.

Total hydrogen ($\mu g \cdot g$-1) measured by TCD				
Reference std.	Certified value	Measured value	3 months at 105°C	3 months at 105° & at RT
762-747	1.8 ±0.4	1.79 1.96	1.16 1.00 1.10	1.23 1.16
		1.88 ±0.12	**1.09 ± 0.08**	**1.20**
510-529	6.1±0.3	8.26 7.63	3.60 3.78 376	3.49 3.33
		7.95 ±0.45	**3.71 ± 0.10**	**3.41**
BS HON-S	1.7±0.3	2.63 2.80	2.55 2.80 3.17	2.31 2.58
		2.72± 0.12	**2.84 ± 0.31**	**2.45**

Appendix F: Pictures of steel alloys

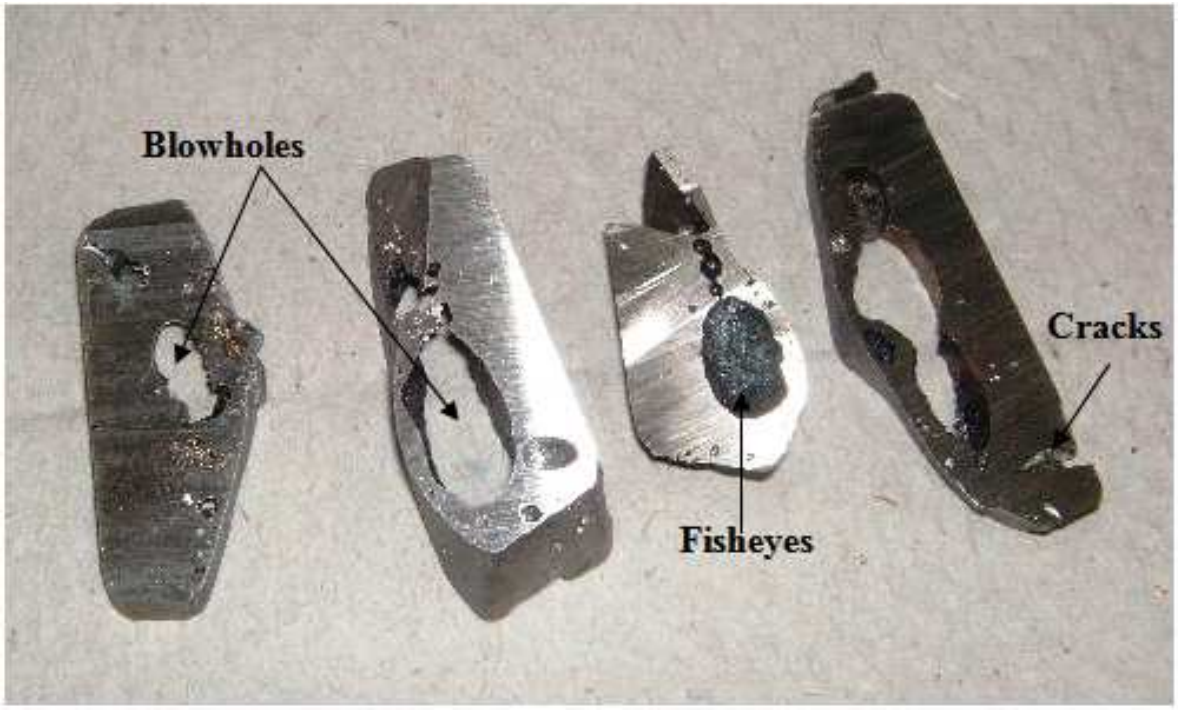

Figure 1G: The 97% Fe + 2 % Mn + 1 % C.

Appendix G: Materials and chemicals

Reference Materials

502-061 (2.19 ± 0.20), 501-529 (6.0 ± 0.20), 762-747 (1.80 ± 0.40) Leco, Lake view Avenue, U.S.A

BS HON-2 (1.9 ± 020), BS HON-S (2.8 ± 0.2) Brammer standard company, Houston, USA

546 (0.61 ± 0.2), Alpha standard, Alpha, Stevensville, Michigan, USA

Reagents

Sodium Hydroxide (NaOH) granules: supported on coal, Merk, Darmstadt, Germany

Magnesium perchlorate ($MgClO_4$), Eltra, Neuss, Germany

Schutze Reagent (I_2O_5) on SiO2, Alpha research, Michigan, USA

Molecular Sieve, J.T. Baker, Deventer, Holland

Solvents

Dichloromethane, 99, 6 %, Merck, Darmstadt, Germany

Methanol, Merck, Darmstadt, Germany

Ethanol 96 % Merck, Darmstadt, Germany

Ridoline C72, Henkel, Düsseldorf, Germany

Acetone, Merck, Darmstadt Germany

Acids

Nitric acid, 65 %, Merck, Darmstadt, Germany

Phosphoric acid, 85 %, Merck, Darmstadt, Germany

Acetic acid, 96 %, Merck, Darmstadt, Germany

Sulfuric acid (H_2SO_4), 95-97 %, Merck, Germany

HCl, 37 %, Merck, Darmstadt, Germany

Bases

Sodium hydroxide pellets, Merck, Darmstadt, Germany

Inhibitor

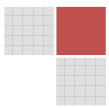

Hexamethylenetetramine ($C_6H_{12}N_4$) (next to Eltra instrument), Merck, Darmstadt, Germany.

Poison

Arsenetrioxide (As_2O_3), 99.999 %, Alfa Aesar, Germany

Melt Extraction instruments

ELTRA, GmbH, Neuss, Germany
Leco GmbH; Mönchengladbach, Germany

Hot extraction instruments

Juwe Bruker, H-MAT 221, Laborgeräte GmbH, Kalkar, Germany

Quadrupole mass spectrometer, Omnistar Balzers instruments, Asslar, Germany

Alloying material

Boron > 99.0 %, Merck, Germany

Carbon, 99.9 %

Silicon, 100 %

Vanadium in FeV, 82.3 %

Titanium 99.99 %

Manganesse, 99.8 %

Iron 99.99 %

Equipment for melting steel alloys

Himmel Oven SGS-02, NETZ, Germany

Equipment for the determination of the concentration of steel alloys

Spark Ablation Optical Emission Spectroscopy from Thermo applied research laboratories 446, Switzerland.

The ICP-OES from Thermo Fischer Scientific, Dreieich,

Instruments for analyzing the morphology of steel alloys

Zeiss AX10 light microscope with Zeiss Axiocamera from Zeiss in Germany

Feld Emissions-Raster Electron Microscope (FE-REM), 1530 with Gemini Electron column from LEO in Germany

Topography of steel samples

The DSM 950 from Carl Zeiss Micromaging GmBH, Gottingen, Germany

Microscope SZX9, from Olympus in Germany.

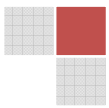

Published articles

N.Mabho, K.Bergers, U.Telgheder, J.Flock, *Talanta*, **2010**, *82*, 1298-1305, Determination of diffusible and total hydrogen concentration in coated and uncoated steel Part I.

K. Bergers, E. Camisão, I. Thomas, N. Mabho, J. Flock, *Steel Research International*, **2010,** *81(7),* p.499-507, Determination of hydrogen in Steel by Thermal Desorption Mass Spectroscopy.

N. Mabho, H.M. Kuß, *GIT Verlag (Wiley),* **2002**, *10*, p1154, Heterogeneity and Homogeneity of Steel Elements by using Capillary X-ray Fluoroscence.

Published papers presented in seminars

03/2010: Presented part of PHd. thesis: The determination of diffusible hydrogen in metallic materials using TDMS at the Institut für Analytische Wissenschaften, **ISAS-eV** (Institute for Analytical sciences) in Dortmund University.

03/2006: Presentation during Master`s degree (Water Science) on: Water Preservation by South African Culture at the Environmental centre at the University of Duisburg-Essen.

03/2002: Presented part of Bachelor work on: Determination of Heterogeneity and Homogeneity of Steel Elements by using Capillary X-ray Fluoroscence at the Institut für Analytische Wissenschaften, **ISAS-eV** (Institute for Analytical sciences) in Dortmund University.

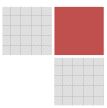

Curriculum Vitae

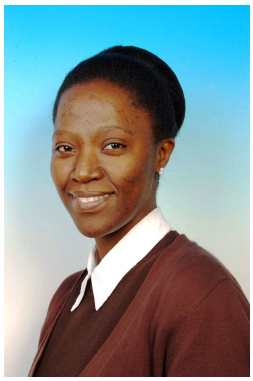

Name:	Mabho
First name:	Nonhlangabezo
Date of birth:	08 September 1978
Place of birth:	Tembisa, South Africa
Home address:	P. O. BOX 348
	Tembisa, 1628, Republic of South Africa
Home contact number:	+2711925 3726, +27786486701
Address in Germany:	Karl-Jahres Straße 169
	47053 Duisburg
Contact number:	+49203 379 1674, +49176 284 47068,

School Education

1986 - 1996:	St.matthew`s Girls High School (Matric Exemption), South Africa

Tertiary Education

1997 - 2001:	National Diploma in Analytical Chemistry at Border Technikon in East London, South Africa
April - Sept. 2001:	Analytical- Chemistry Practical in FAAS, GF-AAS, microwave solid extraction, Potentiometry and Thin Layer Chromatography at Gerhard Mercator University of Duisburg
October 2001 - March 2002:	Surface characterization of Steel using Capillary X-ray fluorescence Spectroscopy in ThyssenKrupp Steel in Germany
June 2002 – June 2003:	Bachelor Degree in Analytical Chemistry at Border Technikon in East London, South Africa

October 2004- March 2007: Master´s study in Water Science at the University of Duisburg-Essen in Germany, Thesis at Interlabor Belp in Switzerland. The topic was the Selenium determination in powdered milk using HG – AAS, ICP-OES, GF-AAS.

July 2007-September 2010 PhD. degree at Duisburg-Essen University und ThyssenKrupp Steel Europe in Germany. The topic was Determination of Diffusible and Total Hydrogen in Coated and Uncoated Steel.

Hobbies

Travelling, Decorating clothes or venues for events and Drawing (art).

References

1. P.D. Dr. Ursula Telgheder (Lecturer)

   University of Duisburg-Essen

   1 Lothar Street

   Duisburg 47048

   E-mail: Ursula.telgheder@uni-due.de

   Contact no.: +49203 379 2534

2. Mr Soto Ndukwana (Group Chairman)

   Ifula Holdings

   51 Wessels Road

   Rivonia 2128

   E-mail: soto@ifula.co.za

   Contact number: +27 11 304 7201, +27 83 326 3466